Dissertation

Development of a Traceable Atomic Force Microscope with Interferometer and Compensation Flexure Stage

Vorgelegt der Fakultät für Maschinenbau
Der Technische Universität Ilmenau

zur Erlangung des akademischen Grades
Doktoringenieur (Dr.-Ing.)

von M.S. Chao-Jung Chen,
Geboren am 19. 01. 1960 in Taoyuan, Taiwan

Gutachter: Univ.-Prof. Dr.-Ing. habil. G. Jäger, TU Ilmenau
Prof. Dr.-Ing. habil. K. Hasche, PTB Braunschweig
PhD Tzeng-Yow Lin, ITRI, Hsinchu/Taiwan
vorgelegt: 07. January 2003
verteidigt: 27. May 2003
Verfahrensnummer: MB 96

Preface

This study is created by Dr. Jia-Ruey Duann, Deputy General Director of Center for Measurement Standards (CMS), and Prof. Dr.-Ing. habil. Gerd Jäger, Head of the Institute of Process Measurement and Sensor Technology (PMS), Faculty of Mechanical Engineering, Technische Universität Ilmenau. When Prof. Jäger visiting to the CMS during the tenth anniversary of National Measurement Laboratory in 1997, he gave some lectures and discussed with the colleagues of Dimensional Measurement Laboratory about the miniature laser interferometer and its applications. I also introduced my project of the development of linewidth measurement and some nanometrology researches in CMS. Prof. Jäger was interested in a Metrological Atomic Force Microscope (MAFM), and long travel range of nanopositioning stage with feedback by laser interferometer. He asked me to be a doctoral student like Mr. Yung-Cheng Wang, a full time doctoral student, at the Technische Universität Ilmenau. But it is impossible for me to go to Ilmenau for four years without working to provide my family. So, Prof. Jäger made a chance of remote doctoral study that I can do the research in the CMS and go to the Technische Universität Ilmenau to report twice per year.

In the 1998 spring, Dr. Jia-Ruey Duann, former Division Chief of the Measurement Standards and Technology Division at CMS, encouraged me to study at the Technische Universität Ilmenau, and promised me that CMS will provide the transportation and daily lives during my study in Germany. Therefore, during my visiting to the Technische Universität Ilmenau in the 1998 autumn, I started to register as a remote doctoral student at PMS. Prof. Jäger acts as my advisor. My study project is “Development of a Traceable Atomic Force Microscope with Interferometer and Compensation Flexure Stage”. The TAFM consists of a commercial Atomic Force Microscope (AFM), two Differential Plane Mirror Laser Interferometers, an Active Error Compensation Flexure Stage, and a super-Invar metrology frame. This instrument will be established to calibrate pitch standards at the National Measurement Laboratory in Taiwan.

Erklärung

Ich versichere, dass ich die vorliegende Arbeit ohne unzulässige Hilfe Dritter und ohne Benutzung anderer als der angegebenen Hilfsmittel angefertigt habe. Die aus anderen Quellen direkt oder indirekt übernommenen Daten und Konzepte sind unter Angabe der Quelle gekennzeichnet.

Bei der Auswahl und Auswertung des Materials haben mir keine Personen entgeltlich/unentgeltlich geholfen.

Weitere Personen waren an der inhaltlich-materiellen Erstellung der vorliegenden Arbeit nicht beteiligt. Insbesondere habe ich hierfür nicht die entgeltliche Hilfe von Vermittlungs- bzw. Beratungsdiensten (Promotionsberater oder anderer Personen) in Anspruch genommen. Niemand hat von mir unmittelbar oder mittelbar geldwerte Leistungen für Arbeiten erhalten, die im Zusammenhang mit dem Inhalte der vorgelegten Dissertation stehen.

Die Arbeit wurde bisher weder im In- noch im Ausland in gleicher oder ähnlicher Form einer Prüfungsbehörde vorgelegt.

Ich bin darauf hingewiesen worden, dass die Unrichtigkeit der vorstehenden Erklärung als Täuschungsversuch angesehen wird und den erfolglosen Abbruch des Promotionsverfahrens zu Folge hat.

Ilmenau, den 18, 10, 2002 Chao-Jung Chen

Dedication

To my parents, You Chen and Chang-Chao Chen, my wife, Shu-Jen Wu, and my children, Jenny, Berry, and Kevin.

Acknowledgments

I would like to express my sincere and respectful gratitude to my advisor, Prof. Dr.-Ing. habil. Gerd Jäger, Head of the Institute of Process Measurement and Sensor Technology, Faculty of Mechanical Engineering, Technische Universität Ilmenau. Without his continuing advice, encouragement, technical guidance and recommendation, this research work would never have been accomplished.

This study was financial supported by the Center for Measurement Standards, Industrial Technology Research Institute (CMS/ITRI). I deeply appreciate Dr. Chang Hsu, General Director of CMS, for his permission of on-job study to me, Dr. Jia-Ruey Duann, Deputy General Director of CMS, for his providing of this oversea study chance, Dr. Victor Tzeny-Yow Lin, Chief of Measurement Standards & Technology Division in CMS, for his recommending me being elected as a candidate of on-job study, Dr. Gwo-Sheng Peng, Manager of Dimensional Measurement Laboratory in CMS, for his continuing technical support and discussion during my study period, Dr. Boh-Sheng Harn, Deputy General Director of CMS, for his encouragement and assistance in researcher exchanging between CMS and Technische Universität Ilmenau. I also would like to thank all my colleagues of Dimensional Measurement Laboratory for their work sharing during my study. I hope to give thanks to Prof. Liang-Chih Chang, advisor of CMS, and Mr. Yen-Liang Chen for the discussion of uncertainty evaluation and programming support, Dr. Chien-Ming Wu, Dr. Sheau-Shi Pan, Mr. Norbert Hofmann, Mr. Wei-Cheng Chang, and Paul Lui, for their assistance in technical discussion and experimental setup. I also give thanks to Dr.-Ing Hans-Joachim Büchner, Dr.-Ing Eberhard Manske, Dr. Yung-Cheng Wang, Dr. Tino Hausotte, Dr. Denys Dontsov, Dr. Holger Wurzbacher, Dr. Detlef Heydenbluth, Mr. Matthias Welter, and Frau Cordula Höring, for their assistance during my study in the Technische Universität Ilmenau in Germany.

Finally, I appreciate my parents, You Chen and Chang-Chao Chen, my wife, Shu-Jen Wu, my children, Jenny, Berry and Kevin, for their patience, understanding, housework sharing, and encouragement throughout my study.

Contents

List of Figures

List of Tables

List of Symbols

A	Distance between the moving mirror and probe tip
B	Dead path
c_{xi}	Sensitivity coefficient of x_i
C	Distance between the reference mirror and probe tip
d	Abbe offset
D	Displacement
$e_{sw}(T)$	Saturated vapor pressure (Pascal)
f	Vapor pressure (Pascal)
H	Step height
I	The rotate inertial of spring
k	Coverage factor
K	The stiffness of the vibration isolator
K_N	The magnitude of a negative stiffness mechanism
K_S	the spring stiffness
l	Length of Spring
L	Displacement
L_a	Lagrangian
m	The number of intersection points
m_1	The mass of dummy stage
m_2	The mass of moving stage
m_3	The mass of spring
m_d	Diffraction order
n	Refraction index of air
n_{tpf}	Refraction index of air, function of temperature t, pressure p, and vapor pressure f
N	Counting of laser interferometer
N_c	Pitch of the reference standards at 20 °C
N_m	Pitch of the standards at temperature T_s
p	Pressure (Pascal)
P	Pitch
P_c	Compression force
q_1	The displacement of dummy stage relative to base
q_2	The displacement of moving stage relative to dummy stage
RH	Relative humidity
s	Standard deviation
SD	Standard Deviation
t	Air temperature (ºC)
t_{90}	Temperature (ºC)

t_s	The temperature of sample (ºC)
T	Absolute temperature (K)
$u(x_i)$	Standard uncertainty of x_i
$u_c(y)$	Combined Standard uncertainty of output estimate y
$u_i(y)$	Component of combined Standard uncertainty $u_c(y)$ of of input x_i
U	Expanded uncertainty
W	Weight
x_i	The displacement of flexure stage in the X direction
y_i	The displacement of flexure stage in the Y direction
Y_c	Pitch of the test standards at 20 °C
Y_m	Pitch of the tested standards at temperature T
α	Coefficient of thermal expansion of the test standards
β	Angle deviation of the flexure stage
δT	Difference of temperature between the reference standards and the test standards
δx	Line center determination
$\delta\alpha$	Difference of the coefficient of thermal expansion between the reference standards and the test standards
$\delta\alpha_{xz}$	Z to X coupling error
$\delta\lambda$	Deviation of laser wavelength
ΔT_s	Deviation in temperature of the reference standards from 20 °C
ε_{P_1}	The error of pitch measurement by the TAFM
ε_{P_2}	The error of pitch calculation by the SPIP software
ϕ	Tilt angle of pitch pattern
γ	Incident angle of the grating diffraction
η	Diffraction angle of the grating diffraction
θ	Angle between laser beam and moving axis of the flexure stage
λ	Laser wavelength in air
λ_0	Laser wavelength in vacuum
λ_f	Stiffness of spring
λ_n	Nonlinearity
λ_{tpf}	Laser wavelength in air, function of temperature t, pressure p, and vapor pressure f
ν	Degrees of freedom
ν_{eff}	The effective degrees of freedom
$\nu_i(y)$	Degrees of freedom of standard uncertainty $u(x_i)$ of input estimate x_i
$\nu(x_i)$	Degrees of freedom of standard uncertainty $u(x_i)$ of input estimate x_i
σ	$1/\lambda_o\,(\mu m^{-1})$
ω	Natural frequency of flexure stage

AFM	Atomic Force Microscope
BIPM	Bureau International des Poids et Mesures
CCL	Consultative Committee for Length
C-AFM	Calibrated Atomic Force Microscope
CMS	Center for Measurement Standards
CTE	Coefficient of Thermal Expansion
DI	Digital Instruments
FEM	Finite Element Method
GUM	Guide to the Expression of Uncertainty in Measurement
ISO	International Organization of Standards
ITRI	Industrial Technology Research Institute
LVDT	Linear Variable Differential Transducer
MAFM	Metrology Atomic Force Microscope
MEMS	Micro Electro Mechanical System
METAS	Metrology and Accreditation in Switzerland
NI	National Instrument
NIST	National Institute of Standards and Technology
NLS	NanoLattice Standard
NMM	Nano-measuring machine
NPL	National Physical Laboratory
NSM	Negative Stiffness Mechanism
NT-MDT	Molecular Devices and tools for NanoTechnology
PI	Physik Instrumente
PMS	Process Measurement and Sensor Technology
PSI	Park Scientific Instruments
PTB	Physikalisch-Technische-Bundesanstalt
RM	Reference Material
RMS	Root Mean Square
SEM	Scanning Electron Microscope
SI	International System of Units
SPIP	Scanning Probe Image Processor
SPM	Scanning Probe Microscope
SRM	Standard Reference Material
STM	Scanning Tunneling Microscope
TAFM	Traceable Atomic Force Microscope
TSMC	Taiwan Semiconductor Manufacturing Company
UMC	United Microelectronics Corporation
WGDM	Working group on Dimensional Metrology

1. Introduction

G. Binnig, H. Rohrer, Ch. Gerber, and E. Weibe developed a Scanning Tunneling Microscope (STM) at IBM in Switzerland in 1982 [1]. The tunneling current between the tip and sample determines the surface texture of the conductive samples. Its use was the first time the microstructure of the surface of an electrical conductor was observed at atomic resolution. G. Binnig, and H. Rohrer won the Nobel Prize in Physics in 1986. G. Binnig, C. F. Quate, and Ch. Gerber developed the Atomic Force Microscope (AFM) in 1986 [2]. This microscope measured the surface profile by the Van der Waal's forces between the tip and the sample. Accordingly, an AFM can measure the micro-texture of conductors, non-conductors and bioengineering materials. The AFM has already been widely applied in materials science, scientific research, biotechnology and the semiconductor industry.

The commercial AFM is normally designed with a tube piezo-actuator for three-dimensional scanning. Figure 1.1 schematically depicts AFM, which consists of a scanner made of a piezo-actuator tube, a laser, a photo-detector, a controller and a cantilever tip. The upper scanner is divided into four electrodes for scanning in the X and Y directions. The lower scanner senses height in the Z direction. The intrinsic properties of the piezo-actuator, such as non-linearity, hysteresis, aging, thermal drift, creep, and coupling error may cause measurement errors, which may reach 20 % of the reading. To reduce major measurement errors mentioned above, an AFM should be periodically calibrated using a traceable standard.

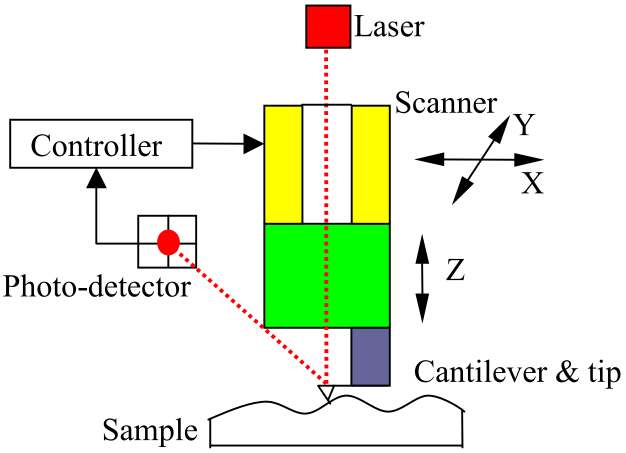

Figure 1.1 Schematic diagram of AFM

The displacements of the AFM must be traceable to the definition of the meter (International System of Units, SI units). For metrological reasons, AFMs are usually feedback-controlled by the applied voltage, a photo-detector, or a capacitance sensor. Some National Measurement

Laboratories have developed metrological AFMs with a traceable displacement sensor, such as a laser interferometer. For instance, Dr. F. Meli assembled a homemade linear flexure stage and a differential plane mirror interferometer in a commercial AFM for pitch measurements [3] at the organization for Metrology and Accreditation in Switzerland (METAS). Prof. K. Hasche and Dr. H.-J. Büchner used three internal laser interferometers to calibrate the capacitance sensors of a Zeiss Veritekt 3 AFM [4,5] at the Physikalisch-Technische-Bundesanstalt (PTB) in Germany. Prof. G. Jäger built a nano-measuring machine with three-axis laser interferometers and two autocollimators with a measuring range of 25×25×5 mm^3 [6] at the Technische Universiät Ilmenau in Germany. A Calibrated AFM was built using a custom-modified AFM controller, flexure stages and laser interferometers, at the National Institute of Standards and Technology (NIST) in the U.S.A. [7].

This research aims to develop a Traceable Atomic Force Microscope (TAFM) for the Center for Measurement Standards (CMS) of the Industrial Technology Research Institute (ITRI) in Taiwan. The TAFM was based on a commercial Dimension Metrology AFM and assembled with a three-axis active compensation flexure stage, two differential plane mirror laser interferometers, an L-shape mirror, and a super-Invar metrology frame. The TAFM was placed on a vibration isolator to eliminate noise due to environmental vibration. A program in LabVIEW was developed to control the movements of the flexure stage, and simultaneously capture the displacements by the laser interferometers (X and Y) and the capacitance sensor (Z) of the AFM. An enclosed box with temperature-controlled circulating water maintains temperature near 20°C and reduces the influences of acoustic and air turbulence.

The TAFM was successfully used to calibrate one-dimensional pitch standards. The pitch of the sample was measured by the TAFM to yield a three-dimensional profile. Then, the X and Y scanned data were interpolated by a program written in MATLAB. Finally, the Scanning Probe Image Processor (SPIP) software was used to calculate the pitch value and the pattern tilt angle [8]. According to the "Guide to the expression of the uncertainty in measurement" (GUM), published by the International Organization of Standards (ISO), the expanded uncertainty of a nominal pitch value of 292 nm was2.5 nm, at a confidence level of 95 % and 29 effective degrees of freedom.

2. State of the art AFM

The Scanning Probe Microscope (SPM) is nowadays an efficient tool for nanometrology such as STM, AFM, Scanning Near-field Optical Microscope (SNOM). The SPM can measure the physical properties of materials with atomic resolution. In 1981, G. Binnig, H. Rohrer, Ch. Gerber, and E. Weibel developed the STM at the IBM Research Laboratory in Switzerland [1]. It was the first successful tunneling experimental to observe vacuum tunneling per se, resolve tunneling spectroscopy and surface topography. But the STM only can measure the conductive materials. For the applications in non-conductive and semi-conductive materials, G. Binnig, C.F. Quate, and Ch. Gerber created an AFM combined the principles of the STM and stylus profiler in 1986[2]. It is capable for all materials with a lateral resolution of 30 Å and a vertical resolution less than 1 Å. Table 2.1 shows the glossary of SPM. They are widely used in fundamental science research, surface topography, biotechnology, and semiconductor industry.

Table 2.1 The glossary of SPM

STM	Scanning Tunneling Microscope
AFM	Atomic Force Microscope
LFM	Lateral Force Microscope
MFM	Magnetic Force Microscope
SCM	Scanning Capacitance Microscope
EFM	Electrostatic Force Microscope
FMM	Force Modulation Microscope
SNOM	Scanning Near field Optical Microscope
SThM	Scanning Thermal Microscope

2.1 Traceability of AFM

There are two scanning types of SPM. One is called “tip scanning”. The other is called “sample scanning”. A tube piezoelectric actuator (scanner) is usually designed as three-dimensional scanning to control the probe tip scanning on a fixed sample in tip scanning type SPM or the sample scanning under the probe tip in sample scanning SPM. Figure 2.1 shows the principles of sample scanning type SPM [9]. A stepper motor moves the sample approaching to the probe tip. A laser beam bounces off the back of the cantilever, then hits onto a position sensitive photo-detector. The SPM processor receives the signal from the PSPD, and then sends applied voltage to the scanner to maintain the cantilever at a certain deflection.

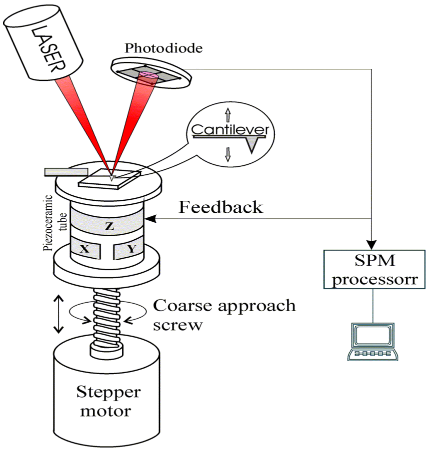

Figure 2.1 Principles of sample scanning AFM [9]

The AFM has been widely applications in many field, including science research, surface roughness analysis, and nonotechnology. Figure 2.2 shows the interaction between probe tip and sample. During the probe tip approaching to the sample surface, there is a Van der Waals Force occurred (attractive force) when the distance between tip and sample decrease to Angstrom level. And there is a Coulombic Force (repulsive force) occurred when the distance is down to fractions of an Angstrom. In generally, the AFM has three operation modes. The Contact mode AFM is operated by scanning a tip attached to the end of a cantilever across the sample. The force between tip and sample remains constant to maintain a constant cantilever deflection. In the non-contact mode AFM, the probe tip is oscillated at a certain frequency, which is slightly higher than the resonance frequency. The amplitude is about a few nanometers. During scanning, the probe tip does not contact sample surface, but oscillates above the absorbed fluid layer on the sample surface. The Intermittent-contact (Tapping) mode AFM is operated by scanning a tip attached to the end of an oscillating cantilever across the sample. The cantilever is oscillated at or near the resonance frequency with a 20 nm to 100 nm amplitude. The advantages of Tapping mode AFM are higher lateral resolution on most samples, less damage to soft samples, and no scraping. It becomes an important AFM technique since it overcomes some of the limitations of both contact and non-contact mode AFM.

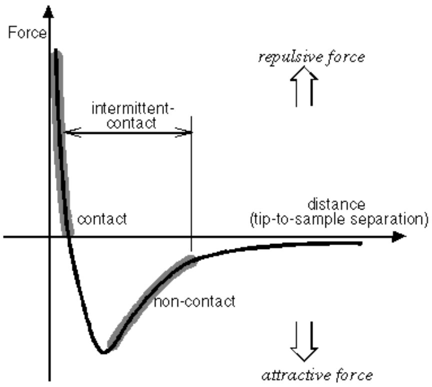

Figure 2.2 Force vs. distance [10]

The SPM has a scanner doing the three-dimensional scanning. The scanner is made of piezoelectric actuator tube. Some intrinsic properties of piezo-actuator such as non-linearity, hysteresis, aging, thermal drift, creep, and coupling can cause measurement errors (see Figure 2.3), which may reach 20 % to the reading. Figure 2.4 shows an example of grating measurement with two AFMs. A result of one AFM is 32.89 µm, a result of another AFM is 40.742 µm. In compliance with metrology standard regulars, the AFM should be periodically calibrated by a traced standard, or combined with accurate displacement sensors to monitor the position scanning . The displacement sensors should be traced to the definition of meter.

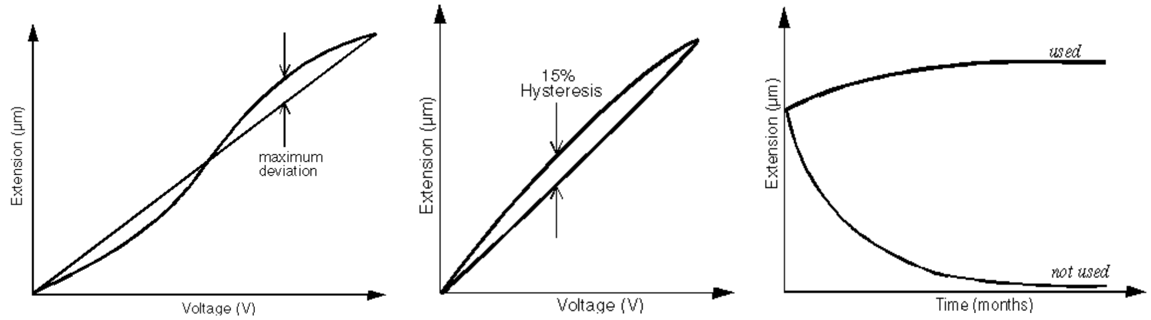

(a). Nonlinearity (b). Hysteresis (c). Aging

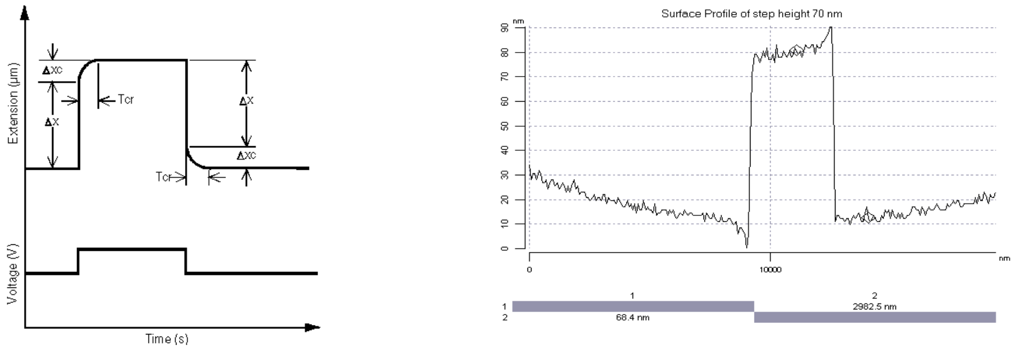

(d). Creep (e). Cross coupling error

Figure 2.3 Intrinsic Properties of AFM [10]

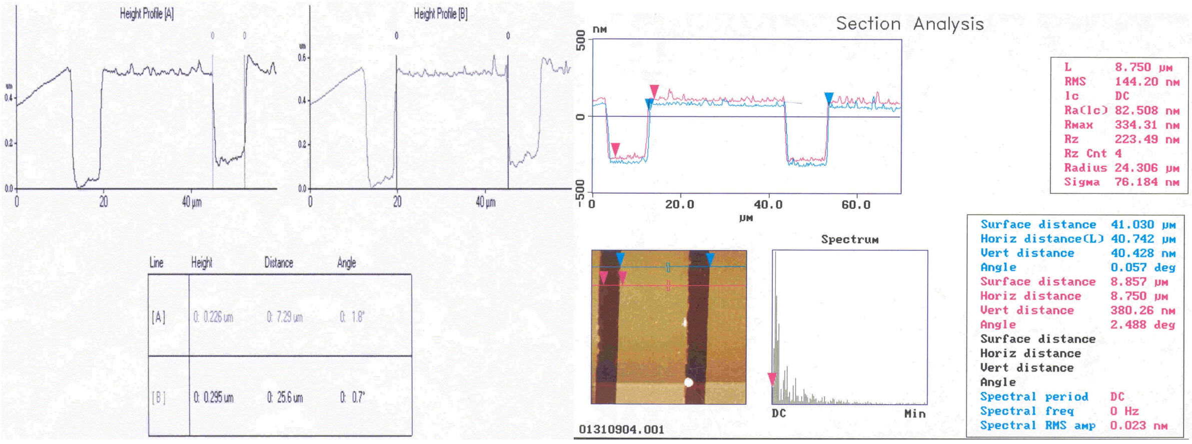

Line	Height	Distance	Angle
[A]	0: 0.226 um	0: 7.29 um	0: 1.8°
[B]	0: 0.295 um	0: 25.6 um	0: 0.7°

```
L         8.750 µm
RMS       144.20 nm
lc        DC
Ra(lc)    82.508 nm
Rmax      334.31 nm
Rz        223.49 nm
Rz Cnt    4
Radius    24.306 µm
Sigma     76.184 nm
```

```
Surface distance     41.030 µm
Horiz distance(L)    40.742 µm
Vert distance        40.428 nm
Angle                0.057 deg
Surface distance     8.857 µm
Horiz distance       8.750 µm
Vert distance        380.26 nm
Angle                2.488 deg
Surface distance
Horiz distance
Vert distance
Angle
Spectral period      DC
Spectral freq        0 Hz
Spectral RMS amp     0.023 nm
```

Figure 2.4 Grating pitch measurement by AFMs

Figure 2.5 shows the traceability of AFM. The AFM users usually need one or two-dimensional Standard Reference Material (SRM) such as a pitch standard to calibrate the displacement sensors periodically. The SRM must be traced to the International System of Units (SI units) via a traceability chain. The national metrology institute investigates a metrological instrument to calibrate the SRM; e.g. a Traceable Atomic Force Microscope assembled with laser interferometer. The wavelength of laser interferometer should be traced to the definition of meter via an iodine stabilized Helium-Neon laser.

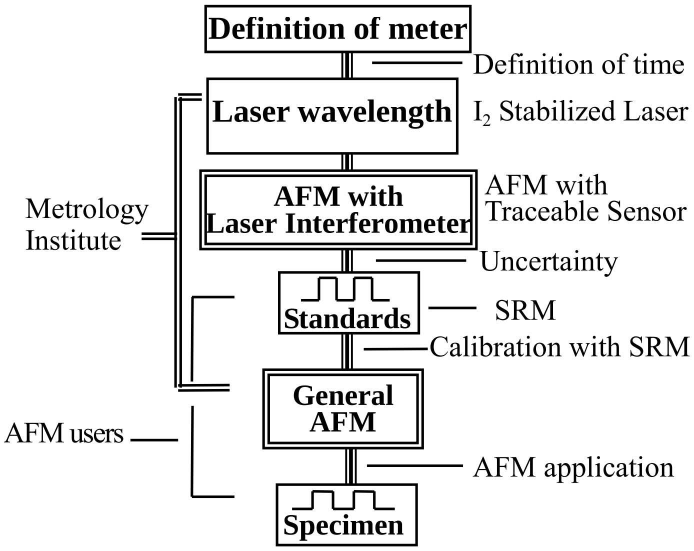

Figure 2.5 Traceability of AFM

The calibration of SRM can be realized by a comparative method or absolute measurement. Figure 2.6 shows a comparative method of pitch standard calibration. Firstly, we have to use a commercial AFM to measure a traced reference pitch standard, then, measure a test standard. Finally, we have to use the Scanning Probe Image Processor (SPIP) developed by Image Metrology company [8] to analyze the pitch value and pattern tilt angle.

We have participated in a 1-D grating international comparison using a DI Dimension 3100M AFM in 2000 [11]. It was coordinated by the Metrology and Accreditation Switzerland (METAS). The nominal values of comparison specimens were 290 and 700 nm pitch gratings (MXS 301CE and MXS 701CE). According to the “Guide to the Expression of Uncertainty in Measurement” [12], the estimated expanded uncertainties at 95% confidence level were 287±2.2 nm and 698.1±5.2 nm [13]. The measuring equation can be expressed as following:

$$Y_c = \frac{N_c Y_m}{N_m}(1 + \delta\alpha\Delta T_s + \alpha\delta T) \tag{2.1}$$

Where Y_c is the pitch of the test standards at 20 °C. N_c is the pitch of the reference standards at 20 °C as given in its calibration certificate. N_m is the pitch of the standards at temperature T_s. Y_m is the pitch of the tested standards at temperature T. $\delta\alpha$ is the difference of the coefficient of thermal expansion between the reference standards and the test standards. ΔT_s is the deviation in temperature of the reference standards from 20 °C. α is the coefficient of thermal expansion of the test standards. δT is the difference of temperature between the reference standards and the test standards.

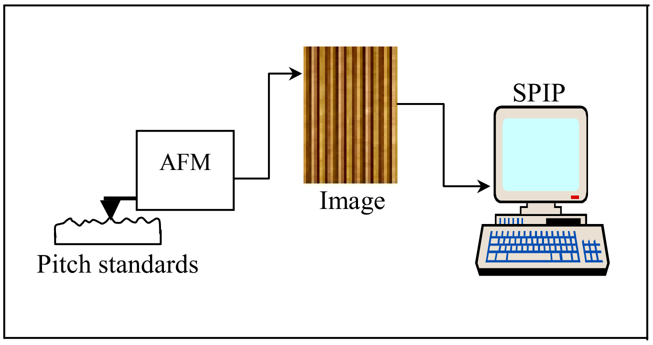

Figure 2.6 Pitch Standard calibration with AFM

Most national standard organizations want to establish the primary measuring instruments to serve the best calibration quality for their countries. The primary measuring instruments should have high stability and productivity and traceability to the SI. The following sections will describe some better designs for the nanometrology in the world. They are Molecular Measuring Machine and Calibrated AFM in United States, Metrology AFM and Nano-Measuring Machine in Germany, and Long-range AFM profiler in Switzerland.

2.2Molecular Measuring Machine at the NIST

The researchers at the National Institute of Standards and Technology (NIST) in United States have developed a measuring instrument called “Molecular Measuring Machine (M^3, see Figure 2.7)”[14-20] with one nanometer of expectant combined standard uncertainty of 50 mm by 50 mm measuring area since 1987. To achieve the goal of the Molecular Measuring Machine, the researchers use a combination of technologies. A STM is used for imaging specimen features. A coarse inchworm actuator and a fine motion flexure stage are used to move the sample to realize the desired range and resolution. The displacement of the STM probe relative to the sample in the XY plane is measured by a homemade laser interferometer (see Figure 2.8). The metrology frame is made of Zerodure with a flatness of 30 nm and right angles between each adjacent reference mirrors (see Figure 2.9). The whole system is operated in an ultra-high vacuum and contained in a precise temperature controlled chamber.

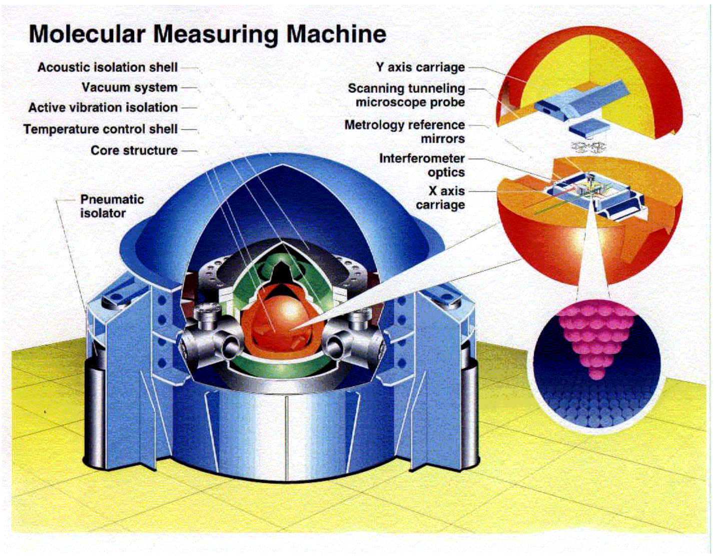

Figure 2.7 Molecular Measuring Machine [14]

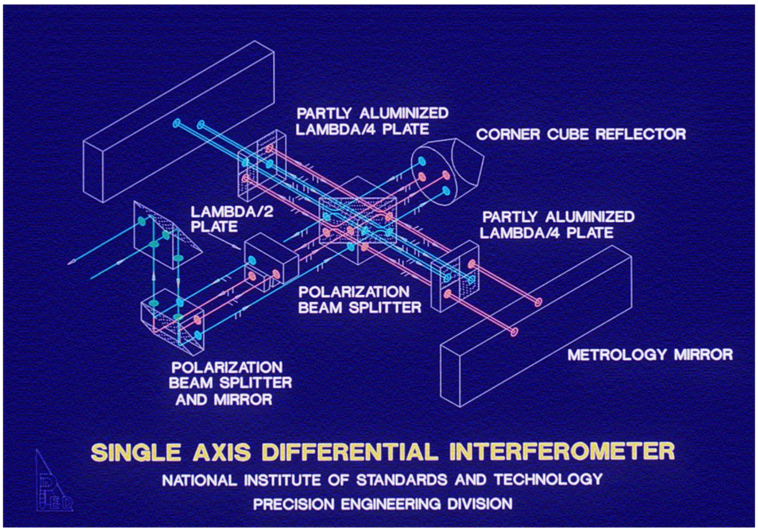

Figure 2.8 Interferometer of the Molecular Measuring Machine[14]

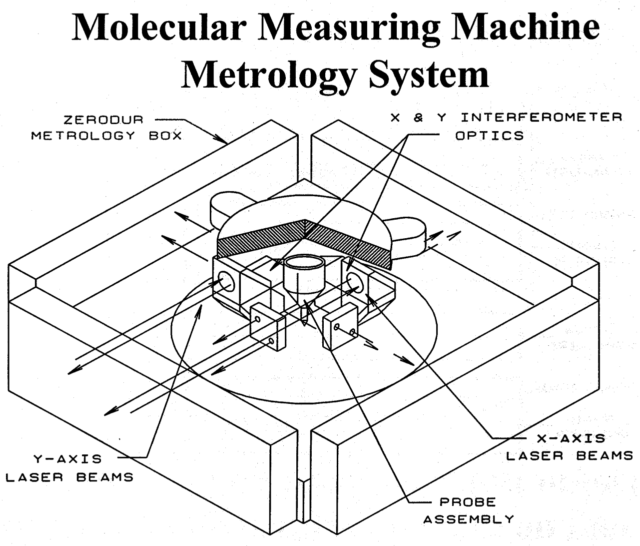

Figure 2.9 Metrology Frame of the Molecular Measuring Machine [14]

The machine core chosen for the machinability, dimensional stability, vacuum compatibility, and thermal conductivity is an Oxygen-free high-conductivity copper sphere with 350 mm in diameter. The core is cut into two pieces, the upper and lower hemispheres. The upper guide way is made into a vee groove and the lower guide way is made into an inverted vee. The guide surfaces are manufactured by diamond turning machining. The carriages are kinematic seated on the guide way with 5 Teflon pads. A specimen is fixed on the Zerodur metrology box, which is kinematically located on the lower carriage. A STM probe with a homemade piezoelectric actuator and a capacitance sensor are located on the upper carriage. The motions in X and Y directions are feedback controlled by laser interferometers and Z motion is controlled by capacitance sensor.

The first measuring result of laser-focused-atom-deposition chromium grating is 212.78 nm with a preliminary expanded uncertainty of 0.02 nm (coverage factor k=2). The uncertainty evaluation is shown in Table 2.2. The estimated combined standard uncertainty u_c is 26 nm for 1 mm measurement.

Table 2.2 The uncertainty evaluation of M^3 (1 mm)

Error sources	Estimated value (nm)	Description
Wavelength of Laser	0.1	$L\times\delta\lambda/\lambda=1$ mm $\times10^{-7}=0.1$ nm
Polarization Mixing	1	$2\lambda_n= 2\times0.5$ nm $=1$ nm
Laser Cosine Error	20	$L\times\theta^2/2=1$ mm $\times(2/300)^2/2=20$ nm
Abbe Offset Error	9	$\sqrt{3}\times d\times\delta\beta=1.73\times10$ mm$\times5\times10^{-7}=9$ nm
Z-to-X coupling Error	13	$\Delta Z\times\delta\alpha_{xz}=650$ nm$\times0.02=13$ nm
Temperature stability	4	$D\times\delta T\times CTE=25$ mm$\times0.005\times3E-5=4$ nm
Sample Cosine Error	0.01	$L\times\theta^2/2=1$ mm $\times(10^{-4})^2/2=0.005$ nm
Line center determination	4	$\sqrt{2}\times\delta x=1.4\times3$ nm$=4$ nm
u_c	26	

2.3 Calibrated Atomic Force Microscope at the NIST

The metric ruler of AFMs, used in semiconductor industry as tools for sub-micrometer dimensional measurement, must be calibrated to perform accurate measurements. Researchers at the NIST have developed a Calibrated AFM (C-AFM) to calibrate standards [21-32]. Figure 2.10 shows the main structure of C-AFM including X and Y- interferometers, a XY flexure stage, a Z-axis flexure stage, a metrology frame, an AFM, and a specimen platform. And a schematic control block diagram is given in Figure 2.11. The X and Y- heterodyne laser interferometers are traced to the SI units via a 633 nm wavelength of the Iodine stabilized He-Ne laser. The motion of Z direction of the sample is achieved by a Queensgate piezoelectric actuator with an integrated capacitance sensor. An X-Y piezo-flexure-stage with a 50 μm range is used to move the sample motion in X and Y directions. The probe tip is located at the intersection of the extension lines of laser beams of X and Y interferometers and can minimize measuring error caused by the Abbe offset. The close loop servo control of AFM tip, laser interferometers and flexures are constructed by Park Scientific Instruments (PSI). A program in LabVIEW is operated in another computer to capture the three dimensional displacements simultaneously. All components are made of low coefficient of thermal expansion materials and located on a metrology frame made of super-Invar.

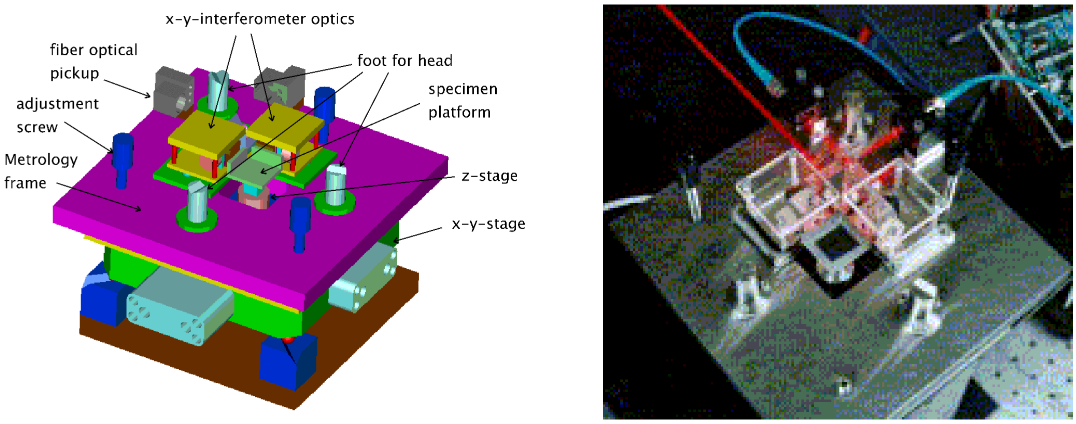

Figure 2.10 Calibrated AFM

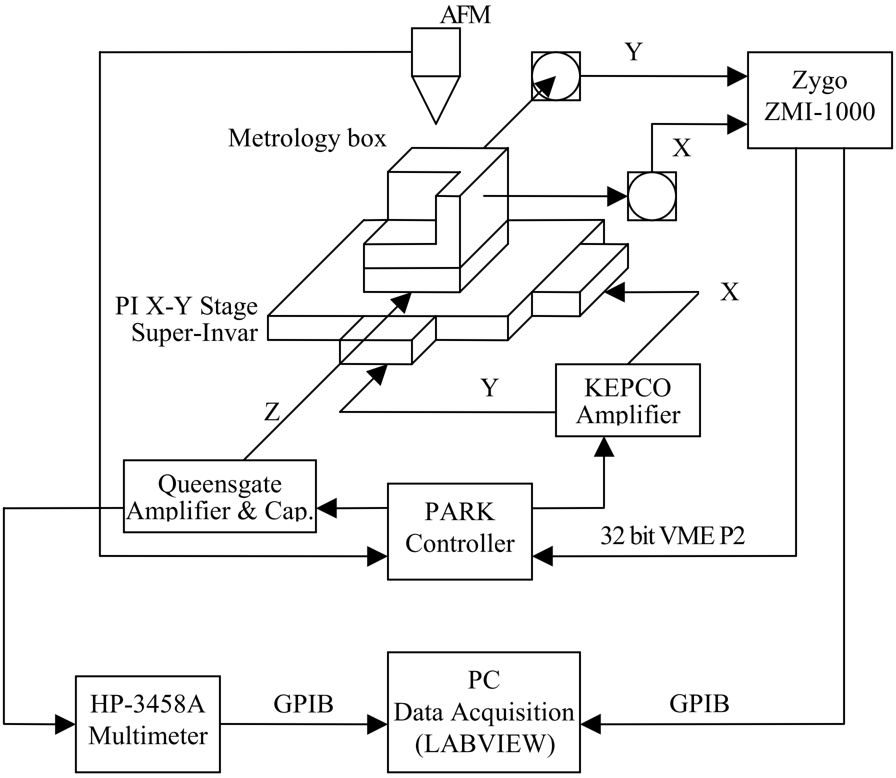

Figure 2.11 Control Block Diagram of C-AFM

The relative expanded uncertainty (k=2) of the first pitch measurement is as low as 1 % on sub-micrometer pitches. The uncertainty budget is shown in Table 2.3 including the effect of sample non-uniformity, reproducibility, edge detection algorithm, resolution of laser interferometer, polarization mixing, error from the deformation of tip, Abbe error, Cosine error, and etc.. D is the measured interval. The Abbe error is proportional to Abbe offset of 2.0 mm and 0.5 arc second tilt over the total range of travel.

Table 2.3 C-AFM uncertainty evaluation for Pitch measurement

Error sources	Estimated value (nm)	Type
Repeatability & sample uniformity	1 SD(standard deviation)	A
Reproducibility	1.6	A
Edge detection algorithm	1.5	B
Resolution of interferometer	0.36	B
Polarization Mixing of interferometer	0.6	B
Laser wavelength in vacuum	0.3×10^{-6}D	B
Index of refraction of air	20.6×10^{-6}D	B
Deformation/Damage of tip	1	B
Abbe error from rotation around Z	0.1×10^{-3}D	B
Cosine Error	1.5×10^{-4}D	B
u_c	$[(1\ \mathrm{SD})^2+(2.5\ \mathrm{nm})^2+(2.1\times10^{-4}\mathrm{D})^2]^{1/2}$	

Table 2.4 shows the uncertainty budget of step height measurements by C-AFM. An example of the measurement of single atomic step of Silicon (111) is shown in Figure 2.12. The single atomic step of Silicon (with native oxide) is 0.314 nm with an expanded uncertainty (k=2) of 0.008 nm.

Table 2.4 C-AFM uncertainty evaluation for Step height measurement

Error sources	Estimated value (nm)	Type
Repeatability & surface texture	1 SD(standard deviation)	A
Uncertainty of z-axis calibration	0.070 %H(Step height)	A
Cosine Error	0.015 %H	B
Abbe errors from offsets in X and Y	0.01 %H	B
Out of plane stage motion	1.5×10^{-2} nm	B
u_c	$[(1\ \mathrm{SD})^2+(1.5\times10^{-2}\ \mathrm{nm})^2+(0.070\ \%\mathrm{H})^2]^{1/2}$	

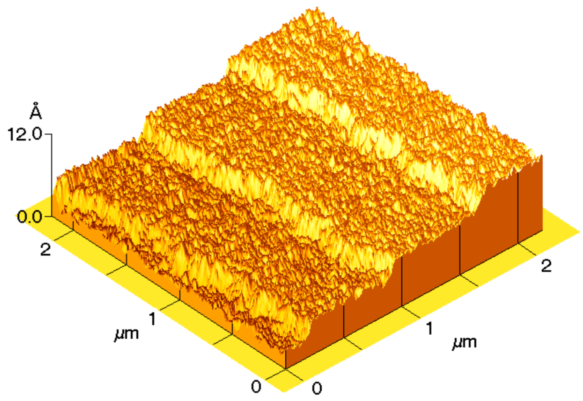

Figure 2.12 Silicon (111) single atomic step specimen with native oxide

2.4 Metrology Atomic Force Microscope at the PTB

Researchers at the Technische Universität Ilmenau, Institute of Process Measurement and Sensor Technology (PMS), in cooperation with the Physikalisch-Technische-Bundesanstalt (PTB), have modified a commercial scanning sample AFM (VERITEKT 3 with a scan range (X,Y,Z) of $70 \times 15 \times 15\ \mu m^3$) by using three miniature laser interferometers and a square mirror [33-39]. It is used for the traceable calibration of SPM standards, step height standards, and tools for measurement tasks in nano-metrology. The original operation principle is sample-scanned by a three-dimensional flexure-hinge stage with piezoelectric actuators and capacitance sensors for close-loop control. The resolutions of each direction are 1.2 nm, 0.25 nm, and 0.25 nm. This AFM has been modified with three miniature laser interferometers developed by PMS and made by SIOS Meßtechnik GmbH in Germany. The calibration of capacitance sensors is accomplished by checking each $\lambda/2$ interval in the whole measuring volume of flexure stage. The schematic diagram of the modified Metrology AFM (MAFM) is shown in Figure 2.13. A probe meets the extension lines of laser beams of interferometers in order to eliminate the Abbe offset.

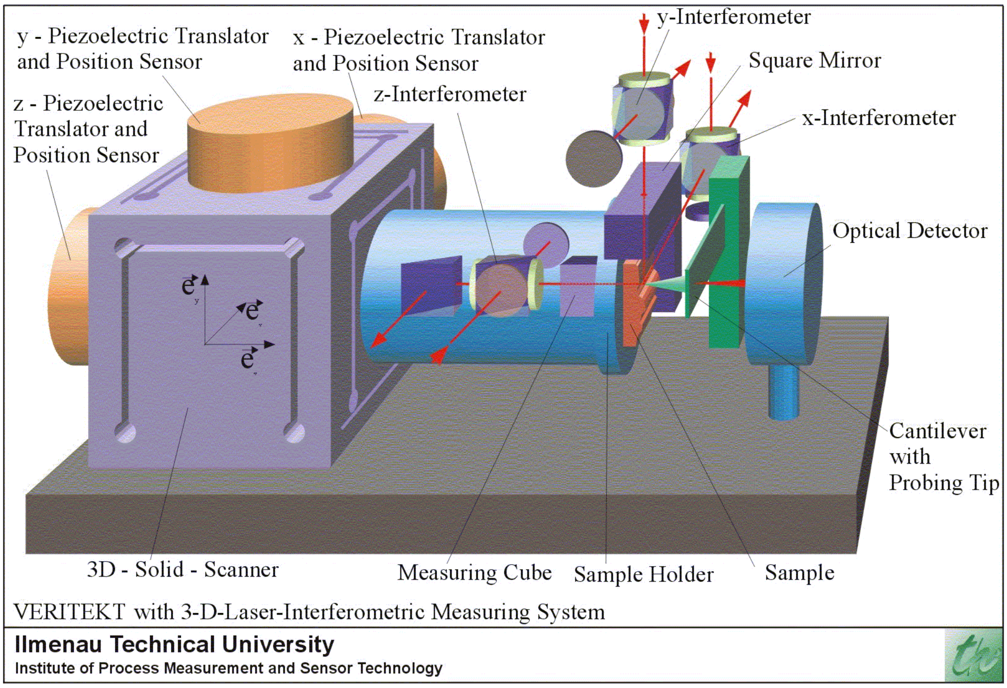

Figure 2.13 Veritekt AFM with 3-D-Laser-interferometric Measuring System

Figure 2.14 shows the mechanical structure of MAFM. The interferometers are served to calibrate the capacitance sensors and reduce the cross coupling errors for all three axes. The uncertainty ($u_{95\%}$) of the laser interferometer at each $\lambda/2$ interval is 1 nm. So, the residual deviations of linearity after compensation are less than 1 nm. The expanded uncertainty of the measurement of any two points within the measuring volume is ($5\ nm + 2 \times 10^{-4}$ D). Where D is the distance in nm. The uncertainty of step height measurement is ($1.1\ nm + 2 \times 10^{-4}$H). Where

H is the height in nm.

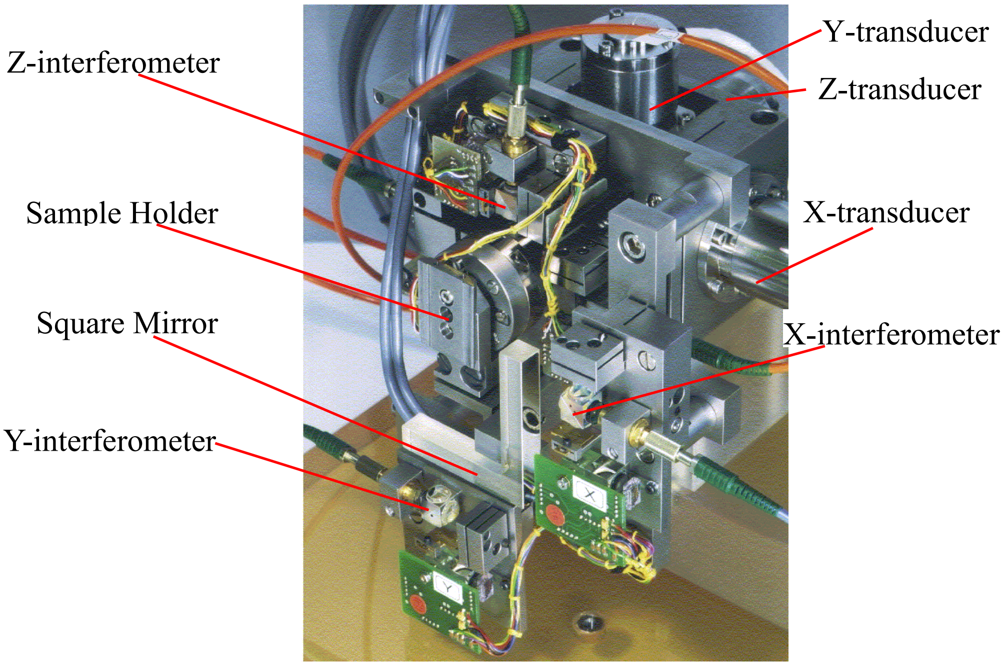

Figure 2.14 Metrology AFM at the PTB

2.5 Nano-Measuring Machine at the Technische Universität Ilmenau

A new nano-measuring machine (NMM) is built at the Institute of Process Measurement and Sensor Technology (PMS) in the Technische Universität Ilmenau in Germany [40-42]. Figure 2.15 shows the positioning stage and electronic system. It is constructed in a measuring range of $25 \times 25 \times 5$ mm^3 with a measuring resolution of 1.2 nm supported by the Thuringian Ministry of Science, Research and Culture.

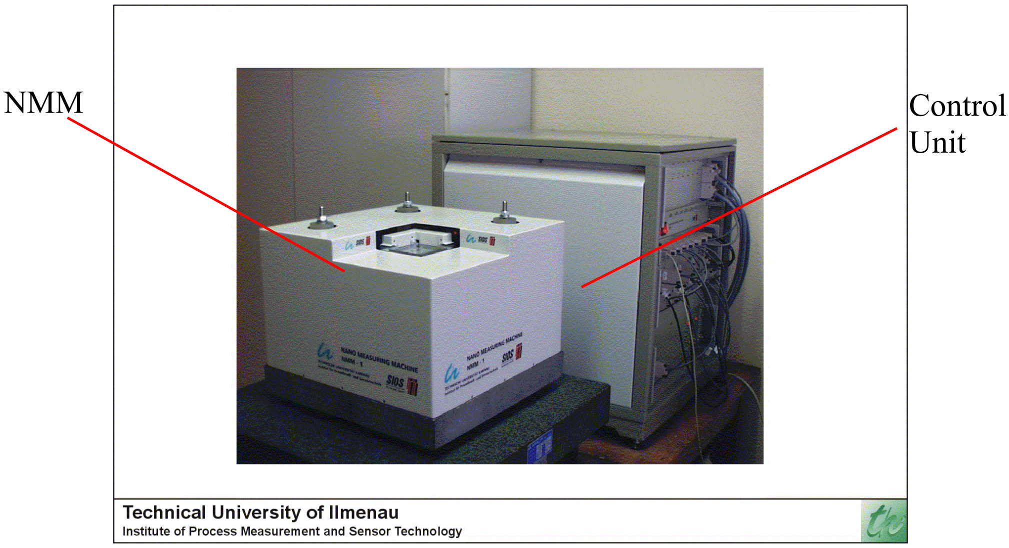

Figure 2.15 Nano-Measuring Machine

To achieve the desired measuring range, high motion speed and positioning resolution, the voice coil actuator and ball bearing guide way are selected for the X and Y linear stages (see Figure 2.16). And four voice coil actuators, independently controlled, are utilized for Z-axis motion and roll and pitch angle errors compensation. This drive system can achieve a motion speed up to 50 mm per second with a positioning resolution of 5 nm within the measuring volume. The displacements of all three axes are recorded and feedback-controlled by plane mirror laser interferometers with a measuring resolution of 1.2 nm made by SIOS Meßtechnik GmbH company. Two autocollimators with a resolution of 0.05 arc second are used to detect the angular deviation of pitch, yaw and roll, and then send to voice coil drivers for the angular compensation.

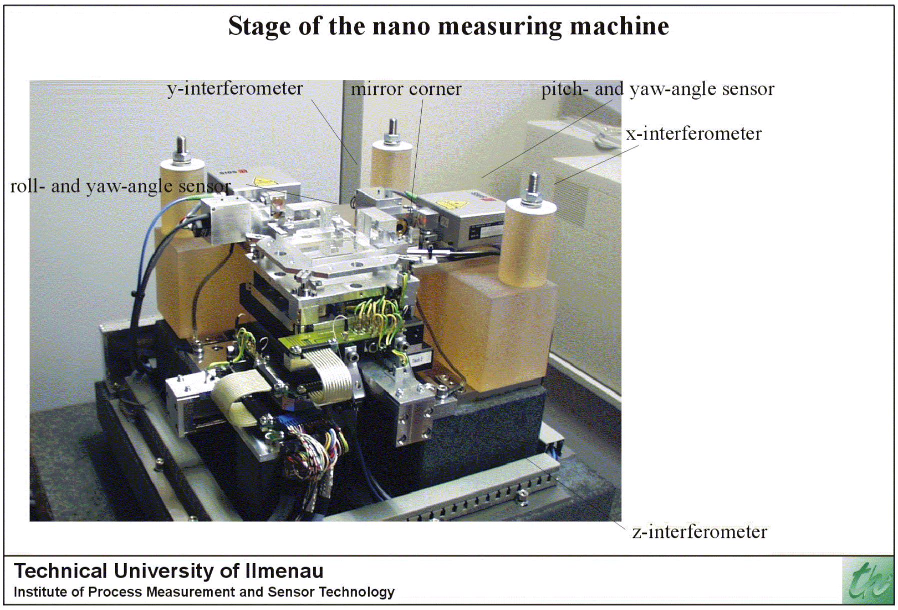

Figure 2.16 Stage of the nano-measuring machine

In order to obtain the best measuring and positioning accuracy, the NMM is arranged in a zero Abbe offset with three plane mirror interferometers, a probe, and two angular sensors. Figure 2.17 shows the realization of the Abbe principle. All the measuring axes of interferometers are aligned to the contact point of the probe tip and the surface of test sample. This construction design can achieve an accurate positioning without any Abbe errors. The sample is located on a mirror corner with flatness of 30 nm peak to valley at all three axes. The mirror corner is feedback-controlled by a three axes drive system via three plane mirror laser interferometers. To avoid the influence from thermal change, the laser interferometers and autocollimators are seated on a main metrology frame made of Zerodur (the coefficient of thermal expansion is near zero in room temperature condition). The preliminary application is equipped with an inductive stylus as a sensing probe. Further modifications will include the assembling of an AFM head and an auto-focus sensor for the applications in material science and nanotechnology.

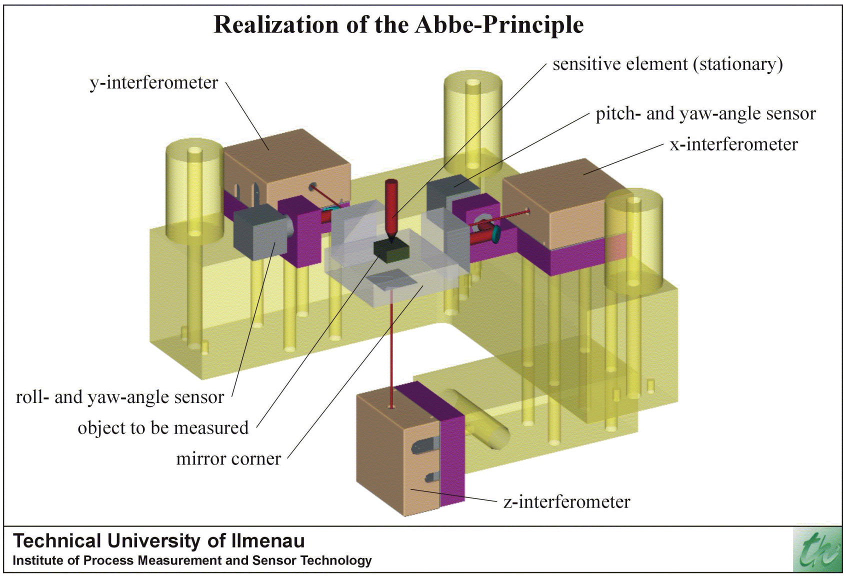

Figure 2.17 Realization of Abbe principle

2.6 Long-range AFM profiler at the METAS

A long-range AFM profiler is built based on a commercial dimension AFM and a homemade linear sample displacement stage at the Metrology and Accreditation in Switzerland (METAS) [43-46]. The mechanical structure is shown in Figure 2.18. It consists of a DI dimension metrology AFM, a linear flexure stage with a motion range of 380 μm, and a double pass differential plane mirror interferometer developed by National Physical Laboratory (NPL). The sample is located at nominally zero Abbe offsets measured by a subnanometer resolution interferometer and the AFM is always operated in the tapping mode.

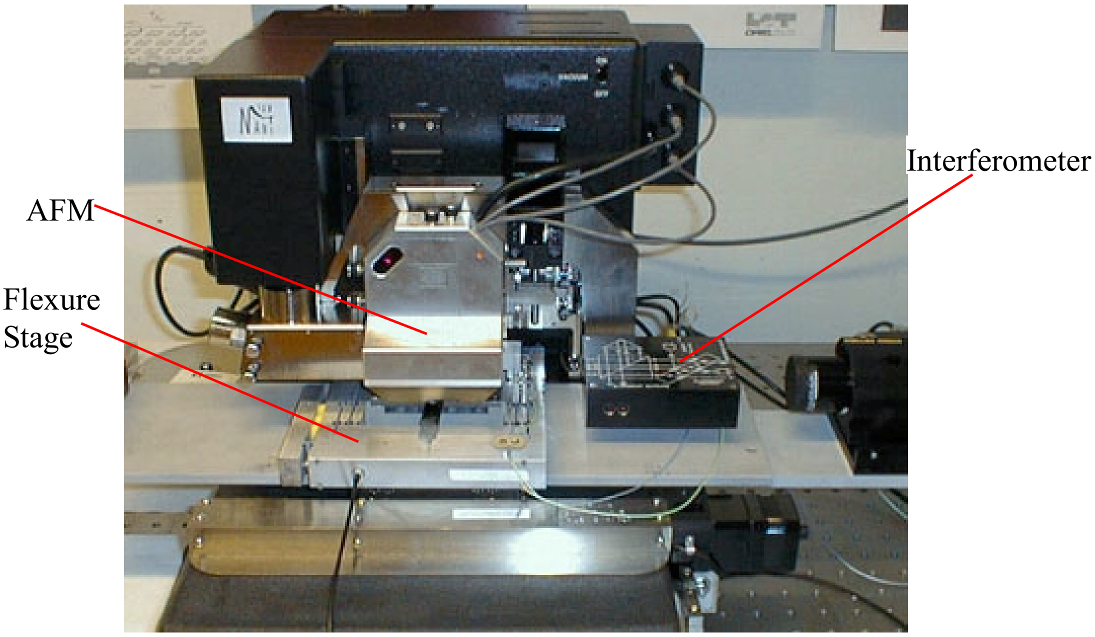

Figure 2.18 Long-range AFM profiler

The measuring principle and instrument structure of long-range AFM profiler are shown in Figure 2.19. The metrology AFM head (a) made by Digital Instruments comprises a parallelogram-type flexure stage in X and Y axes, an individual piezoelectric actuator in Z axis, and three capacitance sensors for all axes. A reference cube is located close to the probe tip as the counter electrode for the capacitance sensors. The scanning range is 70×70×6 μm^3. A homemade linear stage (b) is placed under the AFM head. It includes a single linear stage made of a monolithic double parallelogram flexure-hinge, a piezoelectric actuator and a capacitance sensor. The stage is actuated to a displacement range of 380 μm by a 1000 V piezoelectric actuator (Its nominal stroke is 70 μm) with a lever amplified by a factor of six. It can be performed a highly straight motion with a pitch error of 0.6 arc second and a yaw error of 0.7 arc second.

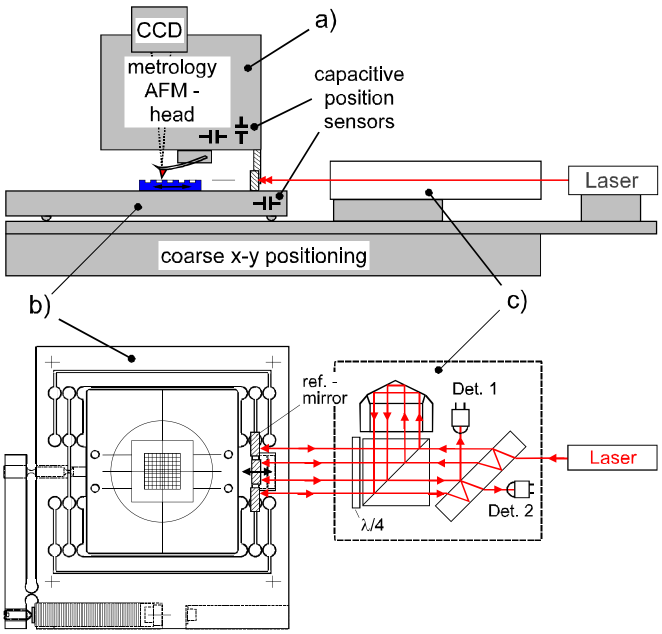

Figure 2.19 Measuring principle of long range AFM profiler

The displacement of the linear stage is feedback-controlled by a capacitance position sensor, and simultaneously measured by the capacitance sensor and a double pass differential plane mirror interferometer [46]. Its first application is used on pitch measurement of periodic structures. The estimated relative combined standard uncertainties for pitch measurements on different range are from 2×10^{-5} to 8×10^{-5}. Table 2.5 shows the combined standard uncertainties (u_c) and effective degrees of freedom (ν_{eff}) of pitch measurements. There are 11 influential quantities including Laser wavelength, refractive index of the air, interferometer nonlinearity, interferometer alignment, sample alignment lateral and horizontal, yaw and pitch of the motion with Abbe offset, temperature deviation, AFM calibration, the repeatability of the measurement in one place and the spread in the different locations. The largest contribution to the total uncertainty is the local pitch variation.

Table 2.5 Uncertainty evaluation for pitch measurement by long-range AFM profiler

Sample	AFM Pitch (nm)	u_c($\times 10^{-5}$) (relative)	ν_{eff}	Diffraction Pitch (nm)	Difference($\times 10^{-4}$) (relative)
Holographic grating	700.989	4.6	88	701.001	0.16
5 μm waffle pattern, top	4999.83	2.1	71		
5 μm waffle pattern, middle	4999.77	1.8	67	5000.4	1.2
5 μm waffle pattern, bottom	4999.83	2.0	72		
3 μm waffle pattern	2999.99	1.9	34	3000.3	1.0
1.8 μm waffle pattern	1800.14	2.8	50	1800.2	0.28
Ruled optical grating	1666.63	7.7	54	1666.39	-1.4

3. Design and Construction of TAFM

Last chapter describes the comparative method of 1-D pitch calibration and some modified metrological AFMs in the world. These metrological AFMs are based on the metrology consideration and special requirements from their industry and science research. There are many high-tech semiconductor manufacturing, biotechnology, Micro Electro Mechanical Systems (MEMS), and nanotechnology in Taiwan. It is important to establish the nanometer-scale standards including linewidth, pitch, step height, and roughness. In the comparative method, a worse expanded uncertainty is associated. It could be better to have a primary standard traceable to the SI rather than to have a secondary standard traceable to other country. Therefore, a project of establishing a nanometrology standard system, supported by the Bureau of Standards, Metrology and Inspection (BSMI), Ministry of Economic Affairs (MOEA), Taiwan. The purpose of the system was set to provide the calibrations of the nano-scale standards from the semiconductor industry, nanotechnology and science research fields. The objectives for the design and construction of a metrological AFM are:

A. The instrument can realize a primary standard of nanometrology in Taiwan.

B. The measuring instrument can measure the micro surface texture on conductor, semiconductor, and nonconductor.

C. The measuring instrument should include a traceable sensor, which can be directly traceable to the SI.

D. The measuring instrument can achieve a resolution of nanometer or sub-nanometer, an expanded uncertainty of nanometer scale, and a measuring range of 100×100×5 μm^3.

E. The measuring instrument should obey the Abbe principle.

F. The test sample volume can be as large as 150×150×5 mm^3.

G. The first application is to provide the 1-D pitch calibration for the Taiwan industry; further applications are 2D grating pitch, step height, and roughness measurements.

According to these considerations, the design of the new traceable AFM can be similar to the above metrological instruments in last chapter. For instances, to build a Molecular Measuring Machine with a measuring range of 50×50×0.1 mm^3 and sub-nanometer resolution and accuracy was an attractive thing. But it needed a big financial support and should be operated in high vacuum chamber. Now it still has some problems in the transducer of z-axis. The C-AFM has a good performance in nanometrology. But the AFM controller was a special custom-modified controller cooperated between the NIST and Park Scientific Instruments

(PSI). It was impossible in this project. In addition, the C-AFM can only measure a small specimen. The MAFM was cooperated between the PTB and the PMS based on a commercial Veritekt 3 AFM made by Curl Zeiss in Germany. But the Veritekt 3 AFM was no more made after 1998. For the considerations of the project budget and the best possibility, the final thought was to follow the design rules of the long-range AFM profiler at the METAS in Switzerland: (1) redesign or find a two-dimensional high precision stage; (2) add a differential laser interferometer; and (3) put hardware integration technique.

After a long-term of technical discussions and a hard work of surveying of AFMs and high accurate flexure stage, a Traceable AFM (TAFM)[13,47-50] was finally established at the Center for Measurement Standards, Industrial Technology Research Institute (CMS/ITRI), Taiwan. The TAFM consists of a commercial Dimension Metrology AFM, two laser interferometers, a flexure stage, a super-Invar metrology frame, a vibration isolator and a temperature controlled water circulator. Figure 3.1 shows the mechanical construction of the TAFM. The AFM head was a DI Dimension Metrology AFM with capacitance sensors at all three axes. The laser interferometers all belong to the type of differential plane mirror laser interferometer made by SIOS Meßtechnik GmbH. The L-shape mirror was 150×18 mm^2 with 30 nm of flatness at each side. The flexure stage was an active-error-compensation flexure stage made by Physik Instruments in Germany. The out-of-plane motion was 0.5 nm, and the angular deviation was 0.5 arc sec. The AFM head and the laser interferometers were fixed on the super-Invar metrology frame. The L-shape mirror was fixed on the flexure stage and the reference mirrors were fixed on the AFM head. The laser interferometers can measure the displacements between the stage and AFM head. A specimen was arranged on the same plane of the X and Y laser interferometers, and the AFM tip was on the intersection point of the lines extended from the X and Y interferometers, in which the error caused by Abbe-offset can be neglected.

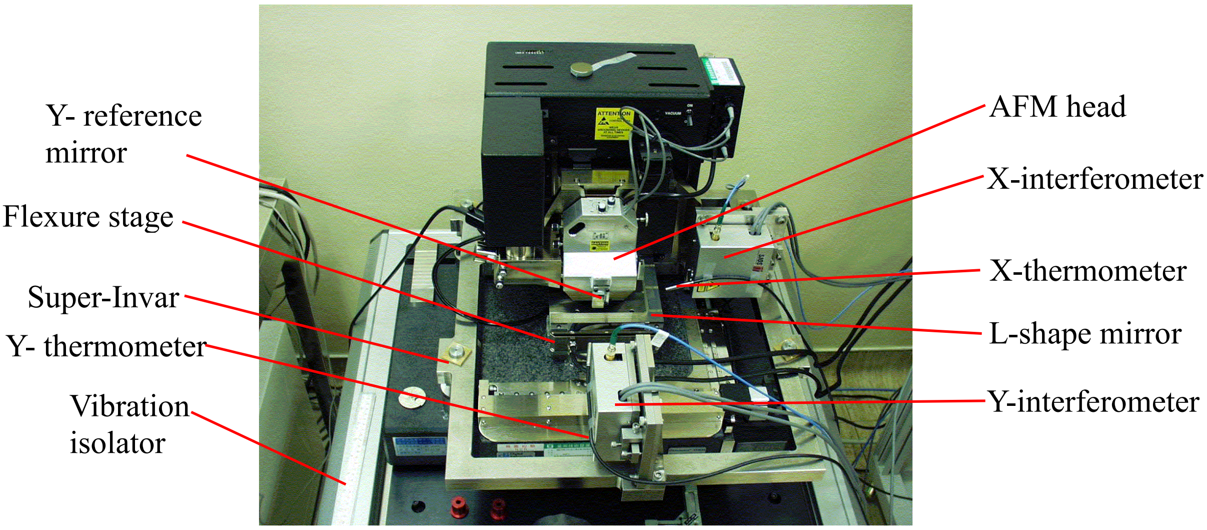

Figure 3.1 Construction of the TAFM

3.1 DI 3100M AFM

The best choice of a commercial AFM for the TAFM currently was the DI 3100M with a Dimension Metrology AFM head [51-53]. It has a coarse motion stage with a travel range of $100\times120\times12$ mm^3 and a positioning accuracy of 6 μm, and a fine scanner with a scanning range of $70\times70\times6$ μm^3. The disadvantage is that it is without the function of the scanning Tunneling microscope.

The Dimension Metrology AFM incorporates a new head and a new scanner design to improve crucial specifications. The improvements over the standard scanning probe microscope included the following:

A. High-resolution sensors and advanced digital closed-loop feedback algorithms that provided the X-Y closed-loop control at any scan size and offset in the scanning range.

B. It had the ability to zoom and offset to a specific region with nanometer accuracy.

C. The Z direction travel was a straight line and perpendicular to the X-Y plane.

The scanner includes a parallelogram flexure stage in the X and Y directions, an individual piezoelectric actuator in the Z direction, and a reference cube used for the electrodes for the all three axes of capacitance sensors. A scanner serves the feedback control of a square measuring area while the Z actuator is sensing the height of the test sample. The resolutions and repeatabilities in the X and Y directions are 1 nm, and the linearity is less than 0.05 %. The resolution in the Z direction is 0.8 nm, and the noise lever is less than 0.04 nm. The orthogonalities within each direction are less than 0.1 degree. The capacitance sensors of the scanner are calibrated by a commercial two-dimensional pitch standard traced to the NIST in United States (STS3-1800P). Figure 3.2 shows the picture of DI 3100M with Dimension Metrology AFM head.

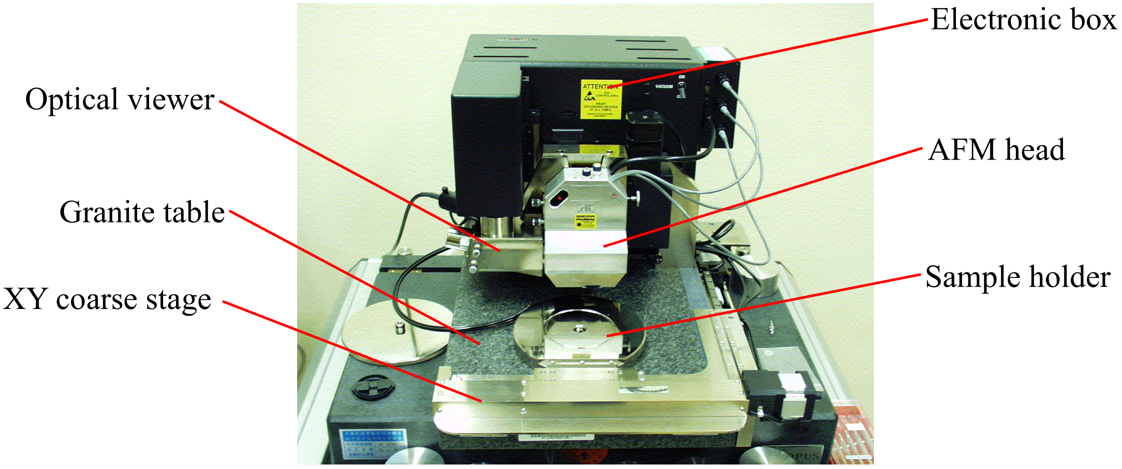

Figure 3.2 Dimension Metrology AFM

According to the application in this project, the AFM controller must be made some changes. The control signals of capacitance sensors and applied voltages of the scanner should be accessed by the user. For this reason modifications of the Controller of the Dimension Metrology AFM head have been done by the Digital Instrumentes company (DI). But the modifications should not influence the original performance of the instrument on the normal operation procedure. A picture of modified controller panel is shown in Figure 3.3.

A. Three signal output ports of capacitance sensors:
  (1). Voltage output port of X-axis capacitance sensor with BNC connector.
  (2). Voltage output port of Y-axis capacitance sensor with BNC connector.
  (3). Voltage output port of Z-axis capacitance sensor with BNC connector.
B. Three external driving voltage ports of the scanner:
  (1). External voltage input port of X-axis PZT driver amplifier with BNC connector.
  (2). External voltage input port of Y-axis PZT driver amplifier with BNC connector.
  (3). External voltage input port of Z-axis PZT driver amplifier with BNC connector.

Figure 3.3 The modified controller of DI AFM

3.2 Differential Plane Mirror Laser Interferometer

Adding a laser interferometer as a displacement sensor is one of the best ways to realize the direct traceability to the SI. It is an important issue of looking for a suitable laser interferometer that can be assembled in this instrument among the products including HP and ZYGO in the United States, NPL in the United Kingdom, and SIOS in Germany [45,54-57]. In this study, a differential plane mirror interferometer was designed to eliminate the influence caused by the dead path in the TAFM. After a surveying, the ZYGO, NPL, and SIOS companies all can supply the differential plane mirror interferometer. The SIOS's product was finally chosen based on the financial consideration and ease to operate and revise. A double pass differential plane mirror interferometer (SP500DD) modified from the standard product of the SP500 interferometer has been accomplished. The specification included a resolution of 0.078 nm, a nonlinearity of 2 nm, a measuring range of 250 mm, a maximum measuring speed of 100 mm/s, and a laser stability of 0.02 ppm. There are four laser beams, two for reference beams and two for measuring beams. It can measure the displacement and angular deviation simultaneously. The picture of SP500DD interferometer is shown in Figure 3.4.

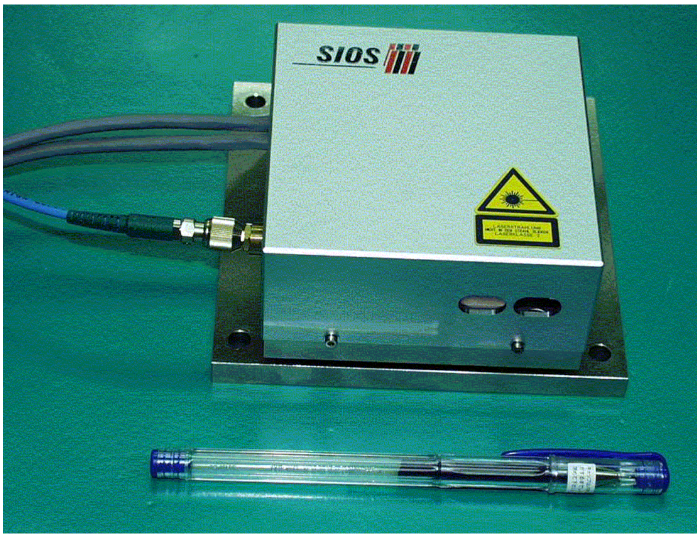

Figure 3.4 SIOS SP500DD interferometer

The optical component arrangement of SP500DD is shown in Figure 3.5. They are 1: collimator and expander for laser beam, 2: beamsplitter, 3: beam-divider with a pair of twin-aperture, 4: optical components of signal analyzer for one measuring axis, 5: scattered-light shield, 6: optical components of signal analyzer for another measuring axis, 7: prism, 9: prism equipped with a piezoelectric vibrator oscillating the measuring beams, 8: alignment flexure for prism (9).

A highly collimated laser beam coming from a collimator (1) is permanently connected to the sensor-head. The laser beam is delivered from a stabilized He-Ne laser through a polarization maintain optical fiber. This highly collimated laser beam is split into two equal-intensity and orthogonal beams by a beamsplitter (2). The deflected beam is further incident onto a two-hole beam-divider (3), in which a pair of parallel beams with a nominal diameter of 1.6 mm and separated by a distance of 5.4 mm is generated. These beams will hereinafter be referred to as the “reference beams”. The transmitted beam is reflected by a prism (9) fixed on an adjustment mount (8) and a piezoelectric vibrator and further incident onto a two-hole beam-divider to form two “measuring beams”. The two pairs of laser beams are reflected by the external reference mirror and moving mirror, then interfered at the beamsplitter, and sent to a pair of signal analyzers (4,6).

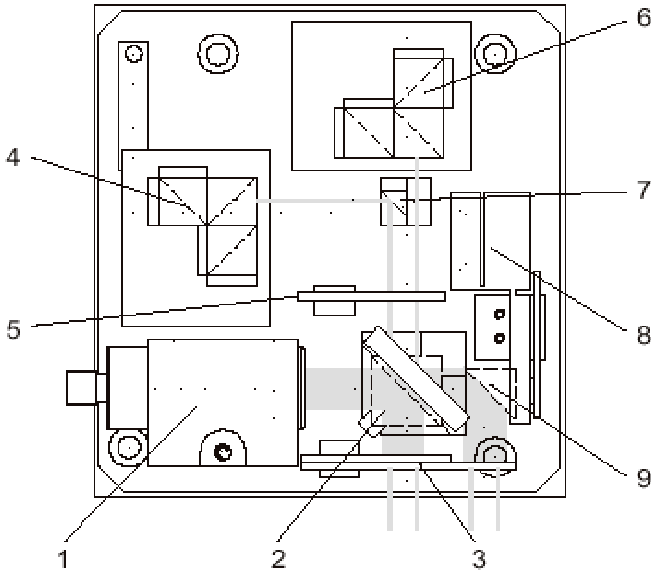

Figure 3.5 Optical arrangement of SIOS interferometer [57]

The displacement measured by SP500DD interferometer can be expressed as equation 3.1, where L is the displacement measured by SP500DD in nm, λ_0 is the vacuum laser wavelength in nm, n is the refraction index of air, and N is the counting number of the interferometer in integer.

$$L = \frac{\lambda_0}{8192n} N \quad \text{(nm)} \tag{3.1}$$

3.3 Active Compensation Flexure Stage

The accuracy of guide way is very important in the precision displacement measurement. There are 6 degrees of freedom of a rigid body in motion. So it contains 6 errors in a one-dimensional positioning stage (including a positioning error in motion axis, two straightness errors orthogonal to each other and to the motion axis, and three angular errors of pitch, yaw, and roll). The driving mechanism will also affect the measuring accuracy. A roller bearing slide-way with a lead-screw and stepping motor (or AC motor) is the traditional motion system with micrometer's accuracy. It can be applied in many fields such as lathe, milling machine, grinding machine, and coordinate measuring machine. For the equipments with subnanometer resolution and even accuracy demand, Some special structures incorporated with appropriate actuators are need. The flexure stage with piezoelectric actuator becomes one of the best solutions in nanotechnology. The parallel spring mechanism was popular in a high-resolution instrument [58-59] in the 1950s, while the flexure stages with piezoelectric actuators are currently widely used in precision Engineering [60-69]. The advantages of flexure stage are with zero-friction, zero backlash, high resolution and small angular error. The only disadvantage is the short travel range. The following sections will introduce the application of flexure stage in the TAFM.

3.3.1 Design rules of Flexure Stage

There are two types of flexure stages called “the Flexure notch” and “the Flexure leaf”. Figure 3.6 shows the mechanism of the flexure stages. The flexure stage is usually made of a monolithic material by wire cutting machine to form a moving part with a pair of notch spring or leaf spring. The flexure notch has a smaller angular deviation and ease to manufacture. It has been widely used in some National Measurement Institutes [3,60-62]. The pitch and yaw deviations can be less than 1 arc sec over 380 μm travel range. The flexure leaf has a big resonance frequency and a compact size. Most of the commercial flexure stages are made of flexure leaf type [63-70].

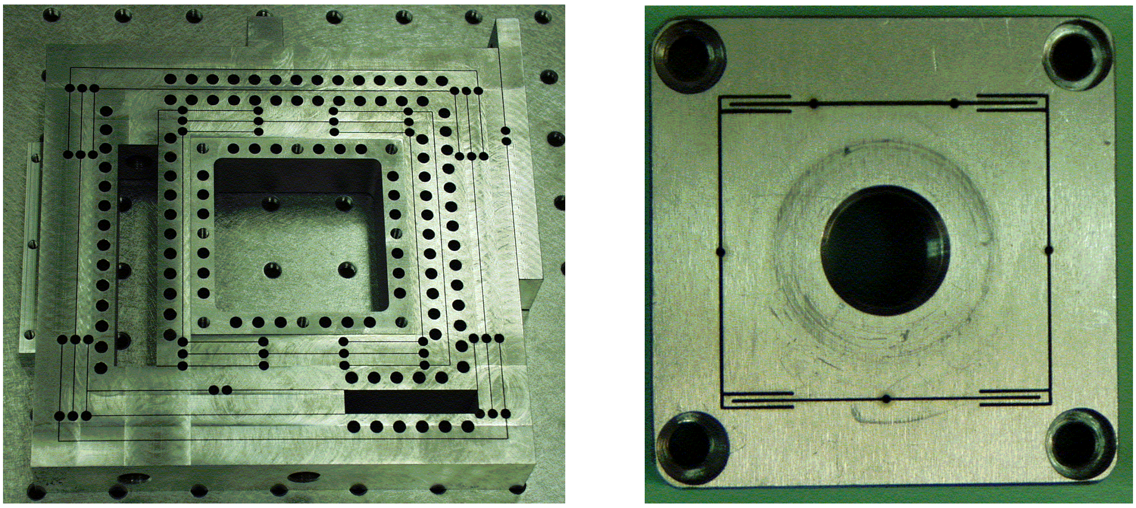
(a). Flexure notch (b). Flexure leaf

Figure 3.6 Flexure stage (Notch and Leaf)

It is helpful for the engineers to have design guides in the choice of the best material and mechanical structure. A theoretical principle and stiffness analysis of double compound flexure stages were studied by Dr. Yeh [72]. Figure 3.7 shows the structure of a double compound flexure stage containing base, moving stage, dummy stages, and springs. The moving stage is driven by a PZT actuator and gets a perfect moving line without straightness error and angular errors that are limited by dummy stages and springs on both sides. The mass of dummy stage, of moving stage, and of spring are m_1, m_2, and m_3 respectively. The displacement of the dummy stage relating to the base is q_1, the displacement of the moving stage relating to the dummy stage is q_2. The rotate inertial of spring is I, the length of spring is l, and the stiffness of spring is λ_f. Then the Lagrangian equation can be expressed as: [71]

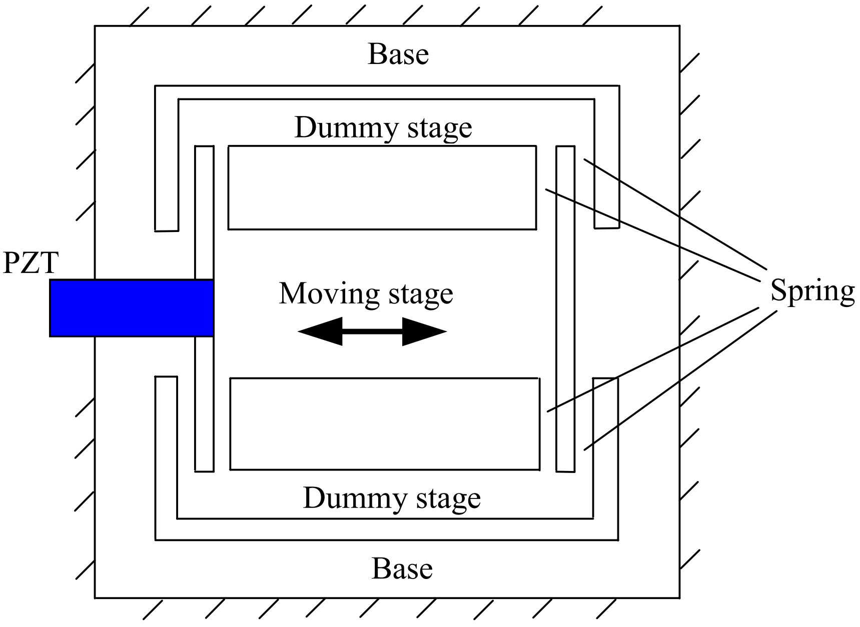

Figure 3.7 Double compound flexure stage

$$
\begin{aligned}
L_a = {} & 2\cdot\frac{1}{2}m_1\cdot\dot{q}_1{}^2+\frac{1}{2}m_2(\dot{q}_1+\dot{q}_2)^2+4\cdot\frac{1}{2}m_3\left(\frac{\dot{q}_1}{2}\right)^2+4\cdot\frac{1}{2}m_3(\dot{q}_1+\frac{\dot{q}_2}{2})^2 \\
& +4\cdot\left(\frac{I}{2}\right)\left(\frac{\dot{q}_2{}^2}{l^2}+\frac{\dot{q}_1{}^2}{l^2}\right)-4\cdot\frac{1}{2}\cdot\lambda_f\cdot\left(q_1{}^2+q_2{}^2\right)
\end{aligned} \tag{3.2}
$$

$$
=m_1\dot{q}_1{}^2+\frac{1}{2}m_2(\dot{q}_1+\dot{q}_2)^2+\frac{m_3\dot{q}_1{}^2}{2}+2m_3\left(\dot{q}_1+\frac{\dot{q}_2}{2}\right)^2+\frac{m_3}{6}(\dot{q}_1{}^2+\dot{q}_2{}^2)-2\lambda_f\left(q_1{}^2+q_2{}^2\right),
$$

where $I=\int x^2dm=\frac{m_3}{l}\int_{-\frac{l}{2}}^{\frac{l}{2}}x^2dx=\left[\frac{m_3}{l}\left(\frac{x^3}{3}\right)\right]_{-\frac{l}{2}}^{\frac{l}{2}}=\frac{m_3l^2}{12}$.

According to the Euler-Lagrange equation:

$$
\frac{d}{dt}(\frac{\partial L_a}{\partial\dot{q}_i})=\frac{\partial L_a}{\partial q_i},\ (i=1\ ,\ 2), \tag{3.3}
$$

two equations can be obtained from equation 3.2.

$$
2(m_1+\frac{m_2}{2}+\frac{8m_3}{3})\ddot{q}_1+(m_2+2m_3)\ddot{q}_2+4\lambda_f q_2=0 \tag{3.4}
$$

and $$2(\frac{m_2}{2}+\frac{2m_3}{3})\ddot{q}_2+(m_2+2m_3)\ddot{q}_1+4\lambda_f q_2=0. \tag{3.5}$$

Assuming $a=2(m_1+\frac{m_2}{2}+\frac{8m_3}{3})$, $b=m_2+2m_3$, $c=4\lambda_f$, $d=2(\frac{m_2}{2}+\frac{2m_3}{3})$, equations 3.4 and 3.5 can be cast as

$$a\ddot{q}_1+b\ddot{q}_2+cq_2=0, \tag{3.6}$$

and

$$d\ddot{q}_2+b\ddot{q}_1+cq_2=0. \tag{3.7}$$

If the springs are in steady free oscillation state and lets

$$q_1=A_1e^{i\omega t}, \qquad \text{and} \qquad q_2=A_2e^{i\omega t}. \tag{3.8}$$

The natural frequency (ω) of flexure stage can be derived as:

$$(b^2-ad)\omega^4+(ca+cd)\omega^2-c^2=0. \tag{3.9}$$

3.3.2 PI Active Flexure Stage

The above section provides a general rule to estimate the natural frequency of the double compound flexure stages. Some engineers like to use the finite element method (FEM) to analyze the characters of the flexure stages such as natural frequency, maximum loading, stiffness, and straightness. After contacting and discussing with the Physik Instrumente (PI) GmbH in Germany (one of the best designers and manufacturers of the flexure stage in the world), a custom-modified flexure stage (P-731K031) was designed and manufactured by the PI, and established in the CMS. This flexure stage [72] was a 3-axis motion stage with error compensation in all moving and rotating axes (see Figure 3.8). The specifications included 100×100×10 μm^3 travel range, 1 nm resolution in X and Y axes, 0.2 nm resolution in z axis, 0.5 nm out of XY plane motion, 0.5 arc sec angular deviation (Pitch, Yaw, and Roll), 150 Hz resonant frequency in X and Y axes and 300 Hz resonant frequency in Z axis at 1.5 kg load. All components were made of super-Invar (a low coefficient of thermal expansion of 0.6×10^{-6}/°C), and feedback-controlled by 6 capacitance sensors inside and an E-710K009 digital controller. Figure 3.9 shows the drawing of the PI flexure stage. An L-shape mirror with a flatness of 30 nm and a square angle error of 1 arc second was located on the top of the flexure stage as the moving mirror of the laser interferometers used.

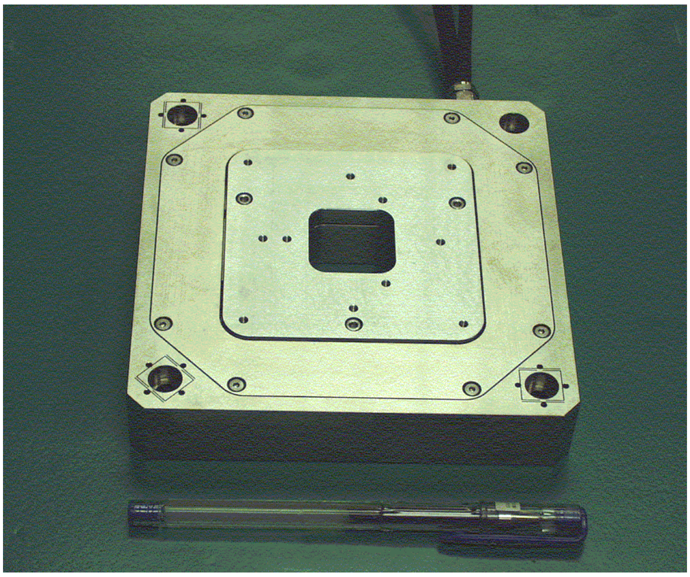

Figure 3.8 PI Flexure stage

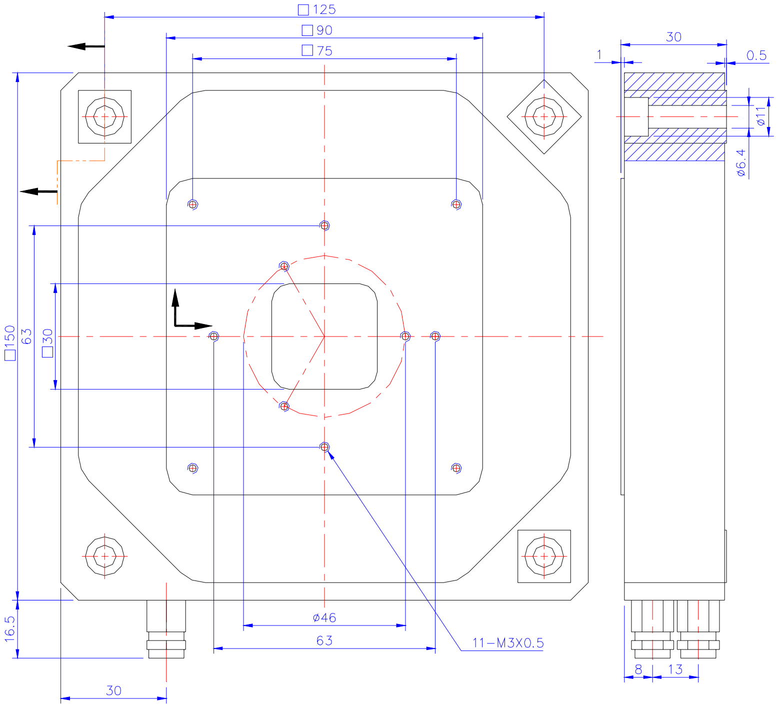

Figure 3.9 Drawing of PI Flexure stage (unit: mm)

3.4 Metrology Frame

In dimensional metrology, a metrology frame should be considered to connect the measuring probe and displacement sensor. It can maintain a constant distance between the probe and displacement sensor. A super-Invar (low coefficient of thermal expansion material) plate shown in Figure 3.10 was used as the metrology frame in the TAFM. The frame was supported on the same granite table of the flexure stage by four sphere-head bolts in quasi-kinematic mounting (one cone, one vee groove and two planes). The AFM head and electronic box were taken apart from the instrument base and fixed on the metrology frame by six screws. The two laser interferometers (X- and Y- axis) were fixed on the same frame with four vertical super-Invar boards and eight screws. Figure 3.11 shows the metrology system of TAFM. The moving mirror was fixed on the flexure stage, and the reference mirrors were fixed on the AFM head. The AFM probe tip was located at the intersection point of the lines extended from the laser beams of the interferometers. This arrangement obeys the Abbe principle [73] and can eliminate the measuring error caused by Abbe offset.

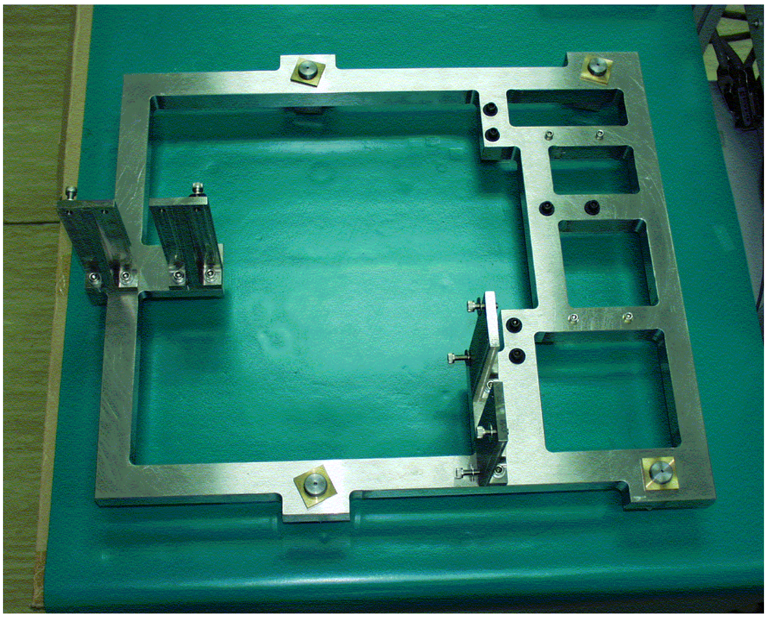

Figure 3.10 Super-Invar metrology frame

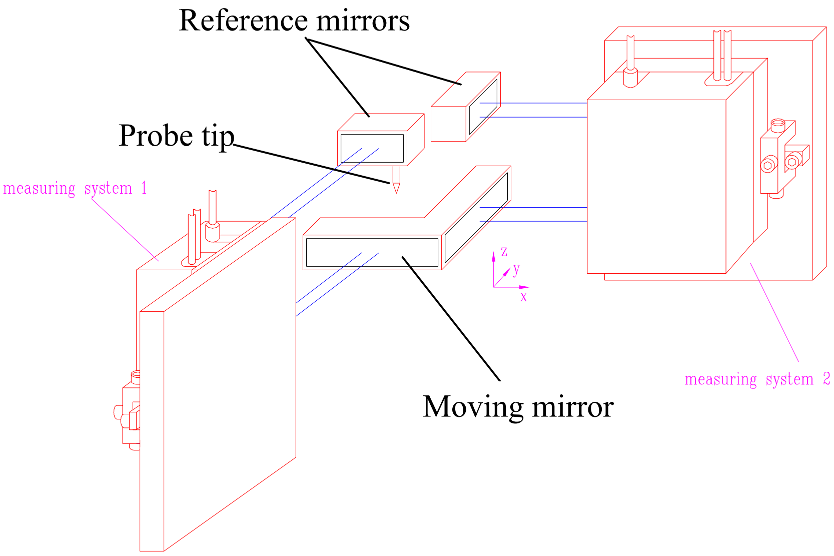

Figure 3.11 Arrangement of metrology system

3.5 Vibration Isolation and Temperature Control

Vibration noise is a big error source for the precision dimensional measurement. A passive pneumatic isolator is the first consideration for the vibration isolation. The passive pneumatic isolator can avoid the vibration noise from the environmental conditions like transportation in the road, people walking in the hall, and other machines in the other rooms. Most passive isolators are employed for the vibration higher than 2 Hz. In this study, a lower natural frequency vibration isolator (Nano-K platform, made by Minus K Technology) based on negative stiffness mechanism (NSM) was applied in the TAFM. The natural frequency can be better than 0.5 Hz in all axes.

A revolutionary concept in low frequency vibration isolation is utilized in the Nano-K vibration isolator [74]. Typically, three isolators are stacked in series: a tilt-motion isolator on the top of a horizontal-motion isolator on the top of a vertical-motion isolator. The negative stiffness mechanism is shown in Figure 3.12. It uses a conventional spring to connect an NSM consisting of two bars or flexures hinged at the center in vertical isolator, supported at their outer ends on pivots, and loaded in compression by force P_c (Figure 3.12(a)). The spring is compressed by weight W to the operating position of the isolator.

The vertical stiffness of the isolator is $K=K_S-K_N$, where K_S is the spring stiffness and K_N is the magnitude of a negative stiffness which is a function of the length of the bars and the force (P_c). The net vertical stiffness is made very low without affecting the static load supporting capability of the spring. Beam-columns connected in series with the vertical motion isolator provide horizontal motion isolating. The horizontal stiffness of the beam columns is reduced by the "beam-column" effect (A beam-column behaves as a spring combined with an NSM). The beam-columns have a horizontal stiffness K_S without the weight load. The lateral bending stiffness is reduced by the "beam-column" effect while loading a weight W (Figure 3.12(b)). This behavior is equivalent to a horizontal spring combined with an NSM so that the horizontal stiffness is $K=K_S-K_N$, and K_N is the magnitude of the beam-column effect. The stiffness of isolator can approach to zero when the spring supports the weight (W). The result is a compact passive isolator capable of very low vertical and horizontal natural frequencies and very high internal structural frequencies (Minus K, US Patents: 5390892, 5310157, 5178357).

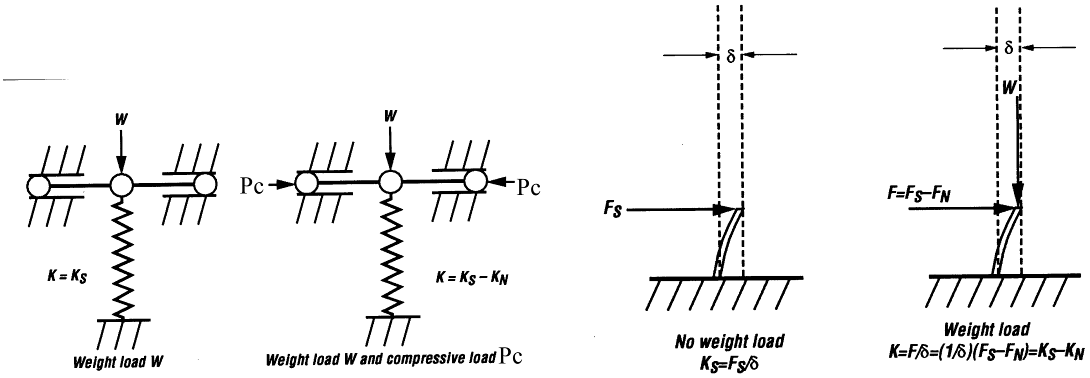

(a) Vertical (b) Horizontal

Figure 3.12 Negative stiffness mechanism

The noise of the laser interferometer caused by conditioning air was about 20 nm. It can be reduced to a few nm by use of a cover. After covering the whole measuring machine, the noise was quickly downed to about 1.5 nm in a few seconds, but the temperature was increased from 20.3°C to 23.7°C within 8 hours. The temperature increasing may be caused by the heat emission of the electronic components of the AFM. The temperature change corresponds to the displacement drift between the reference and the moving mirrors of about 5 μm in Y- axis in one hour. After assembling a temperature control system with circulating water, the temperature inside the cover can be controlled within 20±0.3 °C. The deviation of null displacement caused by the long-term thermal drift was therefore within a few nm. Figure 3.13 shows the cover box with temperature-controlled circulating water inside.

(a). Water ciculation by copper pipe (b). Enclosed box

Figure 3.13 Water circulator for temperature control

3.6 Measuring Method

Figure 3.14 is the schematic diagram of the TAFM [75]. The operation procedures for the

TAFM are as following: First, to assemble the test specimen on the flexure stage and then use the optical microscope of the AFM to find an appropriate testing area. Second, to use the DI AFM to tune the control parameters for a null displacement scanning (0×0 nm^2 scanning range in the XY plane, only at Z height sensing). Then to use a homemade program in LabVIEW in an industrial computer to servo control the two-dimensional scanning of the flexure stage with PI E-710K009 digital control box and GPIB interface, read the voltage of the Z axis capacitance sensor of the AFM, and read the displacements of the flexure stage relative to reference mirror from the differential plane mirror laser interferometers. The displacements of X- and Y-axis of flexure stage from laser interferometers via RS232 interfaces and the voltage of Z-axis of DI AFM via a National Instrument (NI) PCI-6034E AD card are obtained in the same time, while the AFM probe is scanned. Their results can be used to calibrate the grating pitch, step height, and line-width with additional software. Finally, to use a program in Matlab to do the equivalent space interpolation in the X and Y directions, and the SPIP software to calculate the pitch value and the pattern tilt angle.

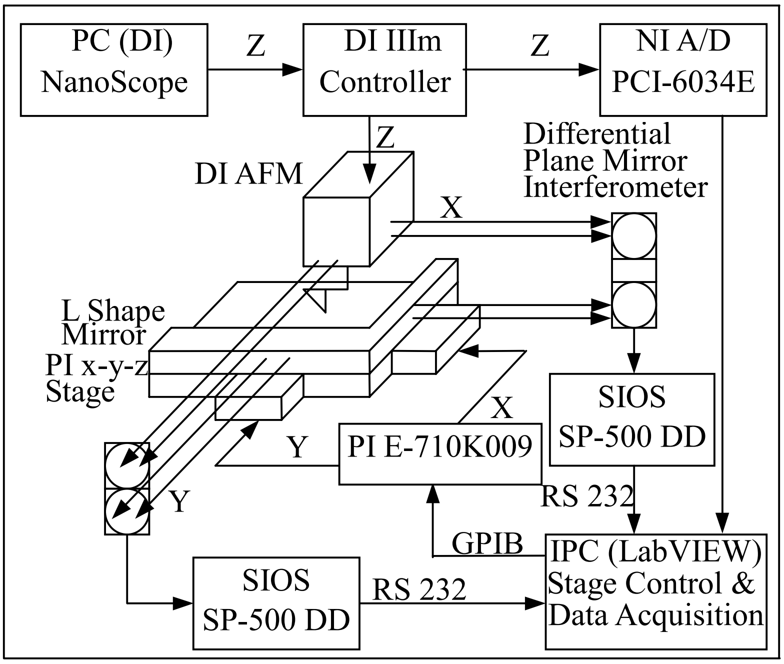

Figure 3.14 Schematic diagram of TAFM

3.7 Assembly Procedure of TAFM

The TAFM was a high accurate instrument traceable to the SI. It contains a commercial Dimension Metrology AFM, a 3-axis active compensation flexure stage, two differential plane mirror laser interferometers, an L-shape mirror, a Super-Invar metrology frame, a vibration isolator, and an enclosed box with temperature-controlled circulatory water. The assembly procedures and tests are described as below.

3.7.1 Install the AFM head

The DI 3100M AFM is originally fixed on instrument base (475 mm×318 mm×76.5 mm).

A. Remove the Dimension Metrology AFM head carefully.

B. Remove the electronic unit and the bridge for the AFM head from the instrument base. Make marks on each cable and connector.

C. Locate the instrument base of the AFM on a granite table (600 mm×400 mm×88 mm) supported by a vibration isolator. Then put the super-Invar metrology frame on the granite table with four sphere-head pivots by quasi-kinematic mounting. Use a high master and adjust the screws of four pivots to a same height of 114.5 mm on the top of super-Invar plate from the granite table.

D. Fix the electronic unit and bridge of the AFM on the super-Invar plate by six screws. Then install the Dimension Metrology AFM head.

E. Figure 3.15 shows the assembly of the AFM and metrology frame. The AFM function was tested by a VLSI standard with a unit cell of 3×3 μm^2 of 2-D grating.

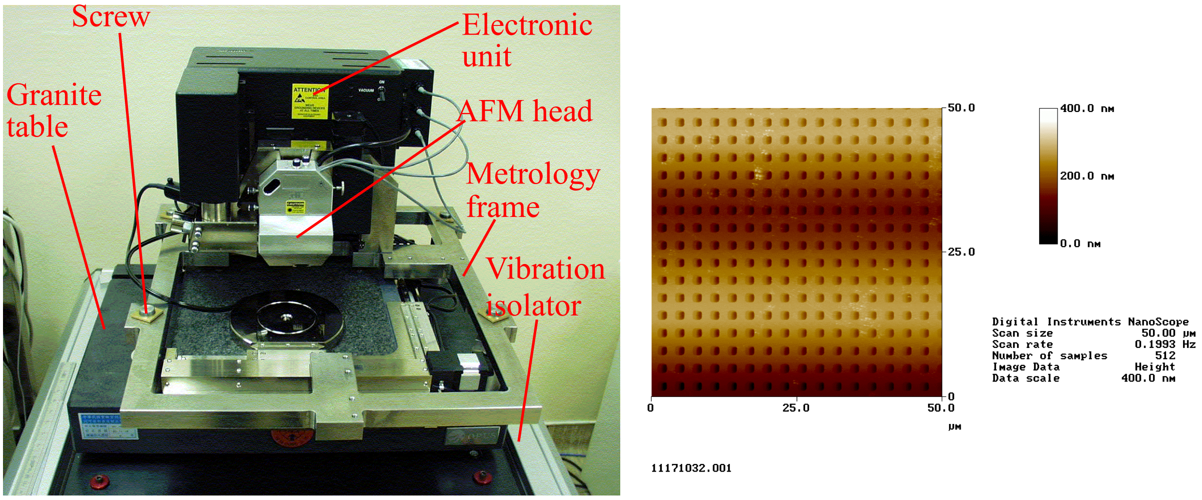

Figure 3.15 Install the AFM head

3.7.2 Install the interferometers

A. Fix four adapting super-Invar boards on metrology frame by eight M6 screws (see Figure 3.16).

B. Fix the sensor heads of differential plane mirror interferometer on the adapting boards by eight M6 screws.

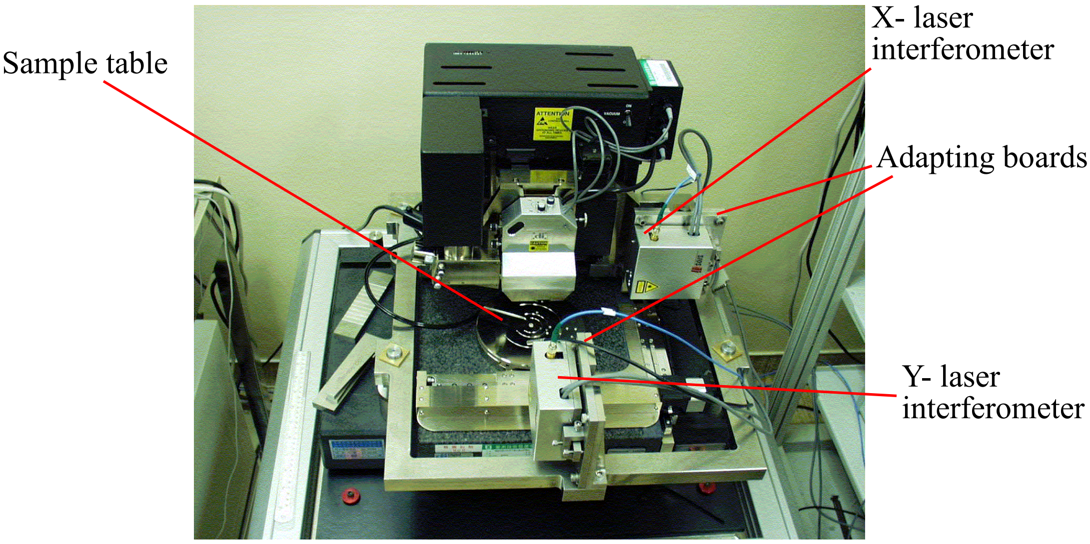

Figure 3.16 Install the interferometers

3.7.3 Install the flexure stage

A. Remove the Y-laser interferometer before the alignment and angular deviation testing of the flexure stage by an autocollimator.

B. The original design of measuring range of the TAFM included a coarse motion of 120 mm × 100 mm × 12 mm and a scanning range of 100 μm × 100 μm × 6 μm. The picture of Figure 3.17(a) shows an angular deviation testing of the X-Y coarse motion with a true square standard (90 ° ± 0.2 ”) and an autocollimator. The yaw error was bigger than 1 arc minute over 50 mm travel. And after adding the flexure stage on the air bearing table (sample table of the DI AFM), the coarse motion system did not work that might be caused by the additional weight of the flexure stage. Therefore, disable the power of the X-Y coarse motion, and disassemble the vacuum chuck and leadscrew drivers.

C. Sequentially install of the adapter board, flexure stage, and true square standard on the vacuum chuck of AFM shown in the right picture (b) of Figure 3.17.

D. Use a linear variable differential transducer (LVDT) to align the true square standard to parallel to the flexure stage while driving the flexure stage in the whole travel range.

E. Assemble an autocollimator and align it to the true square standard. Then install an L-shape mirror on the flexure stage and align it to the autocollimator.

F. Reinstall the Y-interferometer.

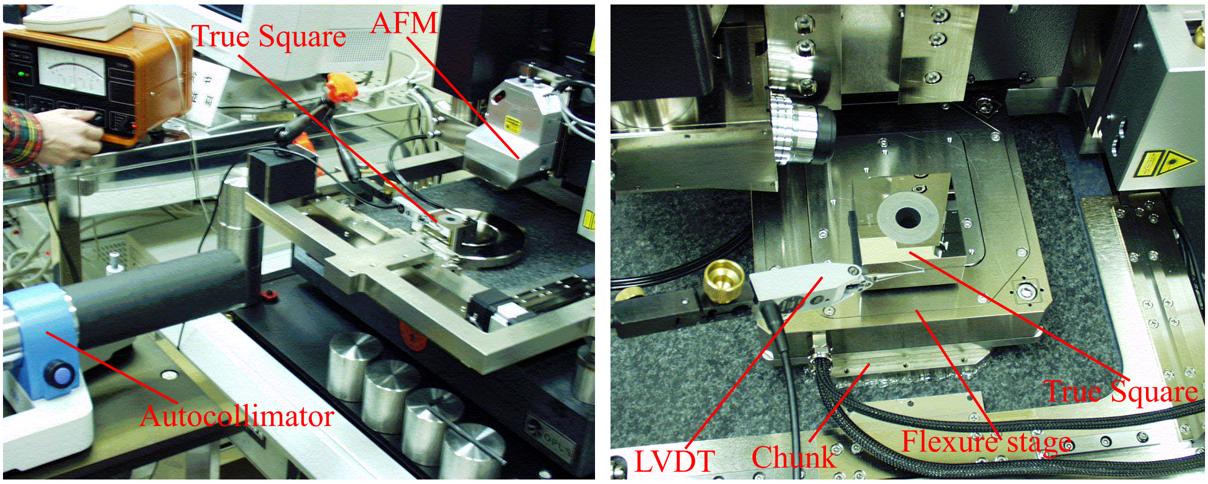

(a). Alignment with autocollimator (b). Install and test of flexure stage

Figure 3.17 Install the flexure stage

3.7.4 Assemble the reference mirrors

A. Careful adhere the reference mirrors on the Dimension Metrology AFM head with Torr Seal (a special adhesive for vacuum components). It needs one day for drying and fixing of the Torr Seal.

B. Fine turn the adjusting screws on the base-plate of sensor head of interferometer till the measuring beam and its reflection beam are vertical to the L-shape mirror.

C. Fine adjust the adjusting screws on the adopter plate of reference mirrors till the reflection reference beam coincides to the incident reference beam. At this moment, a circle signal of interferometer will appear on the screen of oscilloscope. Figure 3.18 shows the assembly of one reference mirror on the AFM head.

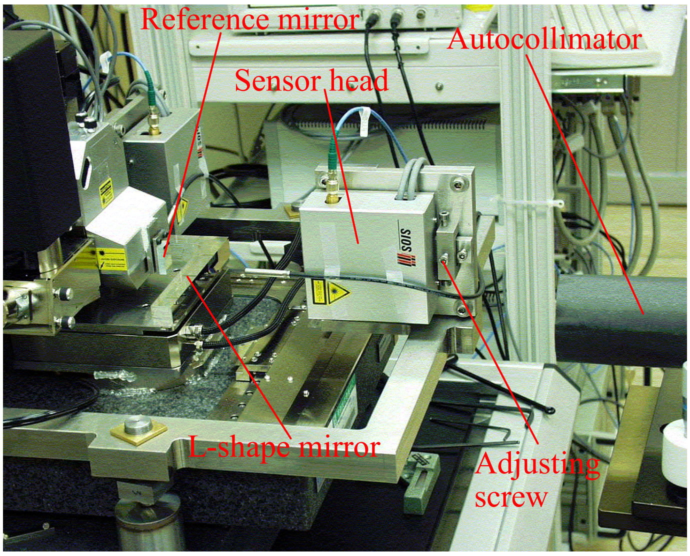

Figure 3.18 Assemble the Y-reference mirror

3.7.5 Align the Interferometers and Flexure stage

A. Connect each set of the analog signals of the interferometers to the oscilloscopes. Iterative adjust of the sensor heads and reference mirrors to get the best signals on the oscilloscopes.

B. Drive the flexure stage for the whole range travel (100 μm) in the X- axis and capture the displacements from the Y-laser interferometer at the same time. Fine knock the base-plate of the flexure stage with a small plastic hammer and test again till the displacements from the Y-laser interferometer approaching to zero. Figure 3.19 shows the final test result of the alignment between the laser interferometers and the flexure stage. The noise of 20 nm caused by the influence of conditioned air.

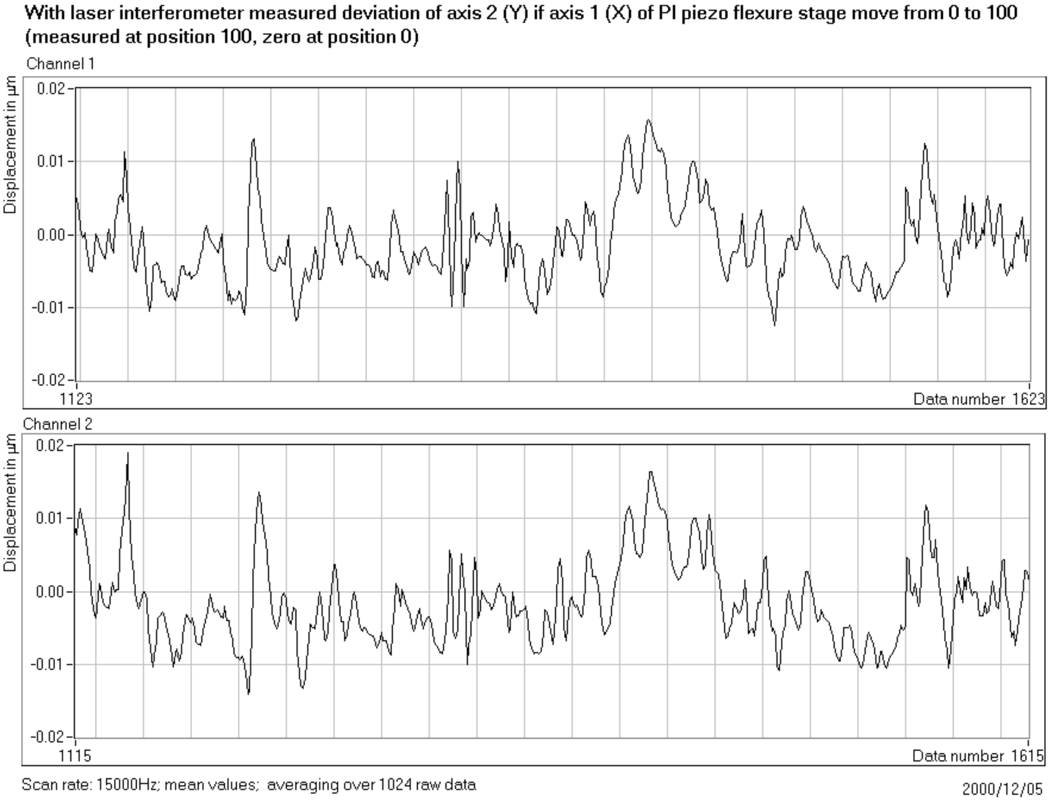

Figure 3.19 Alignment of the interferometers and flexure stage

4. Application in Pitch Measurement

The traceability of the AFMs has been described in section 2.1. The National Metrology Institutes and AFM manufacturers are developing the standards for the calibration of AFM for it's widely use in the semiconductor industry and the fields of nanotechnology. The AFM standards include one-dimensional pitch standards, two-dimensional pitch standards, linewidth standards, roughness standards, and step height standards. For the international comparison on nanometrology, the working group for nanometrology (Working Group 7 on Dimensional Metrology, WGDM-7) of the Consultative Committee for Length (CCL) decided that each entity has to perform the preliminary comparisons on the following five topics [76] at the discussion meeting in Bureau International des Poids et Mesures (BIPM) in June 1998.

Nano1	Line width standards
Nano2	Step height standards
Nano3	Line scales
Nano4	One-dimensional gratings
Nano5	Two-dimensional gratings

In particular, an international comparison with one-dimensional pitch of diffraction gratings was organized by the Metrology and Accreditation in Switzerland (METAS, the previous Swiss Federal Office of Metrology, OFMET) in 1998. The pitch of one-dimensional gratings was mostly measured by Metrological AFM or laser diffractometer. There were 11 participants and 6 National Metrology Institutes using AFM to measure the pitch value. At that time, the CMS did not have any Metrological AFM or laser diffractometer. Therefore, the pitch gratings were measured by comparative method with a commercial AFM. In this study, a TAFM has been established to measure the AFM standards such as one-dimensional pitch, two-dimensional pitch, and step height standards in Taiwan. The following sections will introduce the one-dimensional pitch standards developed by some National Metrology Institutes and AFM manufacturers. The measuring procedures of one-dimensional pitch standards by the TAFM will be also discussed.

4.1 Pitch Standards

A. RM 8090 at the NIST

The Reference Material (RM) 8090 is primarily intended to calibrate the magnification scale of scanning electron microscope (SEM) with nominal pitch ranging from 0.2 μm to 3000 μm [77] in Unite States. It is fabricated by electron beam lithography and metal lift-off on a silicon wafer substrate. The pattern comprises a layer of 10 nm titanium and 40 nm palladium on a 10×10 mm^2 silicon chip. It has the same thickness of silicon wafer; thus it can be inserted into the modern automatic measurement systems. The RM 8090 needs to be carefully mounted, by the user, on the proper SEM stub or wafer type for the user's particular instrument. Figure 4.1 shows the SEM image of the part pattern on RM 8090 with a pitch of 0.2 μm. It was calibrated at the Precision Engineering Division of NIST using a modified metrological Scanning Electron Microscope.

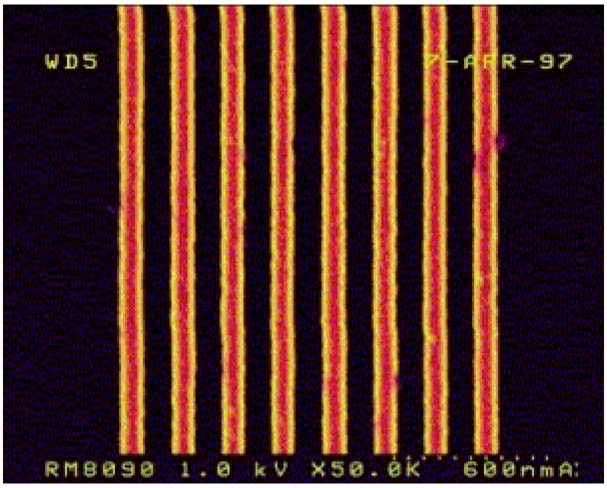

Figure 4.1 RM8090 at the NIST

B. SEM and SPM standards at the NPL

Figure 4.2 shows the picture of the SEM and SPM standards [78], which were developed by the National Physical Laboratory (NPL) in the United Kingdom. They are calibrated by a modified metrological SEM in the NPL and can be mounted on SEM stubs to verify the magnification factors of SPM and SEM. The standards include 2160, 100, and 19.7 lines per millimeter.

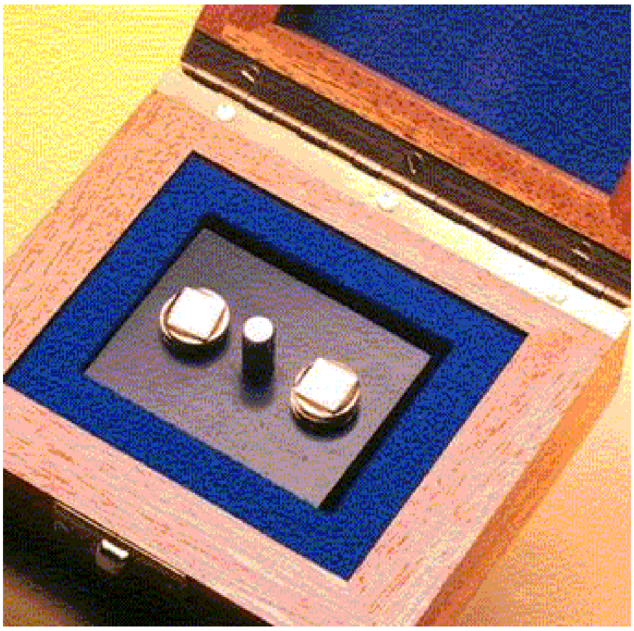

Figure 4.2 SEM and SPM standards at the NPL

C. One-dimensional gratings TDG01 made by NT-MDT

Figure 4.3 shows the AFM image of the one-dimensional diffraction gratings TDG01 [79] made by the Molecular Devices and Tools for NanoTechnology (NT-MDT) in Russia. The diffraction grating TDG01 is intended for sub-micron calibration of the scanning probe microscopes in the X and Y directions. It is formed on an aluminum layer on a glass substrate. The nominal pitch value is 278 nm with an uncertainty of 1 nm.

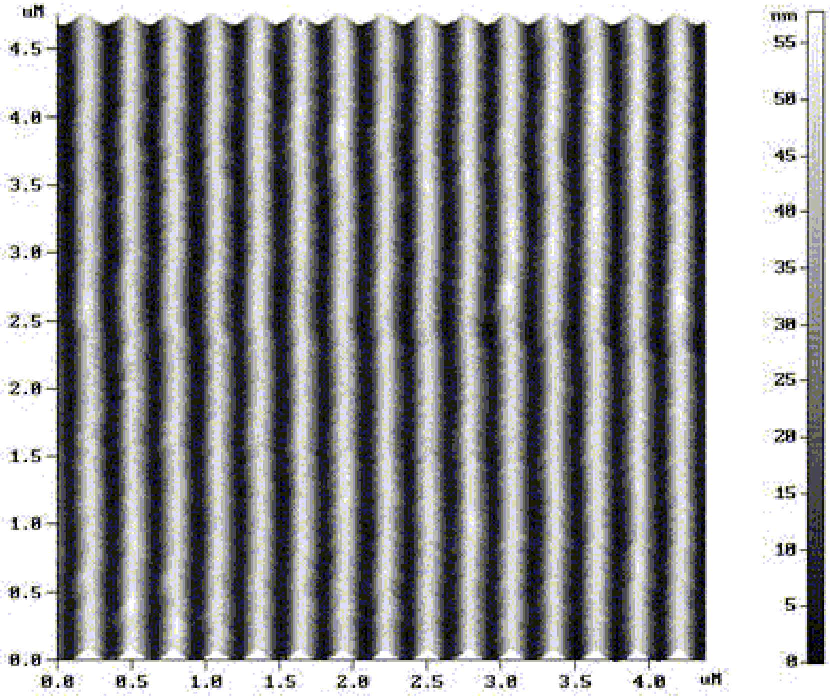

Figure 4.3 One-dimensional gratings TDG01 made by NT-MDT

D. MOXTEK SPM Calibration Standards

The MOXTEK manufactures three types of SPM Calibration Standards [80]. They are one-dimensional gratings (MXS 301CE and MXS 701CE, see Figure 4.4), two-dimensional gratings (MXS 302CE and MXS 702CE), and High Precision Calibration Standards (MXS 301BE). The one and two-dimensional gratings comprise a 60 nm tungsten film on the silicon wafer. The nominal pitch values are 300 nm and 700 nm, and the accuracy is 3 %. The High Precision Calibration Standards consists of a 20 nm titanium layer on the silicon wafer. The nominal pitch value is 300 nm and the accuracy is 1 %. The MXS 301CE and MXS 701CE were chosen for the international comparison of one-dimensional gratings in 1998 [76].

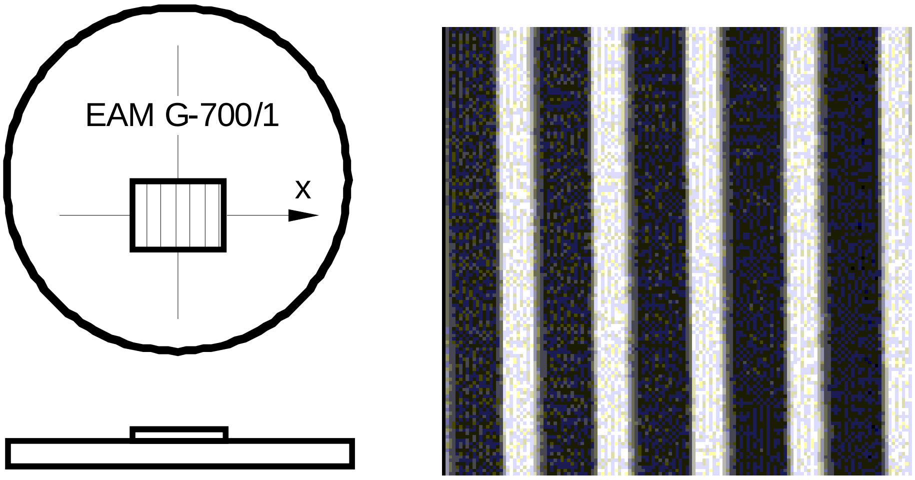

Figure 4.4 MOXTEK SPM Calibration Standards

E. NanoLattice Pitch Standards made by VLSI

The VLSI Standards Incorporated is one of the standards suppliers for the semiconductor industry. The NanoLattice Standard (NLS)[81] shown in Figure 4.5 is the newest SEM pitch calibration standard. It has a 0.1 μm nominal pitch required for SEM magnification calibration and characterization of non-linearity across the field of view. The NIST Traceable NanoLattice consists of a 1 mm × 1 mm grating etched in silicon with a nominal pitch of 100 nm. When mounted on a wafer, the chip is placed in a recessed pocket so that it is coplanar to the surface of a wafer with a tolerance of ±15 μm.

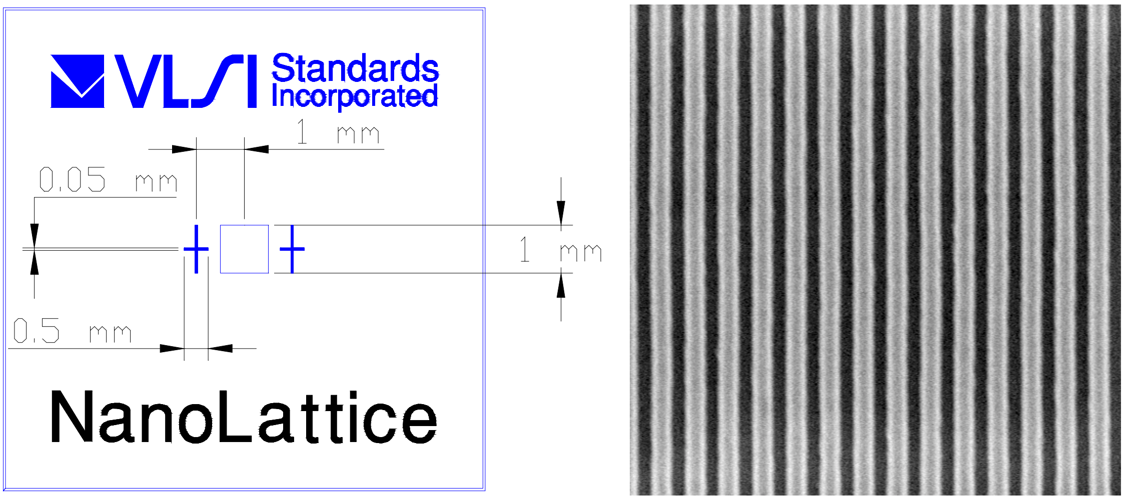

Figure 4.5 NanoLattice Pitch Standards made by VLSI

4.2 Pitch Measurement by TAFM and SPIP

After finishing the establishment of TAFM, the first application was to measure the one-dimensional pitch of diffraction gratings: First, to measure the surface texture of sample and capture the displacements of the X and Y directions from the laser interferometers and Z-capacitance of the AFM. Second, to do the equivalent space interpolation in the X and Y directions by use a program in Matlab. Finally, to calculate the pitch value and the pattern tilt angle by feeding the interpolated data from the Matlab program into the SPIP software. A MXS 301BE high precision one-dimensional pitch standard made by Moxtek acts as a check standard to assess the TAFM. The measuring procedure is described as following: [82]

4.2.1 Pitch Calibration by TAFM

A. Locate the MXS 301BE sample on the flexure stage of TAFM shown in the Figure 4.6. The grating's direction is perpendicular to the X direction. Rotate the sample till the angle deviation about less than 6 °.

B. Use the optical microscope of the TAFM to find an appropriate area (without contamination and defects), then turn on the flexure stage, laser interferometers, and temperature-controlled water circulator.

C. Wait about one night for the temperature in the enclosed box near to 20 °C.

D. Use the DI AFM scanning an area larger than 10 times of the nominal pitch value to tune the control parameters of the AFM.

E. The TAFM uses the sample-scanning mode and the cantilever tip must be at stationary in XY plane. Therefore, change the scanning area to zero in the XY plane, and let the AFM only operating in Z height sensing.

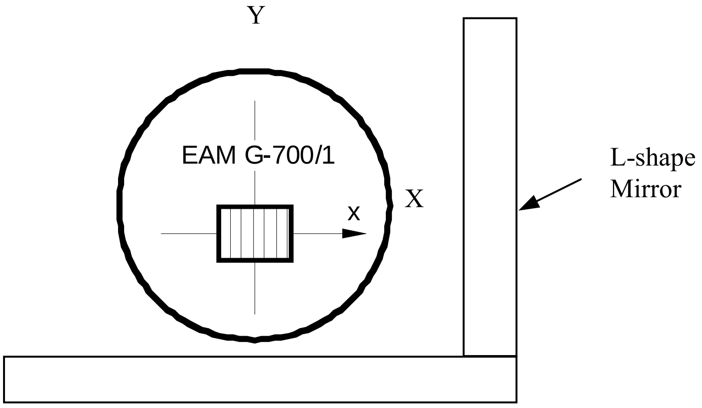

Figure 4.6 Sample locating in the TAFM

F. Run the 2d_scan_frontend_h.vi (see appendix 9.1) program written in LabVIEW. The control panel on the screen is shown in Figure 4.7.

Speed of Piezo Stage
(Only valid for MA-scan)
Maximalwert: 30
(about 5s for 0.1mm at 0.02)

Number of steps 512
Delay beteen steps [s] 0.0000
Tolerance of Displacement Data Ax1 0.0400
Tolerance of Displacement Data Ax2 0.0400

Speed Axis 1 fw 0.0200
Speed Axis 1 bw 0.0010
Speed Axis 2 0.0200
Speed Axis 4 0.0200
Path for saved tracedata c:\data\scandata.txt

Scan range [µm] Axis1 3.000
Number of points Axis 1 [0,32768] 26000
Points for speed up/down Axis1 6000
Tolerance of endposition [µm] Axis1 0.0000
Delay between movements [s] Axis1 0.00
Step size [µm] Axis2 0.02362
Number of Points [0,32768] Axis2 6000
Points for speed up/down Axis2 600
Tolerance of endposition [µm] Axis2 0.0000
Delay between movements [s] Axis2 0.00
Scan range [µm] Axis2 3.000

Figure 4.7 TAFM operation panel

G. Key in the number of steps of each scanning line in the X direction, tolerances in the X and Y directions, scanning speeds, scanning range, step size between lines in the Y direction, and output data filename.

H. Push the “start” function icon, and push the “interf.Conf.” function icon to adjust the configuration of laser interferometers.

I. Choose the “Scan MA Step 1 RS232” function icon and push the “Start Scan” function icon to measure the sample. The measuring data will put into the preset filename in step G. Measuring data include the X- and Y- displacements from laser interferometers and the Z-displacement from the capacitance sensor of the AFM.

4.2.2 Interpolation by Matlab Program

A. Use a program written in Matlab (see appendix 9.2) to do the equivalent space interpolation in the X and Y directions of the file obtained from the TAFM.

B. The output includes the interpolation ranges of the X and Y directions (t_{xx} and t_{yy}), a 3D image of interpolation area (see Figure 4.8), and a data file of every Z height of each cross point with equivalent space in the X and Y directions.

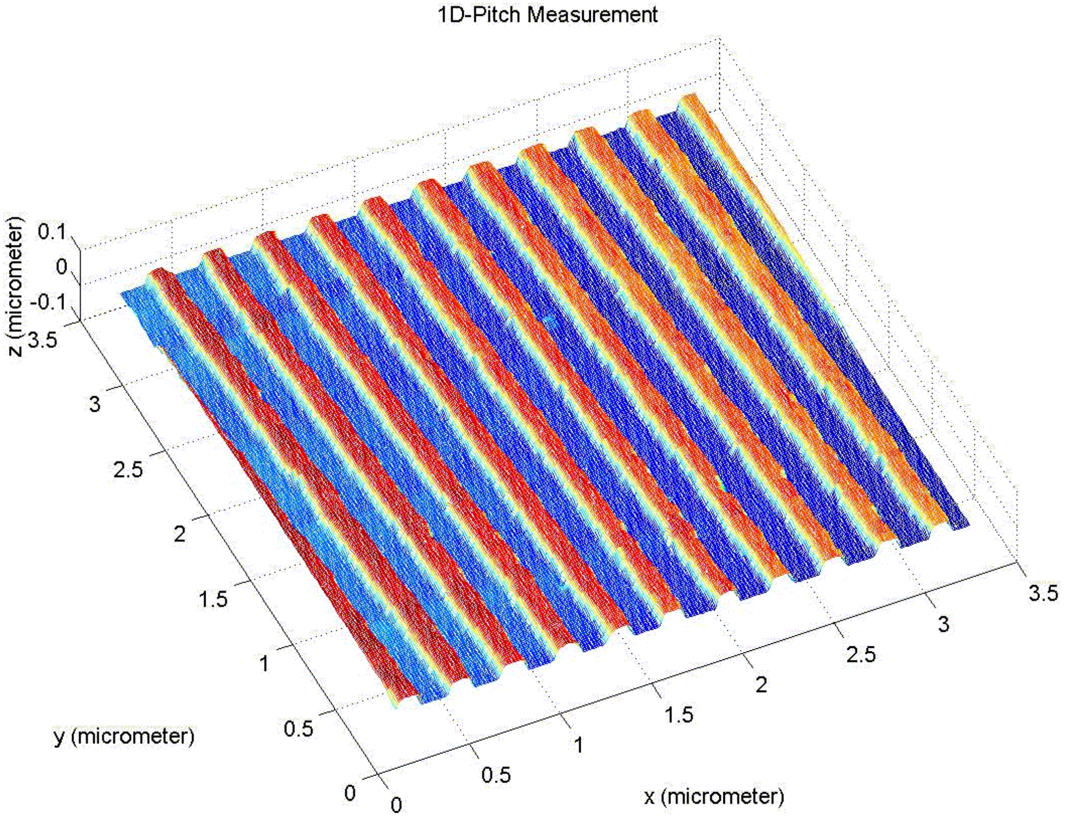

Figure 4.8 3D image after interpolation by Matlab

4.2.3 Calculation the Pitch Value by the SPIP Software

A. Run the SPIP software, and key in the data filename created by the Matlab interpolation program shown in Figure 4.9.

B. Key in the t_{xx} and t_{yy} into the blanks of “X Size” and “Y Size”, interpolation points of the X and Y directions into “Number of X, Y Pixels”, then choose a Data type of “ASCII” and push the “Guess All” function.

C. Choose the “Fourier Menu” function in the SPIP main panel, a “Fourier Menu” panel will show in the screen.

D. Choose the “Parallel Lines” function on the “Fourier Menu” panel, a two-dimensional image of calibration area and a panel “Unit Cell and Calibration results” will appear in the screen shown in Figure 4.10.

E. The value of the cross of row “a vector” and column “Length” is the average value of pitch calibration. And the value of the cross of row “a vector” and column “Angle” is the average value of the pattern tilt angle.

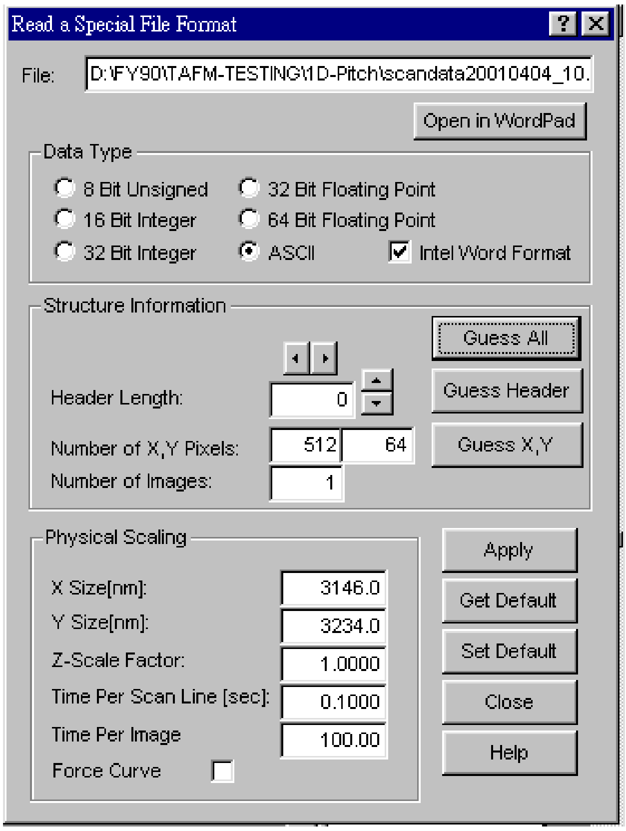
Read a Special File Format

File: D:\FY90\TAFM-TESTING\1D-Pitch\scandata20010404_10.

Data Type

○ 8 Bit Unsigned ○ 32 Bit Floating Point
○ 16 Bit Integer ○ 64 Bit Floating Point
○ 32 Bit Integer ● ASCII ☑ Intel Word Format

Structure Information

Header Length: 0
Number of X,Y Pixels: 512 64
Number of Images: 1

Physical Scaling

X Size[nm]: 3146.0
Y Size[nm]: 3234.0
Z-Scale Factor: 1.0000
Time Per Scan Line [sec]: 0.1000
Time Per Image 100.00
Force Curve ☐

Figure 4.9 SPIP parameters input panel

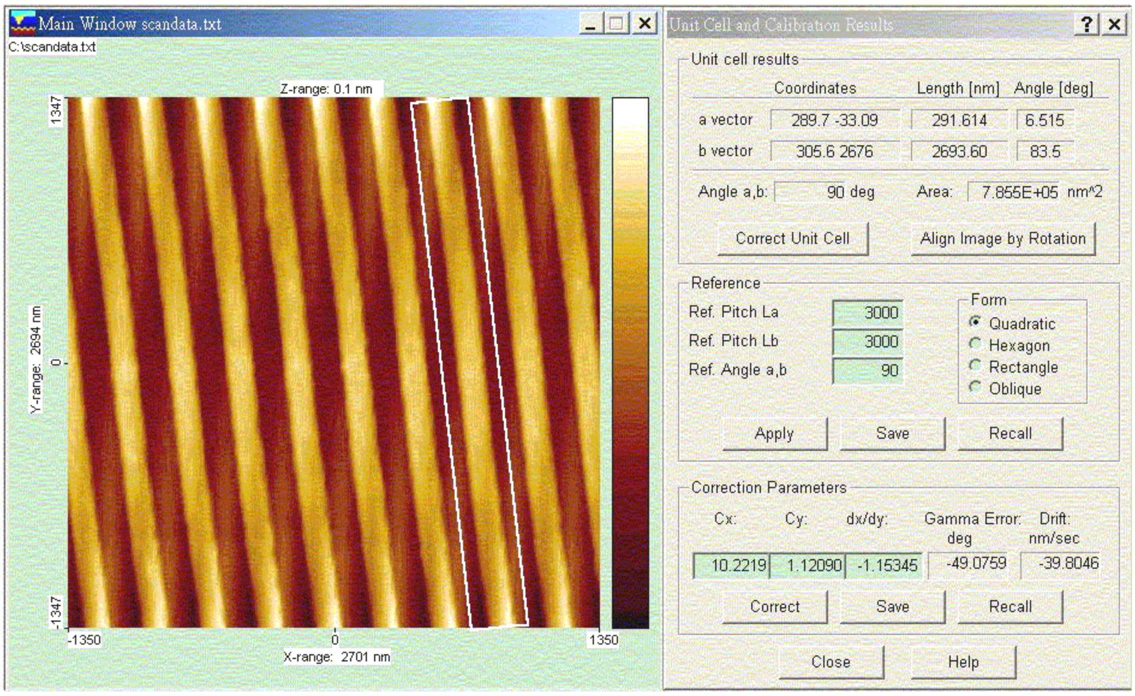

Unit Cell and Calibration Results

Unit cell results

	Coordinates	Length [nm]	Angle [deg]
a vector	289.7 -33.09	291.614	6.515
b vector	305.6 2676	2693.60	83.5

Angle a,b: 90 deg Area: 7.855E+05 nm^2

Reference

Ref. Pitch La 3000
Ref. Pitch Lb 3000
Ref. Angle a,b 90

Form
● Quadratic
○ Hexagon
○ Rectangle
○ Oblique

Correction Parameters

Cx:	Cy:	dx/dy:	Gamma Error: deg	Drift: nm/sec
10.2219	1.12090	-1.15345	-49.0759	-39.8046

Figure 4.10 Pitch calculation result by SPIP

5. Result and Discussion

5.1 AFM test

A VLSI STS3-1800P standard (two-dimensional pitch standards with grid pitch of 10 µm×10 µm, and depth of 180 nm) was used to test the maximum measuring range, noise level, and linearity [83-84]. The DI Dimension Metrology AFM was always operating in "Tapping mode". Figure 5.1 shows the maximum range test of the DI AFM. The measuring range was 70 µm×70 µm in the X and Y directions. The scanning rate was 0.5008 Hz. The left picture shows the height in the Z direction (0~500 nm). The right picture shows the voltage output of capacitance sensor in the Z direction. It can be exported for the application of TAFM.

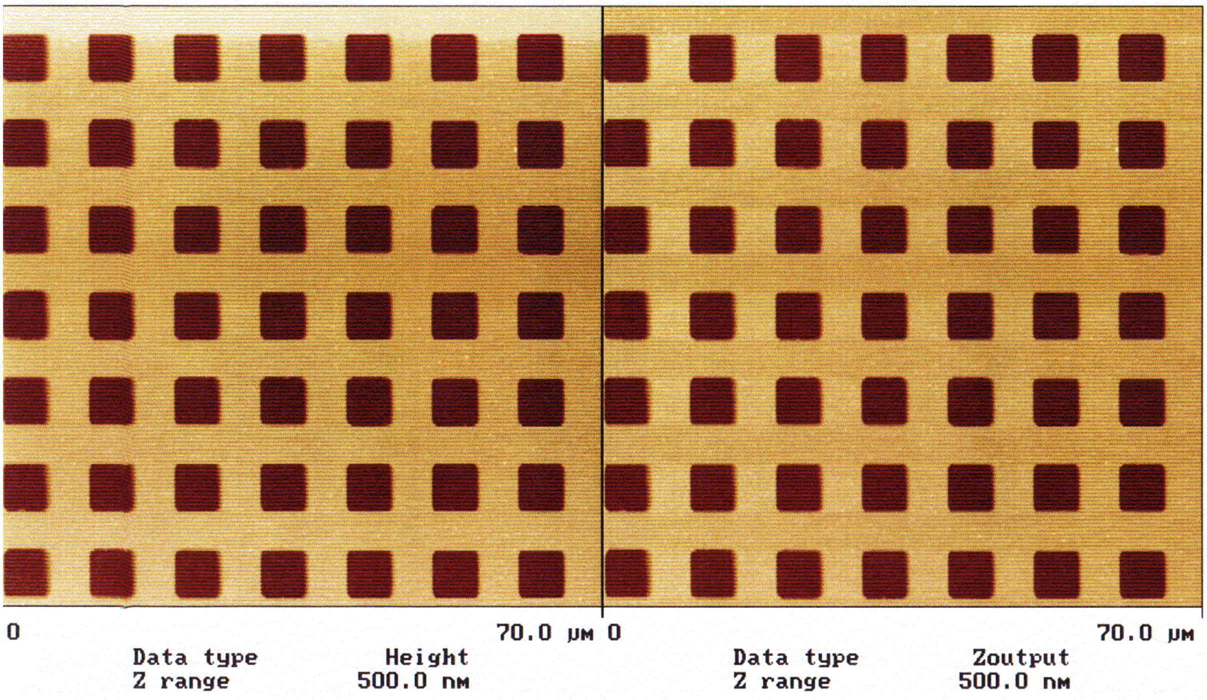

Figure 5.1 Maximum measuring range test (X and Y)

The noise level testing is shown in Figure 5.2. The scanning range was changed to 1 nm × 1 nm. The scanning rate was 9.766 Hz. The number of measuring points of each scanning line was 256, and the scanning lines were 256. The result of noise level testing in the Z direction was 0.039 nm (RMS, Root Mean Square).

The linearity test in the X direction is shown in Figure 5.3. The displacements of scanner of the DI Dimension Metrology AFM were close-loop-controlled by three capacitance sensors, one for each axis. This test was to check the relations between the applied voltage and time, and the relation between the displacement and time during scanning. The upper Figure shows the applied voltage versus time, and the lower Figure shows the displacement versus time. The results of linearity test in X and Y directions were less than 0.05 %.

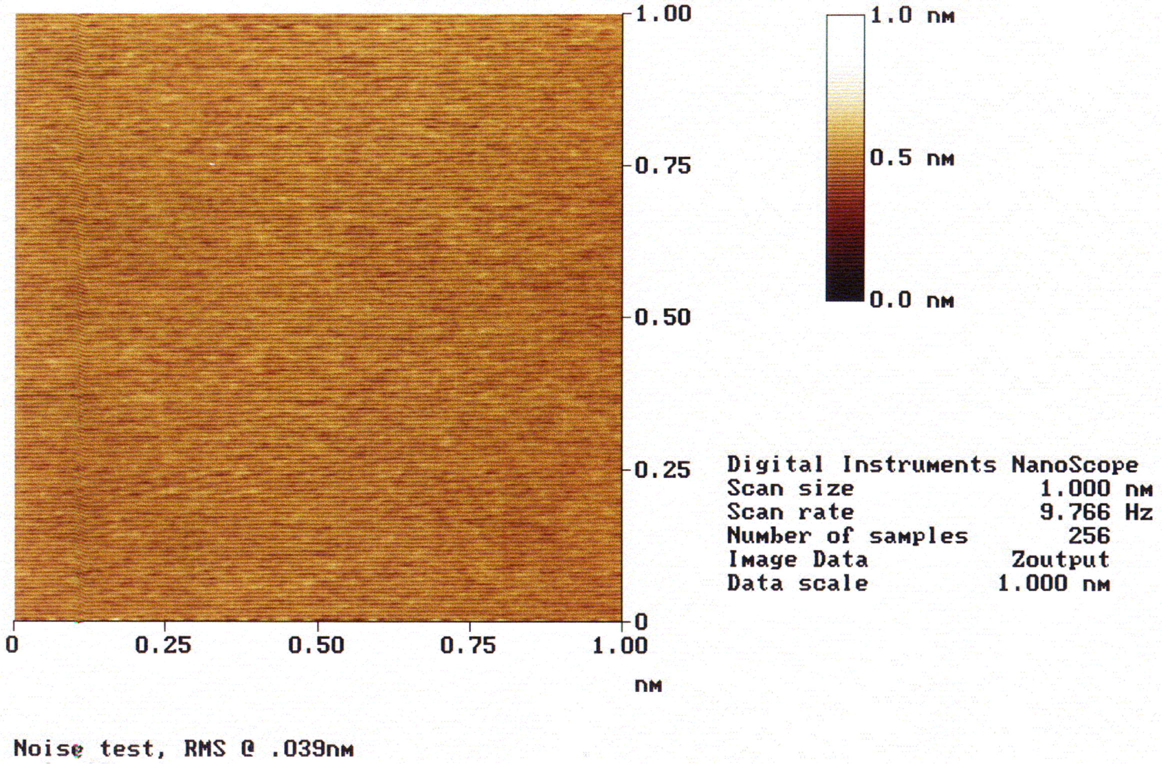

Figure 5.2 Noise level test

Figure 5.3 Linearity test in X direction with constant speed

5.2 Laser interferometer test

A program in LabVIEW was developed to test the noise of the SIOS differential plane mirror laser interferometers. The measuring noise of laser interferometer affected by conditioned air (in a temperature-controlled laboratory without an enclosed cover) was about 20 nm in 17 second shown in Figure 5.4. The signal-sampling rate of laser interferometers was 6000 samples/second, and the average number of samples was 1024 of each channel. The X-direction's interferometer included two signals of 1A and 1B, and Y-direction's interferometer included two signals of 2A and 2B.

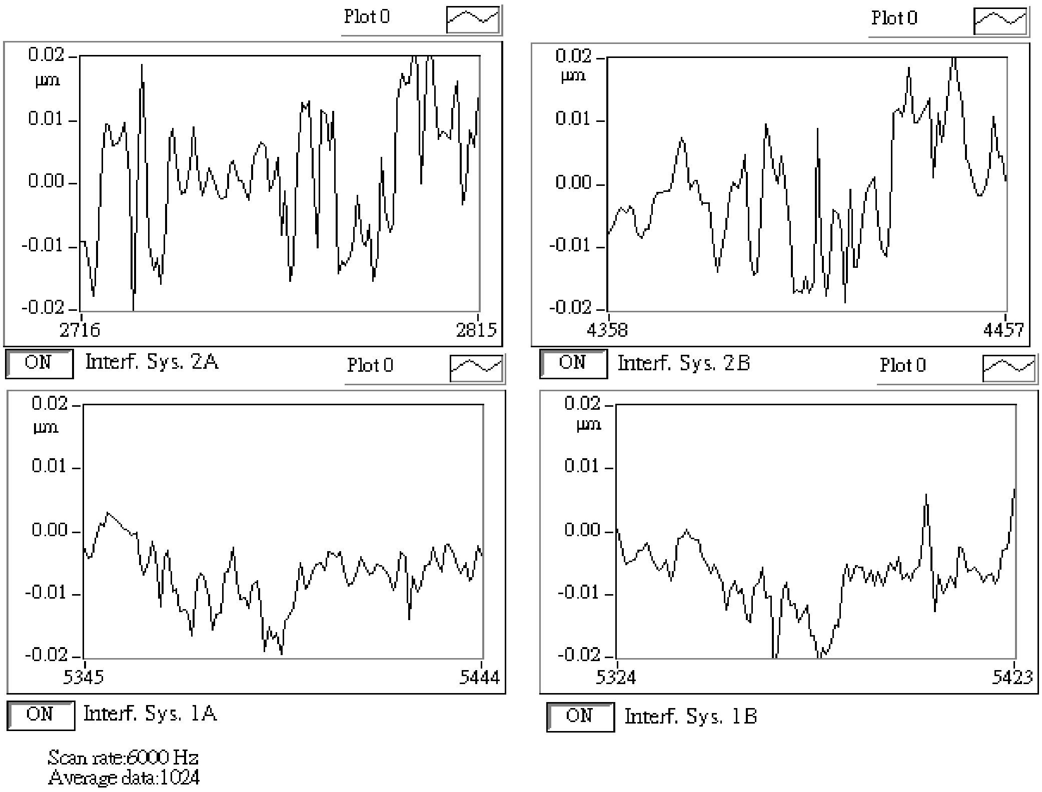

Figure 5.4 Interferometer noise without enclosed cover

After adding an enclosed box made of stainless steel sheets and thermal isolation material to cover the whole measuring machine, the noise of laser interferometers was reduced to about 2 nm in 18 seconds as shown in Figure 5.5. The signal-sampling rate was 1024 samples/second, and the average number of samples was 128 of each channel. The X-direction's interferometer included channel 1 and channel 2, and Y-direction's interferometer included channel 3 and channel 4.

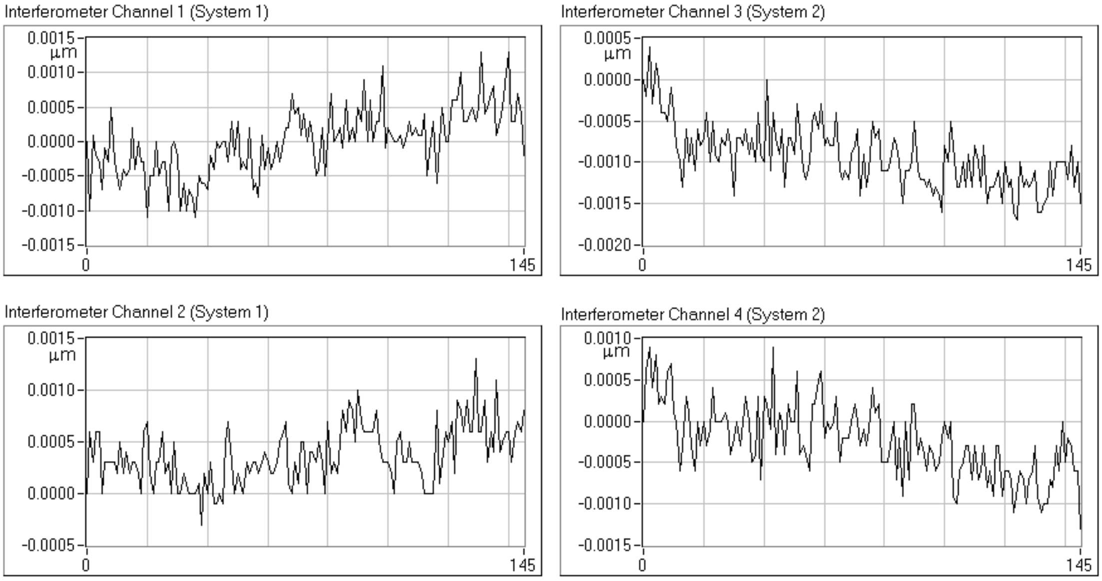

Scan rate: 1024 Hz
Averaging over 128 raw data

Figure 5.5 Interferometer noise with enclosed cover

5.3 Active compensation flexure stage test

A program in LabVIEW was written to test the performances of PI P-710K031 compensation flexure stage. Figure 5.6 shows the positioning noise at zero point. The displacements were measured by its capacitance sensors inside. The variation in the X direction (Axis 1) was less than 4 nm in 5.5 seconds. The variation in the Y direction (Axis 2) was less than 2.5 nm in 5.5 seconds. The variation in the Z direction (Axis 4) was less than 1 nm in 5.5 seconds.

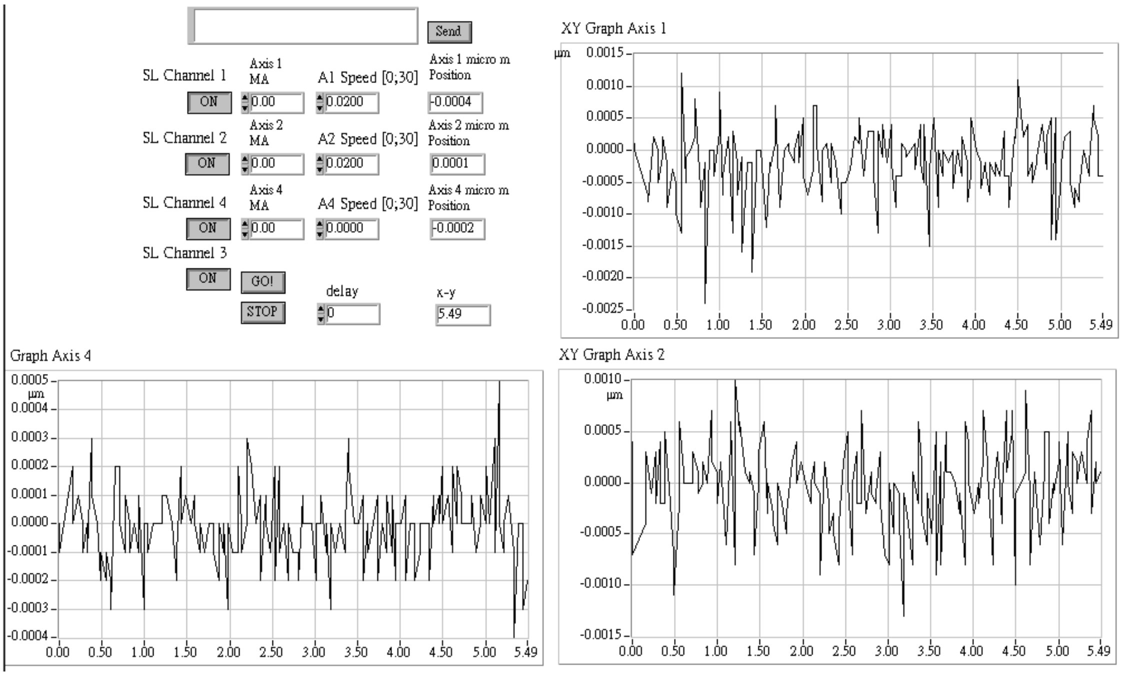

SL Channel 1
Axis 1 MA: 0.00
A1 Speed [0;30]: 0.0200
Axis 1 micro m Position: -0.0004
SL Channel 2
Axis 2 MA: 0.00
A2 Speed [0;30]: 0.0200
Axis 2 micro m Position: 0.0001
SL Channel 4
Axis 4 MA: 0.00
A4 Speed [0;30]: 0.0000
Axis 4 micro m Position: -0.0002
SL Channel 3
delay: 0
x-y: 5.49

Figure 5.6 Positioning noise at zero point

Figure 5.7 shows the crosstalk while the stage was moving from 0 to 100 μm in the X direction (Axis 1). The variation in the Y direction (Axis 2) was less than 4.5 nm. The variation in the Z direction (Axis 4, according to the definition of PI stage) was about 1 nm. Figure 5.8 shows the variation in the Z direction while stage was scanning in the X and Y directions. The scanning included 100 μm of forward and backward scanning lines (512 points) in the X direction, and 10 μm of spacing in the Y direction. The variation in the Z direction was about 1 nm.

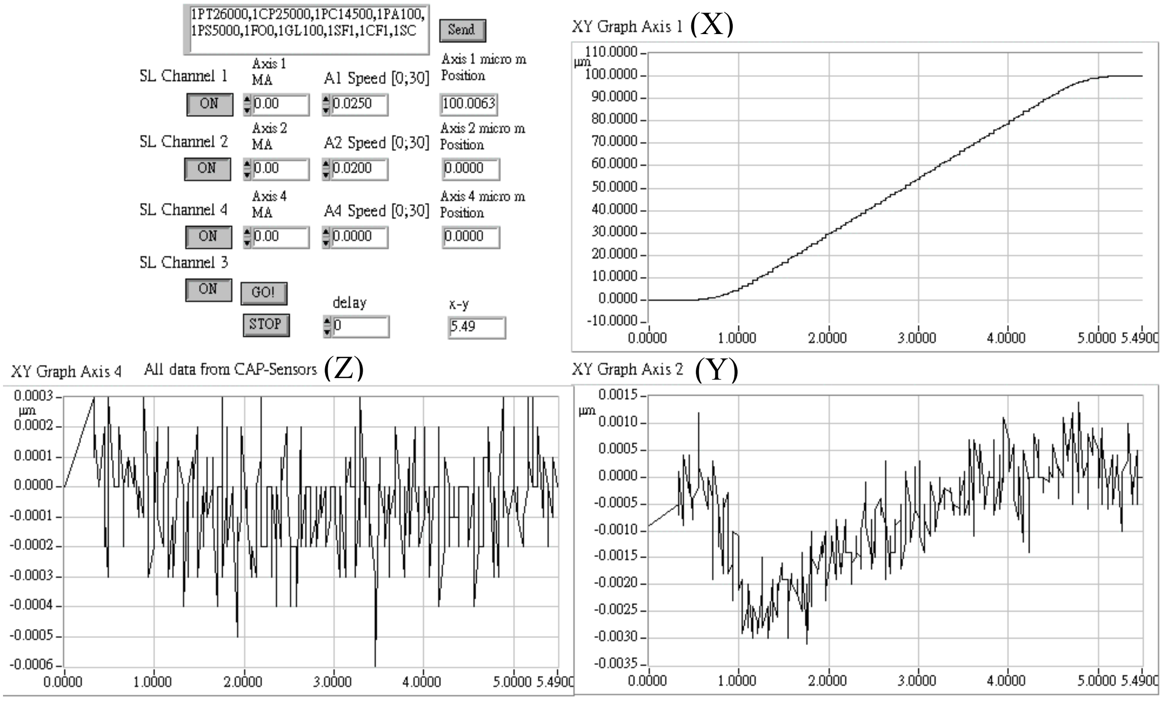

```
1PT26000,1CP25000,1PC14500,1PA100,
1PS5000,1FO0,1GL100,1SF1,1CF1,1SC
```

SL Channel 1 ON; Axis 1 MA 0.00; A1 Speed [0;30] 0.0250; Axis 1 micro m Position 100.0063

SL Channel 2 ON; Axis 2 MA 0.00; A2 Speed [0;30] 0.0200; Axis 2 micro m Position 0.0000

SL Channel 4 ON; Axis 4 MA 0.00; A4 Speed [0;30] 0.0000; Axis 4 micro m Position 0.0000

SL Channel 3 ON

delay 0

x-y 5.49

Figure 5.7 Crosstalk error while moving in X direction

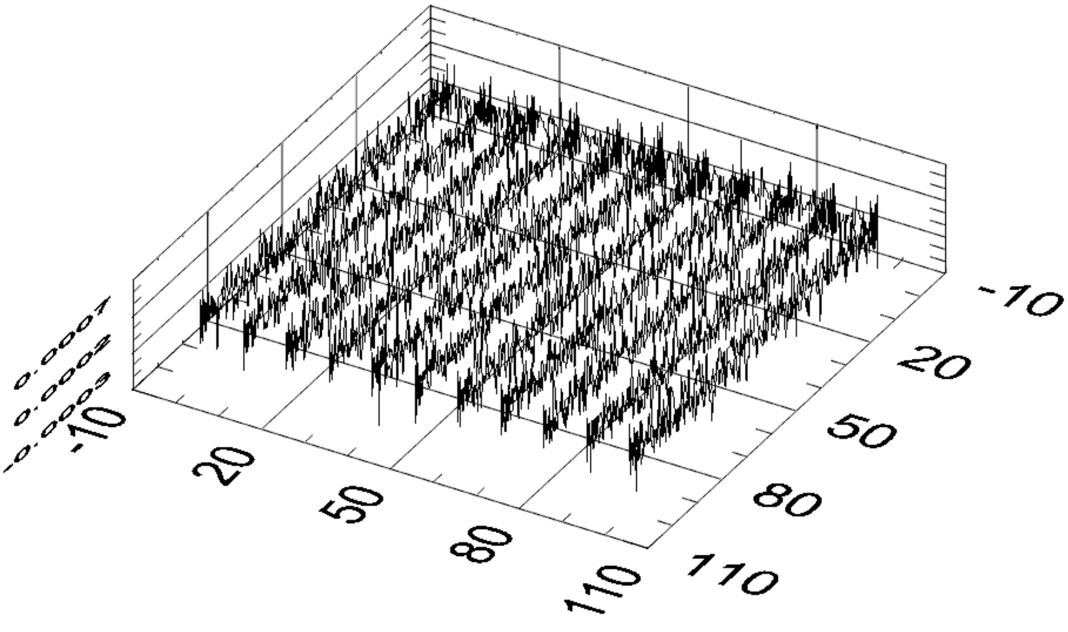

Figure 5.8 X-Y scanning test of flexure stage

Figure 5.9 shows the positioning calibration of flexure stage in the X direction by ZYGO Z-1000 laser interferometer calibrated by PI [85]. The deviations in the X and Y directions were less than 4 nm, and the deviation in the Z direction was less than 1 nm.

X (μm)	X (μm)	Y (μm)	Z (μm)	X (μm)	X (μm)	Y (μm)	Z (μm)
5	0.0018	0.0011	0.0006	55	0.0018	0.0012	0.0003
10	0.0023	0.0012	0.0006	60	0.0030	0.0008	0.0004
15	0.0026	0.0015	0.0005	65	0.0017	0.0015	0.0004
20	0.0020	0.0014	0.0004	70	0.0020	0.0010	0.0008
25	0.0029	0.0008	0.0004	75	0.0016	0.0010	0.0006
30	0.0020	0.0015	0.0006	80	0.0015	0.0006	0.0004
35	0.0012	0.0008	0.0005	85	0.0015	0.0010	0.0005
40	0.0019	0.0012	0.0002	90	0.0019	0.0019	0.0005
45	0.0015	0.0017	0.0007	95	0.0017	0.0015	0.0003
50	0.0038	0.0021	0.0003	100	0.0025	0.0013	0.0005

Figure 5.9 Calibration by laser interferometer

Figure 5.10 is a noise test in z-axis of the TAFM with a 3μm × 3μm scanning area. The data were taken from the internal capacitance sensors of PI flexure stage. There were 128 scanning lines in Y-axis and 512 scanning points at each scanning line in X-axis. It took about 42 seconds for each scanning line. Each noise test took one and half-hour. The specimen was MXS 310BE made by Moxtek Company with a nominal pitch of 292 nm. The noise of PI flexure stage in z-axis (out-of-plane motion) was less than 0.5 nm measured by the internal capacitance sensor.

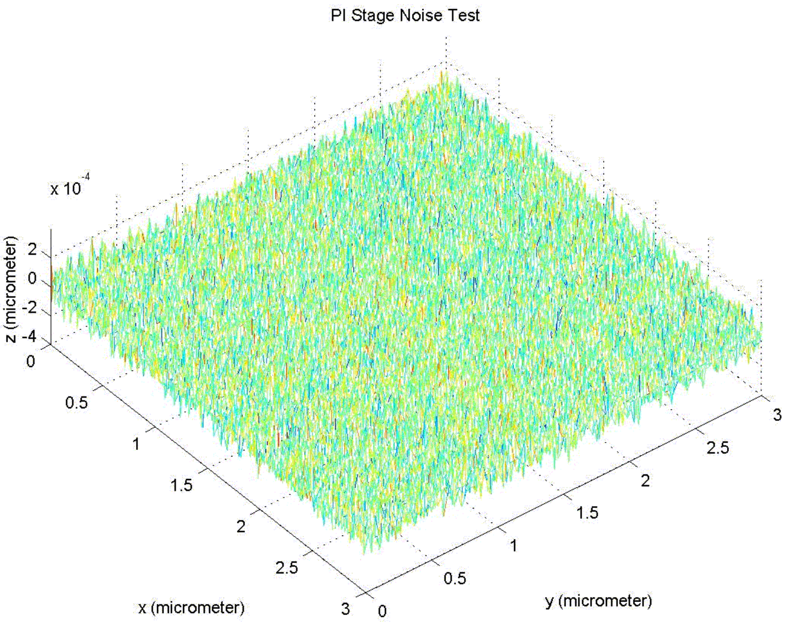

Figure 5.10 Noise test of PI flexure stage by capacitance sensor

5.4 Temperature test

The noise of laser interferometer in air conditioned room was about 20 nm. After cover the whole measuring instrument with an enclosed box. The noise could decrease to about 2 nm in 18 seconds (see Figure 5.5). However, the temperature increased from 20.3°C to 23.7°C within 8 hours (see Figure 5.11). The temperature changing may be caused by the heat emission of the electronics of the DI AFM. The displacement deviation between reference mirror and moving mirror was about 5 μm in y-axis in one hour. After assembling a temperature control system with circulating water, the temperature can be controlled within 20±0.3 °C. Figure 5.12 shows the temperature variation in the enclosed box with temperature control system in 48 hours.

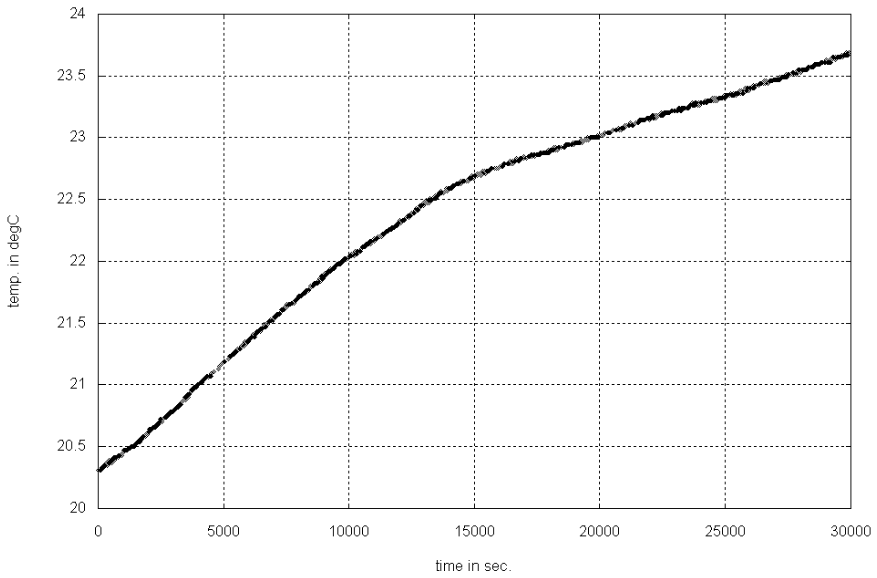

Figure 5.11 Temperature variation without temperature control

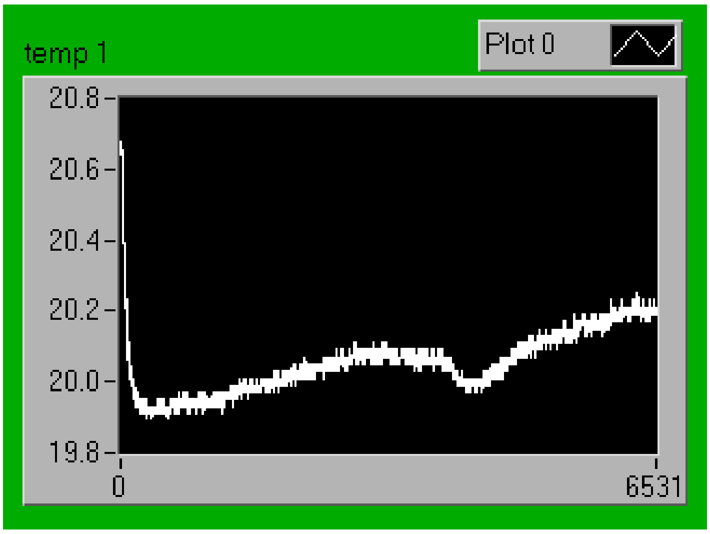

Figure 5.12 Temperature variation with circulating water in 48 hours

Figure 5.13 and Figure 5.14 show the results of pitch measurement on the same scanning area of the Moxtek MXS 301BE 1-D gratings sample [80]. The AFM was only controlled at the Z-height sensing and the sample scanning in XY plane was controlled by the PI flexure stage.

The displacements of X- and Y- axes were read by the SIOS differential laser interferometers and the displacement of Z-axis is read by the capacitance sensor of the AFM. In the image of Figure 5.13, there were some drifts in all three axes: 1μm in X-axis, 3.8 μm in Y-axis, and 0.1 μm in Z-axis. They were caused by the temperature change due to heat emission from the electronic unit of the AFM, and the biggest drift was in Y-axis. After adding a temperature-controlled system with circulating water, a better result was obtained as displayed in Figure 5.14. There was no drift in Z-axis, but there were still about 20 nm drifts in X- and Y- axes in 20 minutes.

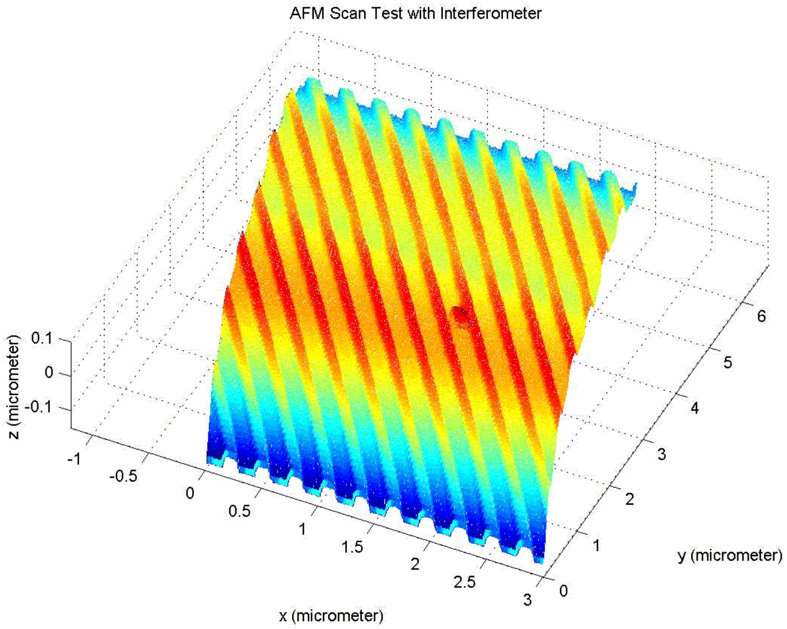

Figure 5.13 TAFM test without temperature control

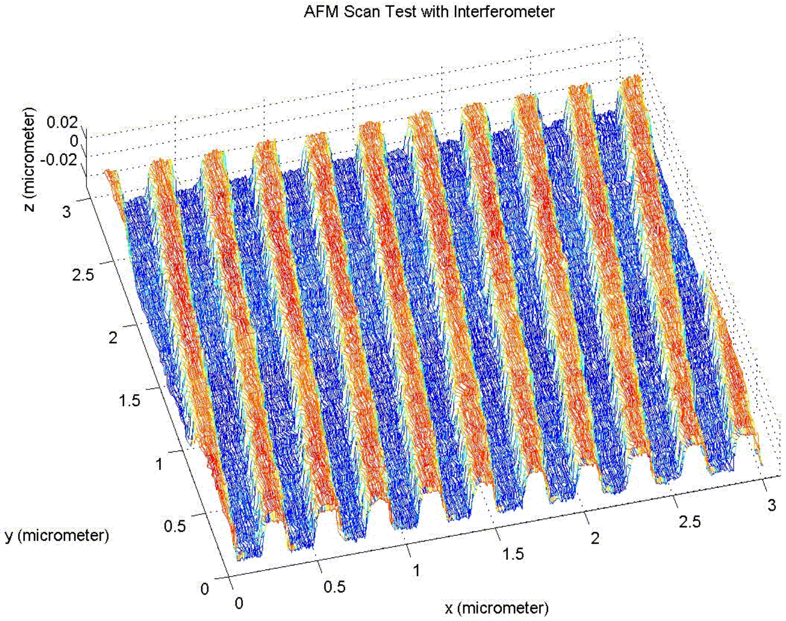

Figure 5.14 TAFM test with temperature control

5.5 Vibration noise test

Figure 5.15 shows the natural frequency test of vibration isolator (see Figure 3.1) by using a PCB 393B31accelerator (S/N: 5113) and a HP 35670 analyzer (S/N: 3613A03665). The period of one cycle is 2.929688 - 0.9375 = 1.992188 (sec). So, the natural frequency equals 1/1.992188 = 0.50196 (Hz). After the assembly of the TAFM, the noise level of AFM in the Z direction became to 0.67 nm (RMS, see Figure 5.16). And a few nm noises appeared at the output signal of the TAFM shown in Figure 6.3 on page 78. A more sensitive accelerator also was used to measure the natural frequency of metrology frame. A 9 Hz natural frequency in vertical direction was obtained.

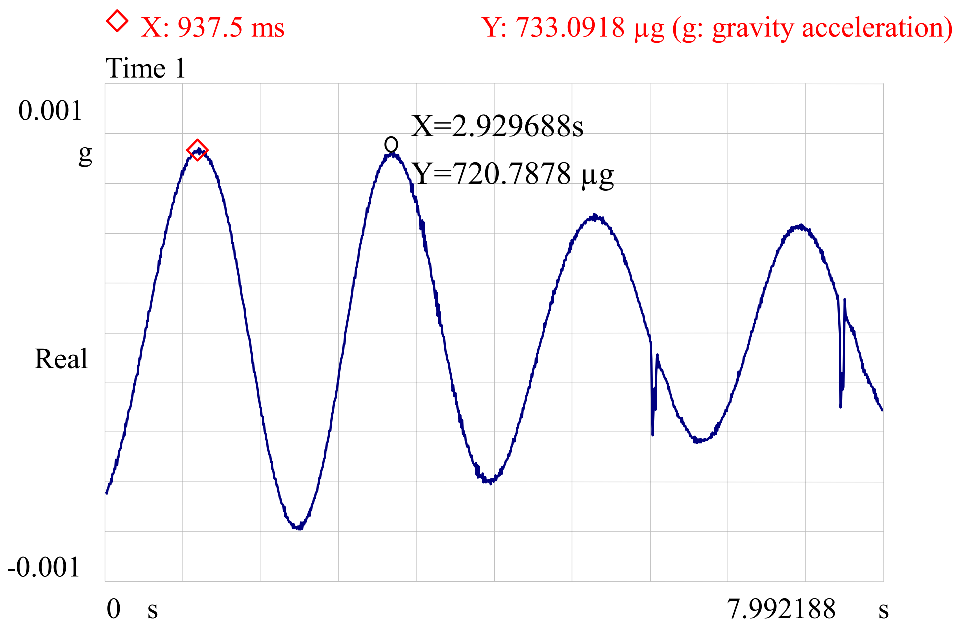

Figure 5.15 Natural Frequency test of vibration isolator

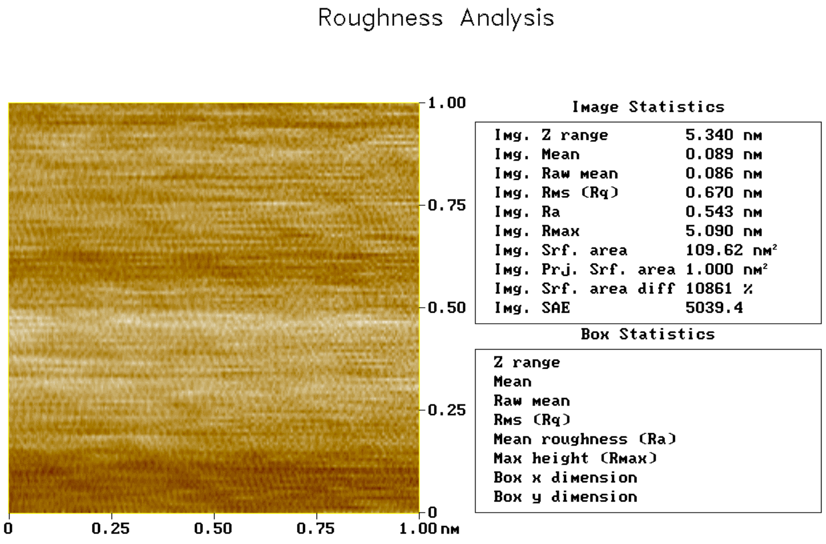

```
Image Statistics
Img. Z range          5.340 nm
Img. Mean             0.089 nm
Img. Raw mean         0.086 nm
Img. Rms (Rq)         0.670 nm
Img. Ra               0.543 nm
Img. Rmax             5.090 nm
Img. Srf. area        109.62 nm²
Img. Prj. Srf. area 1.000 nm²
Img. Srf. area diff 10861 %
Img. SAE              5039.4
Box Statistics
Z range
Mean
Raw mean
Rms (Rq)
Mean roughness (Ra)
Max height (Rmax)
Box x dimension
Box y dimension
```

Figure 5.16 Noise of AFM

5.6 Pitch Measurement

Table 5.1 shows the results of pith measurement by the TAFM. First, to obtain a set of three-dimensional surface texture. Then, to do the equivalent space interpolation in the X and Y directions by use of a program written in MATLAB. Finally, to calculate the pitch value and the pattern tilt angle by use of the SPIP software. The measuring area was 3.5×3.5 μm^2 in XY plane. The average pitch value of 16 measurements was 291.63 nm. And the standard deviation was 0.071 nm.

Table 5.1 Pitch Measurements

Number	Angle ϕ (°)	Pitch P (nm)
1	1.022	291.734
2	1.421	292.202
3	0.400	292.002
4	0.983	291.815
5	2.639	291.778
6	1.757	292.065
7	1.431	291.552
8	1.807	291.492
9	2.348	291.299
10	2.382	291.363
11	2.174	291.281
12	2.417	291.434
13	2.441	291.453
14	2.066	291.682
15	2.254	291.570
16	2.653	291.377

5.7 Uncertainty Evaluation of Pitch Measurement

According to the “ Guide to the Expression of Uncertainty in Measurement” [12], the first important thing is to establish a measuring equation to follow measuring method and the sample to be tested. The measurand may be not measured directly, and may be determined by some parameters such as laser wavelength, temperature, pressure, humidity, and mechanical structure. The second procedure is to evaluate the standard uncertainties of every error source. They can be estimated by the calibration certificates or by experiences. Then, calculation of the estimated combined standard uncertainty is done by the square root of the combined variance. Finally, the effective degrees of freedom and the coverage factor to get the expanded uncertainty are calculated.

5.7.1 Measuring Equation

According to the calibration procedure of pitch measurement, the pitch value and the pattern tilt angle were calculated by the FFT function of the SPIP software (version 1.92). The SPIP software was developed by Image Metrology Cooperation [8]. It was difficult to get the analysis model and measuring equation. So, a simulative model was described as below:

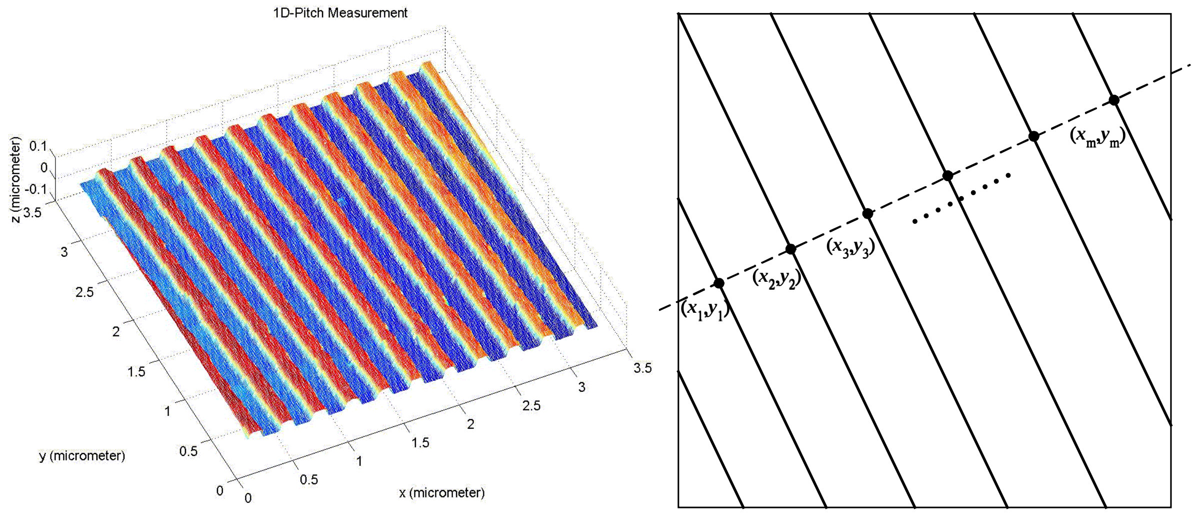

(a).Three-dimrnsional profile by Matlab program (b).Mathematics simulation

Figure 5.17 Simulate of pitch measurement

Figure 5.17 shows a three-dimensional profile after interpolating by the program in Matlab, and a mathematics simulation of measuring procedures. Making a dash line perpendicular to the pitch pattern yields the intersection points (x_1, y_1), (x_2, y_2), (x_3, y_3)… (x_n, y_n) as shown in Figure 5.17(b). The average pitch value *P*, according to the measuring procedures, can be expressed as:

$$P=\frac{1}{m-1}\sum_{i=1}^{m-1}\left[(x_{i+1}-x_i)^2+(y_{i+1}-y_i)^2\right]^{1/2}+\varepsilon_{P_1}+\varepsilon_{P_2}, \qquad (5.1)$$

where ε_{P_1} is the error of pitch measurement by the TAFM, ε_{P2} is the error of pitch calculation by the SPIP software, (x_i, y_i) are the intersection points, and m is the number of intersection points. The x_i and y_i are obtained from the laser interferometers while the sample is moving by the flexure stage. So x_i and y_i are the displacements of flexure stage in the X and Y directions. The displacements can be expressed:

$$x_i, y_i=\left(\frac{\lambda_0}{8192\,n_{tpf}}\right)N\left[1-\frac{\theta^2}{2}\right]+d(\sin\beta), \qquad (5.2)$$

λ_0 : Laser wavelength in vacuum,

n_{tpf}: Refractive index of air, function of air temperature t, air pressure p, and vapor pressure f,
N : Counting of laser interferometer,
θ : Angle between the laser beam and moving axis of the flexure stage,
β : Angle deviation of the flexure stage,
d : Abbe offset.

The dimension of the sample to be tested may be changed if the surrounding condition varies. So the calibration result must be corrected to a value at 20 ˚C. Figure 5.18 shows the diagram block of displacement measurement by laser interferometer. The equation 5.2 can be changed to:

$$x_{i(20)}, y_{i(20)} = [1+\alpha(20-t_s)]\left[A - B - C + \frac{\lambda_0}{8192\, n_{tpf}} N(1-\frac{\theta^2}{2}) + d(\sin\beta)\right]$$

$$= F(\lambda_0, n_{tpf}, N, \alpha, t_s, A, B, C, \theta, d, \beta). \tag{5.3}$$

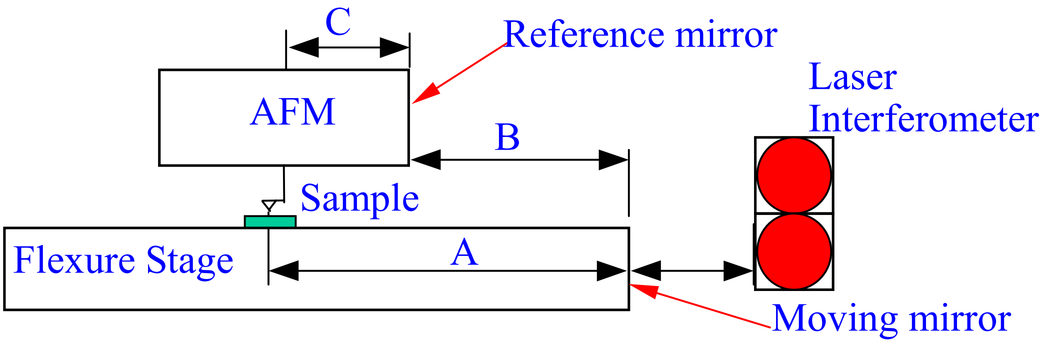

Figure 5.18 Diagram block of displacement measurement

In equation 5.3: t_s is temperature of sample to be tested; α is coefficient of thermal expansion of sample to be tested; $\frac{\lambda_0}{n_{tpf}}$ is the laser wavelength in the air; A is the distance between the moving mirror and probe tip; B is the distance between the moving mirror and reference mirror (Dead path); C is the distance between the reference mirror and probe tip. The laser wavelength in air will be changed while the surrounding condition is changing. The refractive index of air must be corrected by Edlén [86-89] and Wexler formulas with the air temperature, air pressure, and relative humidity. Equation 5.4 shows the laser wavelength in air.

$$\lambda_{tpf} = \frac{\lambda_o}{n_{tpf}} = \frac{\lambda_o}{1 + A_\lambda \times B_\lambda - C_\lambda} \tag{5.4}$$

$$A_\lambda = \frac{p\left[8343.05 + 2406294\,(130 - \sigma^2)^{-1} + 15999\,(38.9 - \sigma^2)^{-1} 10^{-8}\right]}{96095.43}$$

$$B_\lambda = \frac{[1 + p(0.601 - 0.00972\ t_{90})10^{-8}]}{1 + 0.003661\ t_{90}}$$

$$C_\lambda = f(3.7345 - 0.0401\sigma^2)10^{-10}$$

$f = RH \times e_{sw}(T)/100$

$$e_{sw}(T) = \exp[\sum_{i=0}^{6} A_i \times T^{i-2} + A_7 \times l_n(T)] \tag{5.5}$$

$A_0=-2.9912729\times10^3$

$A_1=-6.0170128\times10^3$

$A_2=1.887643854\times10^1$

$A_3=-2.8354721\times10^{-2}$

$A_4=1.7838301\times10^{-5}$

$A_5=-8.41504171\times10^{-10}$

$A_6=4.4412543\times10^{-13}$

$A_7=2.858487$

In Equation 5.5:

p : Pressure (Pascal)

t_{90}: Temperature (°C)

σ : $1/\lambda_o(\mu m^{-1})$

f : Vapor Pressure (Pascal)

RH: Relative Humidity

$e_{sw}(T)$: Saturated Vapor Pressure (Pascal)

T: Absolute temperature (K)

5.7.2 Standard Uncertainty

The error sources of pitch measurement contain the laser wavelength of interferometer, refractive index of air, coefficient of thermal expansion, temperature of sample, mechanical structure, dead path, alignment, straightness, Abbe offset, and practical measuring deviation. The error budget will be described in detailed as follow.

5.7.2.1 Laser wavelength of interferometer

A. Laser wavelength in vacuum

The laser interferometers were used to measure the motions of the PI flexure stage in the X and Y directions. The vacuum wavelength of laser interferometer from the calibration certificate was 632.991234 nm. It was calibrated by a stabilized Iodine He-Ne laser. The deviation of vacuum wavelength was $\pm 1.27\times 10^{-8}$ μm and was attributed as a rectangular distribution in pitch measurement. Then the standard uncertainty of vacuum wavelength $u(\lambda_0)$ was $1.27\times 10^{-8}/\sqrt{3} = 0.73\times 10^{-8}$ (μm); the sensitivity coefficient $\frac{\partial F}{\partial \lambda_0}$ was $1.5798\,L$ μm^{-1} (see section 5.7.3 on page 62). The estimated bounds of $\pm 1.27\times 10^{-8}$ μm for the vacuum wavelength are believed to be reliable to 10 percent (The relative uncertainty was $\Delta u(x_i)/\ u(x_i)=0.1$). This gives the degrees of freedom $\nu(\lambda_0)=50$, as derived by equation 5.6 [12].

$$\nu(x_i) \approx \frac{1}{2}\frac{u^2(x_i)}{\sigma^2[u(x_i)]} \approx \frac{1}{2}\left[\frac{\Delta u(x_i)}{u(x_i)}\right]^{-2} \tag{5.6}$$

B. Nonlinearity

According to the specifications of the SIOS SP 500DD laser interferometer, the nonlinearity was 2 nm. Its contribution in pitch measurement was attributed as a retangular distribution. Then the standard uncertainty of nonlinearity $u(\lambda_n)$ was 1.15 nm, and the sensitivity coefficient was 1 (see table 5.2 on page 64). The relative uncertainty was $\Delta u(x_i)/\ u(x_i)=0.1$, which gives the degrees of freedom $\nu(\lambda_n)=50$, as derived by equation 5.6.

5.7.2.2 Refractive index of air

The measurement of length is made in the ambient conditions; therefore, a correction must be applied to the laser wavelength in air. The laser wavelength in air will be varied due to the changes of the refractive index of air. The refractive index of air is determined by the Edlén's formula with parameters of air temperature, air pressure, and relative humidity. During the period of pitch measurement, the laser wavelength must be corrected according to the air temperature, air pressure, and relative humidity.

A. Edlén's formula

The laser wavelength in air is corrected by the revised Edlén formula [87-88]. The expanded uncertainty of Edlén's formula is 3×10^{-8}. Its contribution was attributed as a rectangular distribution of pitch measurement. The standard uncertainty of Edlén formula

$u(n_{tpf})$ was 1.732×10^{-8}, and the sensitivity coefficient $\frac{\partial F}{\partial n_{tpf}}$ was $-0.9997L$ (see section 5.7.3 on page 62). The relative uncertainty was $\Delta u(x_i)/\ u(x_i)=0.1$, which gives the degrees of freedom $\nu(n_{tpf})=50$, as derived by equation 5.6.

B. Air temperature

The air temperature in the enclosed box of the TAFM was controlled within (20 ± 0.3) °C. Its contribution in pitch measurement was attributed as a rectangular distribution. The standard uncertainty of air temperature $u(t)$ was 0.173 °C, and the sensitivity coefficient $\frac{\partial F}{\partial t}$ was $9.53 \times 10^{-7}\,L$ °C^{-1} (see section 5.7.3 on page 62). The relative uncertainty was $\Delta u(x_i)/\ u(x_i)=0.1$, which gives the degrees of freedom $\nu(t)=50$, as derived by equation 5.6.

C. Air pressure

The expanded uncertainty of barometer was 50 Pa, and the sensitivity coefficient $\frac{\partial F}{\partial p}$ was $-2.68\times 10^{-9}L$ Pa^{-1} (see section 5.7.3 on page 62). The contribution in pitch measurement was attributed as a rectangular distribution. Therefore the standard uncertainty of air pressure $u(p)$ was 28.87 Pa. The relative uncertainty was $\Delta u(x_i)/\ u(x_i)=0.1$, which gives the degrees of freedom $\nu(p)=50$, as derived by equation 5.6.

D. Relative Humidity

The relative humidity was varied within ±10 %, and the sensitivity coefficient $\frac{\partial F}{\partial f}$ was $8.5\times 10^{-9}L$ %$^{-1}$ (see section 5.7.3 on page 63). Its contribution was attributed as a rectangular distribution. The standard uncertainty of relative humidity $u(f)$ was 5.77 %. The relative uncertainty was $\Delta u(x_i)/\ u(x_i)=0.1$, which gives the degrees of freedom $\nu(f)=50$, as derived by equation 5.6.

5.7.2.3 Coefficient of thermal expansion

The material of pitch standards was silicon wafer. The coefficient of thermal expansion (CTE) was $(2.55 \pm 1) \times 10^{-6}$ °C^{-1}. It contributed a rectangular distribution in pitch measurement. Therefore the standard uncertainty of the coefficient of thermal expansion $u(\alpha)$ was 0.577×10^{-6} °C^{-1}, and the sensitivity coefficient $\frac{\partial F}{\partial \alpha}$ was 0 (see section 5.7.3 on page 63). The relative uncertainty was $\Delta u(x_i)/\ u(x_i)=0.1$, which gives the degrees of freedom $\nu(\alpha)=50$, as derived by equation 5.6.

5.7.2.4 Temperature of sample

The air temperature in the measuring volume was controlled within (20±0.3) °C. Assuming that the temperature change of the sample was as the same as that of the air temperature. Thus the standard uncertainty of sample temperature $u(t_s)$ was 0.173 °C, and the sensitivity coefficient was $-2.55 \times 10^{-6} L$ °C^{-1} (see section 5.7.3 on page 63). The relative uncertainty was $\Delta u(x_i)/\ u(x_i)=0.1$, which gives the degrees of freedom $\nu(p)=50$, as derived by equation 5.6.

5.7.2.5 Mechanical structure (Metrology loop)

The TAFM was built based on a commercial AFM and assembled with a 3-axis flexure stage, two laser interferometers, an L-shape mirror, and a super-Invar metrology frame. The positions of laser interferometer, probe, and stage were affected by temperature-change. In Figure 5.18, A is the distance between the moving mirror and probe tip, B is the distance between the moving mirror and reference mirror, and C is the distance between the reference mirror and probe tip.

A. Distance between the moving mirror and probe tip(A)

The material of the flexure stage was super-Invar with a coefficient of thermal expansion of 0.6×10^{-6} °C^{-1}. The distance of A was about 82 mm, and the estimated sample temperature changing was 0.025 °C, which was the same as the air temperature-change during one pitch measurement. So the change of A equals $82 \times 0.6 \times 10^{-6} \times 0.025 = 1.23$ (nm). Assuming that its contribution was attributed a rectangular distribution. The standard uncertainty of flexure stage $u(A)$ was 0.36 nm, and the sensitivity coefficient was 1 (see section 5.7.3 on page 63). The relative uncertainty was $\Delta u(x_i)/\ u(x_i)=0.2$, which gives the degrees of freedom $\nu(A)=12.5$, as derived by equation 5.6.

B. Distance between the reference mirror and probe tip(C)

The material of the AFM head was Aluminum alloy with a coefficient of thermal expansion of 23×10^{-6} °C^{-1}. The distances of C were about 48 mm in X-axis and 30 mm in Y-axis. The dimension of reference mirror mount was 8 mm (super-Invar) and the thickness of reference mirror was 6 mm (Quartz). An estimated material temperature-change was 0.025 °C during each pitch measurement. Therefore, the changes of C were $(48\times23+8\times0.6+6\times8)\times10^{-6}\times0.025 = 28.92$ (nm) associated with a standard uncertainty $u(C)$ of 8.35 nm in X-axis (Rectangular distribution), and $(30\times23+8\times0.6+6\times8)\times10^{-6}\times0.025 = 18.57$ (nm) associated with a standard uncertainty of 5.36 nm in Y-axis (Rectangular distribution). The sensitivity coefficient was -1 (see section 5.7.3 on page 63). The relative uncertainty was $\Delta u(x_i)/\ u(x_i)=0.2$, which gives the degrees of freedom $\nu(C)=12.5$, as derived by equation 5.6.

5.7.2.6 Dead path (B)

The estimated dead path (B) was 20 mm as shown in Figure 5.18. The combined standard uncertainty of refractive index of air $u(n_{tpf})$ was 0.222×10^{-6}. The deviation of B is $20 \times 0.222 \times 10^{-6} \times (0.05/0.3) = 0.74$ (nm). Assuming that its contribution was attributed as a rectangular distribution. The standard uncertainty $u(B)$ was 0.21 nm, and the sensitivity ceofficient was –1 (see section 5.7.3 on page 63). The relative uncertainty was $\Delta u(x_i)/u(x_i)=0.2$, which gives the degrees of freedom $\nu(B) =12.5$, as derived by equation 5.6.

5.7.2.7 Stage alignment

The laser beam of the interferometer must parallel to the moving axis (X) of the flexure stage used. The deviation of the flexure stage was about 20 nm read from Y-axis laser interferometer over the whole 100 µm travel range in X-axis. So the deviation of angle between laser beam and moving axis of flexure stage was $\pm \tan^{-1} \dfrac{20}{100000} \approx \pm 1'$ (see Figure 5.19 (a)). Assuming that its contribution was attributed as a rectangular distribution. The standard uncertainty of alignment $u(\theta)$ was 0.57735 ’ or 2.9089×10^{-4}, and the sensitivity coefficient was 0 (see section 5.7.3 on page 63). The relative uncertainty was $\Delta u(x_i)/u(x_i)=0.2$, which gives the degrees of freedom $\nu(\theta) =12.5$, as derived by equation 5.6.

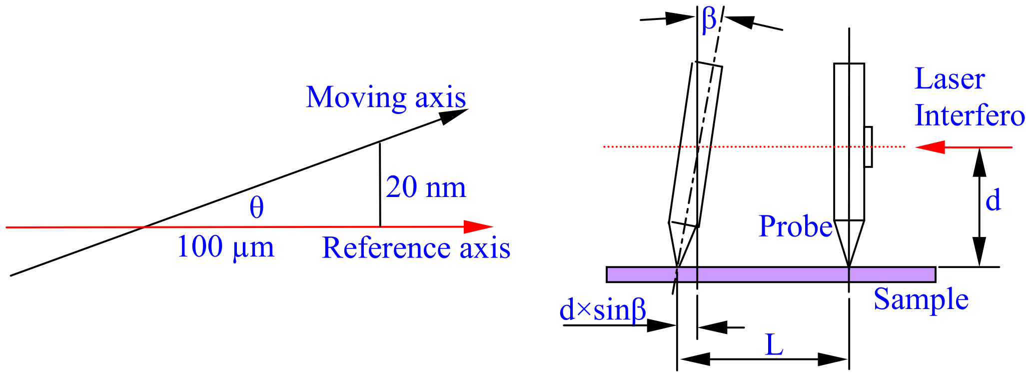

(a) Stage alignment error (b) Abbe error

Figure 5.19 Stage alignment error and Abbe error

5.7.2.8 Abbe error

The Abbe error can be calculated by the Abbe offset, the vertical distance between the measuring axis and the standard axis. The Abbe error is $d \times \sin\beta$ (see Figure 5.19(b)). The Abbe offset was less than 1 mm and the angular deviation was 0.5 arc sec, therefore the standard uncertainty of angle deviation $u(\beta)$ was 0.289 ” (1.4×10^{-6}). The sensitivity coefficient of angle deviation $\frac{\partial F}{\partial \beta}$ was 1 mm (see section 5.7.3 on page 63). The relative uncertainty was $\Delta u(x_i)/\ u(x_i)=0.2$, which gives the degrees of freedom $\nu(\beta)=12.5$, as derived by equation 5.6.

5.7.2.9 Measurement repeatability

A. TAFM by use of laser interferometer

The SIOS differential plane mirror laser interferometer can measure the displacements of a moving flexure stage. In a pitch measurement experiment, the displacement in X-axis was 3146.63 nm and the displacement in Y-axis was 3242.97 nm. The standard uncertainties in X-axis and Y-axis were $u(N_x)=s_x/\sqrt{16}/0.077=3.75$ and $u(N_y)=s_y/\sqrt{16}/0.077=147.5$, respectively, where s_x and s_y are standard deviation of displacement measurements in the X and Y directions, respectively. The sensitivity coefficient was 0.077 nm and the degrees of freedom were 15.

B. Matlab program and SPIP software

In practice, the pitch measurement was carried out by a TAFM, a Matlab program and a SPIP software. The average pitch value was 292.63 nm and the standard deviation was 0.282 nm of 16 measurements. So the sensitivity coefficient was 1 and the degrees of freedom were 15.

According to above information, the standard uncertainty of the TAFM $u(\varepsilon_{P_1})$ was $0.282/\sqrt{16}=0.071$ (nm). The standard uncertainty of SPIP software $u(\varepsilon_{P_2})$ was 0.048 nm, sensitivity coefficient was 1 and the degrees of freedom were 39 (see appendix 9.3).

5.7.3 Sensitivity Coefficient

The sensitivity coefficient is calculated by partial differentiating each parameter of the measuring equation. The equation 5.1 (see page 54) can be expanded as:

$$P=\frac{1}{m-1}\left\{\begin{array}{l}\left[(x_2-x_1)^2+(y_2-y_1)^2\right]^{1/2}+\left[(x_3-x_2)^2+(y_3-y_2)^2\right]^{1/2}+\cdots\cdots\\+\left[(x_{m-1}-x_{m-2})^2+(y_{m-1}-y_{m-2})^2\right]^{1/2}+\left[(x_m-x_{m-1})^2+(y_m-y_{m-1})^2\right]^{1/2}\end{array}\right\}+\varepsilon_{P_1}+\varepsilon_{P_2}\ . \quad (5.7)$$

The sensitivity coefficients of x_i are derived by the partial differentiating the equation 5.7: (where Ø indicate the angle between the normal of grating and X- axis.)

$$c_{x_1} = \frac{\partial P}{\partial x_1} = \frac{1}{m-1} \times \frac{1}{2}\left[(x_2 - x_1)^2 + (y_2 - y_1)^2\right]^{-1/2} \times (-2)(x_2 - x_1) \approx -\frac{(x_2 - x_1)}{P(m-1)} \approx -\frac{\cos\phi}{m-1} \ ,$$

$$c_{x_2} = \frac{\partial P}{\partial x_2} = \frac{1}{m-1} \times \begin{Bmatrix} \frac{1}{2}\left[(x_2 - x_1)^2 + (y_2 - y_1)^2\right]^{-1/2} \times 2(x_2 - x_1) \\ + \frac{1}{2}\left[(x_3 - x_2)^2 + (y_3 - y_2)^2\right]^{-1/2} \times (-2)(x_3 - x_2) \end{Bmatrix} \approx 0 \approx c_{x_3} \approx c_{x_4} \approx \cdots \approx c_{x_{m-1}} \ ,$$

$$c_{x_m} = \frac{\partial P}{\partial x_m} = \frac{1}{m-1} \times \frac{1}{2}\left[(x_m - x_{m-1})^2 + (y_m - y_{m-1})^2\right]^{-1/2} \times 2(x_m - x_{m-1}) \approx \frac{(x_m - x_{m-1})}{P(m-1)} \approx \frac{\cos\phi}{m-1} .$$

Alternatively, it can also obtain the sensitivity coefficients of y_i by partial differentiating the equation 5.7:

$$c_{y_1} = \frac{\partial P}{\partial y_1} \approx -\frac{\sin\phi}{m-1} ,$$

$$c_{y_2} = \frac{\partial P}{\partial y_2} \approx 0 \approx c_{y_3} \approx c_{y_4} \approx \cdots \approx c_{y_{m-1}} ,$$

$$c_{y_m} = \frac{\partial P}{\partial y_m} \approx \frac{\sin\phi}{m-1} .$$

The x_i and y_i are obtained from the laser interferometers while the sample is moving by the flexure stage. So x_i and y_i are the displacements of the flexure stage in the X and Y directions, respectively. The sensitivity coefficients of each parameter of the displacement from the laser interferometers can be obtained as following (where L is the displacement):

$$\frac{\partial F}{\partial \lambda_0} = \left[1 + \alpha(20 - t_s)\right]\frac{1}{8192\, n_{tpf}} N(1 - \frac{\theta^2}{2}) \approx \frac{L}{\lambda_0} = \frac{L}{0.632991234 \ \mu m} = 1.5798\, L \mu m^{-1} ,$$

$$\frac{\partial F}{\partial n_{tpf}} = -\left[1 + (20 - t_s)\right]\frac{\lambda_0}{8192\, {n_{tpf}}^2} N(1 - \frac{\theta^2}{2}) \approx -\frac{L}{n_{tpf}} \approx -\frac{L}{1.000273} = -0.9997\, L ,$$

$$\frac{\partial F}{\partial t} = \frac{\partial F}{\partial n_{tpf}} \frac{\partial n_{tpf}}{\partial t} = \frac{\partial F}{\partial n_{tpf}} \left[A\frac{\partial B}{\partial t} - \frac{\partial C}{\partial t} \right] \approx 9.53 \times 10^{-7} L \ {}^{\circ}C^{-1} ,$$

$$\frac{\partial F}{\partial p}=\frac{\partial F}{\partial n_{tpf}}\frac{\partial n_{tpf}}{\partial p}=\frac{\partial F}{\partial n_{tpf}}\left[A\frac{\partial B}{\partial p}+B\frac{\partial A}{\partial p}\right]\approx -2.68\times 10^{-9}L\ Pa^{-1},$$

$$\frac{\partial F}{\partial f}=\frac{\partial F}{\partial n_{tpf}}\left[\frac{\partial n_{tpf}}{\partial f}+\frac{\partial n_{tpf}}{\partial (RH)}\right]\approx 8.5\times 10^{-9}L\ \%\mathrm{RH}^{-1},$$

$$\frac{\partial F}{\partial N}=\left[1+\alpha(20-t_s)\right]\frac{\lambda_0}{8192\ n_{tpf}}(1-\frac{\theta^2}{2})\approx\frac{\lambda_0}{8192\ n_{tpf}}=0.077\quad nm\ ,$$

$$\frac{\partial F}{\partial \alpha}=(20-t_s)\left[A-B-C+\frac{\lambda_0}{8192n_{tpf}}N(1-\frac{\theta^2}{2})+d\times\sin\beta\right]\approx 0\ ,$$

$$\frac{\partial F}{\partial t_s}=-\alpha\left[A-B-C+\frac{\lambda_0}{8192n_{tpf}}N(1-\frac{\theta^2}{2})+d\times\sin\beta\right]\approx -\alpha L\ ^{\circ}C^{-1},$$

$$\frac{\partial F}{\partial A}=\left[1+\alpha(20-t_s)\right]\approx 1\ ,\quad \frac{\partial F}{\partial C}\approx -1\ ,$$

$$\frac{\partial F}{\partial B}=-\left[1+\alpha(20-t_s)\right]\approx -1,$$

$$\frac{\partial F}{\partial \theta}=-\left[1+\alpha(20-t_s)\right]\frac{\lambda_0}{8192\ n_{tpf}}N\theta\approx -\theta L\approx 0\ ,$$

$$\frac{\partial F}{\partial \beta}=d\times\cos\beta\ .$$

5.7.4 Combined Standard Uncertainty

According to the "Guide to the expression of uncertainty in measurement"[12], the combined standard uncertainty can be expressed:

$$u_c^2(y)=\sum_{i=1}^{N}\left[\frac{\partial f}{\partial x_i}\right]u^2(x_i)+2\sum_{i=1}^{N-1}\sum_{j=i+1}^{N}\frac{\partial f}{\partial x_i}\frac{\partial f}{\partial x_j}u(x_i,x_j)\ . \tag{5.8}$$

Substituting the results of the sensitivity coefficients and the standard uncertainties into equation 5.8, the combined standard uncertainty of pitch measurement can be obtained as:

$$\begin{aligned}u_c^{\,2}(P)&=c_{x_1}^2u^2(x_1)+c_{x_m}^2u^2(x_m)+c_{y_1}^2u^2(y_1)+c_{y_m}^2u^2(y_m)+u^2(\varepsilon_{P_1})+u^2(\varepsilon_{P_2})\\&=\frac{2\cos^2\phi}{(m-1)^2}u_c^{\,2}(x)+\frac{2\sin^2\phi}{(m-1)^2}u_c^{\,2}(y)+u^2(\varepsilon_{P_1})+u^2(\varepsilon_{P_2})\end{aligned}\quad , \tag{5.9}$$

where

$$u_c^{\,2}(x)=[\frac{\partial F}{\partial \lambda_0}]^2[u(\lambda_0)]^2+[\frac{\partial F}{\partial n_{tpf}}]^2[u(n_{tpf})]^2+[\frac{\partial F}{\partial \alpha}]^2[u(\alpha)]^2+[\frac{\partial F}{\partial t_s}]^2[u(t_s)]^2+[\frac{\partial F}{\partial \theta}]^2[u(\theta)]^2+[\frac{\partial F}{\partial N_x}]^2[u(N_x)]^2$$
$$+[\frac{\partial F}{\partial \beta}]^2[u(\beta)]^2+[\frac{\partial F}{\partial A}]^2[u(A)]^2+[\frac{\partial F}{\partial C}]^2[u(C)]^2+[\frac{\partial F}{\partial B}]^2[u(B)]^2 \quad , (5.10)$$

and

$$u_c^{\,2}(y)=[\frac{\partial F}{\partial \lambda_0}]^2[u(\lambda_0)]^2+[\frac{\partial F}{\partial n_{tpf}}]^2[u(n_{tpf})]^2+[\frac{\partial F}{\partial \alpha}]^2[u(\alpha)]^2+[\frac{\partial F}{\partial t_s}]^2[u(t_s)]^2+[\frac{\partial F}{\partial \theta}]^2[u(\theta)]^2+[\frac{\partial F}{\partial N_y}]^2[u(N_y)]^2$$
$$+[\frac{\partial F}{\partial \beta}]^2[u(\beta)]^2+[\frac{\partial F}{\partial A}]^2[u(A)]^2+[\frac{\partial F}{\partial C}]^2[u(C)]^2+[\frac{\partial F}{\partial B}]^2[u(B)]^2 \quad . (5.11)$$

Table 5.2 shows the error budget including the error sources, estimated uncertainty, error type, distribution, standard uncertainty, sensitivity coefficient, and degrees of freedom.

Table 5.2 Error budget (X direction)

Error (x_i)	Estimated Uncertainty	TYPE	Distribution	Standard Uncertainty	$\frac{\partial F}{\partial x_i}$	$\left\lvert\frac{\partial F}{\partial x_i}u(x_i)\right\rvert$	ν_i
Laser Interferometer						1.15 nm	50
Wavelength(λ_0)	1.27×10^{-8} μm	B	$1/\sqrt{3}$	0.73×10^{-8} μm	$1.5798L_x$ μm^{-1}	0.012×10^{-6} L_x	(50)
Non-linearity(λ_n)	2 nm	B	$1/\sqrt{3}$	1.15 nm	1	1.15 nm	(50)
Refractive index of Air						0.222×10^{-6} L_x	50
Formular	3×10^{-8}	B	$1/\sqrt{3}$	1.732×10^{-8}	-0.9997 L_x	0.0173×10^{-6} L_x	(50)
Temperature(t)	0.3 °C	B	$1/\sqrt{3}$	0.173 °C	9.53×10^{-7} L_x °C^{-1}	0.165×10^{-6} L_x	(50)
Air Pressure(p)	50 Pa	B	$1/\sqrt{3}$	28.87 Pa	-2.68×10^{-9} L_x Pa^{-1}	0.0774×10^{-6} L_x	(50)
Relative Humidity	10 %	B	$1/\sqrt{3}$	5.77 %	8.5×10^{-9} L_x %$^{-1}$	0.049×10^{-6} L_x	(50)
CTE(α)	1×10^{-6} °C^{-1}	B	$1/\sqrt{3}$	0.577×10^{-6} °C^{-1}	0	0	50
Sample Temperature (t_s)	0.3 °C	B	$1/\sqrt{3}$	0.173 °C	-2.55×10^{-6} L_x°C^{-1}	0.441×10^{-6} L_x	50
Mechanical structure						8.36 nm	12.5
A	1.23 nm	B	$1/2\sqrt{3}$	0.36 nm	1	0.36 nm	(12.5)
C	28.92 nm	B	$1/2\sqrt{3}$	8.35 nm	-1	8.35 nm	(12.5)
Dead Path (B)	0.74 nm	B	$1/2\sqrt{3}$	0.21 nm	-1	0.21 nm	12.5
Stage alignment (θ)	1’	B	$1/\sqrt{3}$	0.577 ’	0	0	12.5
Abbe error (β)	0.5 ”	B	$1/\sqrt{3}$	0.2886 ”	1 mm	1.4 nm	12.5
Pitch Measuring (N_x)	$u(N_x)$	A	1	$u(N_x)$	0.077 nm	0.077 $u(N_x)$ nm	15

Table 5.2 Error budget (Y direction)

Error (y_i)	Estimated Uncertainty	TYPE	Distribution	Standard Uncertainty	$\frac{\partial F}{\partial y_i}$	$\left\lvert\frac{\partial F}{\partial y_i} u(y_i)\right\rvert$	ν_i
Laser Interferometer						1.15 nm	50
Wavelength(λ_0)	1.27×10^{-8}μm	B	$1/\sqrt{3}$	0.73×10^{-8}μm	$1.5798 L_y$ μm^{-1}	$0.012\times10^{-6} L_y$	(50)
Non-linearity(λ_n)	2 nm	B	$1/\sqrt{3}$	1.15 nm	1	1.15 nm	(50)
Refractive index of Air						$0.222\times10^{-6} L_y$	50
Formular	3×10^{-8}	B	$1/\sqrt{3}$	1.732×10^{-8}	$-0.9997 L_y$	$0.0173\times10^{-6} L_y$	(50)
Temperature(t)	0.3 °C	B	$1/\sqrt{3}$	0.173 °C	$9.53\times10^{-7} L_y$ °C^{-1}	$0.165\times10^{-6} L_y$	(50)
Air Pressure(p)	50 Pa	B	$1/\sqrt{3}$	28.87 Pa	$-2.68\times10^{-9} L_y$ Pa^{-1}	$0.0774\times10^{-6} L_y$	(50)
Relative Humidity	10 %	B	$1/\sqrt{3}$	5.77 %RH	$8.5\times10^{-9} L_y$ %$^{-1}$	$0.049\times10^{-6} L_y$	(50)
CTE(α)	1×10^{-6}°C^{-1}	B	$1/\sqrt{3}$	0.577×10^{-6}°C^{-1}	0	0	50
Sample Temperature (t_s)	0.3 °C	B	$1/\sqrt{3}$	0.173 °C	$-2.55\times10^{-6} L_y$°C^{-1}	$0.441\times10^{-6} L_y$	50
Mechanical structure						5.37 nm	12.5
A	1.23 nm	B	$1/2\sqrt{3}$	0.36 nm	1	0.36 nm	(12.5)
C	18.57 nm	B	$1/2\sqrt{3}$	5.36 nm	-1	5.36 nm	(12.5)
Dead Path (B)	0.74 nm	B	$1/2\sqrt{3}$	0.21 nm	-1	0.21 nm	12.5
Stage alignment (θ)	1’	B	$1/\sqrt{3}$	0.577’	0	0	12.5
Abbe error (β)	0.5 ”	B	$1/\sqrt{3}$	0.2886 ”	1 mm	1.4 nm	12.5
Pitch Measuring (N_y)	$u(N_y)$	A	1	$u(N_y)$	0.077 nm	$0.077\ u(N_y)$ nm	15

In table 5.1, the mean value of 16 pitch measurements is 291.63 nm, and the standard uncertainty is 0.071 nm. Substituting the values of table 5.2 into equation 5.10 and 5.11, the combined standard uncertainty of displacements in the X and Y directions can be expressed as:

$$\begin{aligned} u_c^{\,2}(x) &= (1.15\text{ nm})^2 + (0.222\times10^{-6} L_x)^2 + (0.441\times10^{-6} L_x)^2 + (8.36\text{ nm})^2 + (0.21\text{ nm})^2 \\ &\quad + (1.4\text{ nm})^2 + (0.077\ u(N_x)\text{ nm})^2 \\ &= (8.56\text{ nm})^2 + (0.49\times10^{-6} L_x)^2 + (0.077\ u(N_x)\text{ nm})^2 \end{aligned} ,$$

$$\begin{aligned} u_c^{\,2}(y) &= (1.15\text{ nm})^2 + (0.222\times10^{-6} L_y)^2 + (0.441\times10^{-6} L_y)^2 + (5.37\text{ nm})^2 + (0.21\text{ nm})^2 \\ &\quad + (1.4\text{ nm})^2 + (0.077\ u(N_y)\text{ nm})^2 \\ &= (5.67\text{ nm})^2 + (0.49\times10^{-6} L_y)^2 + (0.077\ u(N_y)\text{ nm})^2 \end{aligned} ,$$

and simplified as:

$$u_c(x) = \sqrt{(8.56\text{ nm})^2 + (0.077\ u(N_x)\text{ nm})^2 + (0.49\times10^{-6} L_x)^2}\ , \tag{5.12}$$

$$u_c(y) = \sqrt{(5.67\text{ nm})^2 + (0.077\ u(N_y)\text{ nm})^2 + (0.49\times10^{-6} L_y)^2}\ . \tag{5.13}$$

Substituting equation 5.12 and 5.13 into equation 5.9, the combined standard uncertainty of pitch measurement is expressed as:

$$\begin{aligned} u_c^{\,2}(P) = {} & \frac{2\cos^2\phi}{(m-1)^2}[(8.56\,\mathrm{nm})^2 + (0.49\times10^{-6}L_x)^2 + (0.077\times u(N_x)\,\mathrm{nm})^2] \\ & + \frac{2\sin^2\phi}{(m-1)^2}[(5.67\,\mathrm{nm})^2 + (0.49\times10^{-6}L_y)^2 + (0.077\times u(N_y)\,\mathrm{nm})^2] + (0.048\,\mathrm{nm})^2 + u^2(\varepsilon_{P_1}) \end{aligned},$$

where $u(N_x) = u(L_x)/0.077$, the combined standard uncertainty of pitch measurement can be rearranged as:

$$u_c(P) = \left\{ \begin{array}{l} \dfrac{1}{(m-1)^2}\left[\begin{array}{c} \left((12.11\,\mathrm{nm})^2 + (0.69\times10^{-6}L_x)^2 + (1.414\,u(L_x)\,\mathrm{nm})^2\right)\cos^2\phi + \\ \left((8.02\,\mathrm{nm})^2 + (0.69\times10^{-6}L_y)^2 + (1.414\,u(L_x)\,\mathrm{nm})^2\right)\sin^2\phi \end{array} \right] \\ + (0.048\,\mathrm{nm})^2 + u^2(\varepsilon_{P_1}) \end{array} \right\}^{1/2} \qquad (5.14)$$

5.7.5 Expanded Uncertainty

Generally, the expanded uncertainty *U* is intended to provide an interval about the result of a measurement that may be expected to encompass a large fraction of the distribution of values that could reasonably be attributed to the measurand [12]. The expanded uncertainty is obtained by multiplying the combined standard uncertainty $u_c(y)$ by a coverage factor *k*:

$$U = ku_c(y)\,. \qquad (5.14)$$

The coverage factor *k* is chosen on the basis of the level of confidence required of the interval *y-U* to *y+U*. It can be found from the *t*-distribution at a confidence level t_c and degrees of freedom ν.

Substituting the measuring result of table 5.1 into equation 5.14, yields the combined standard uncertainty of the 292 nm pitch standard $u_c(P)$:

$$\begin{aligned} u_c(P) &= \left\{ \begin{array}{l} \dfrac{1}{10^2}\left[\begin{array}{c} \left((12.11\,\mathrm{nm})^2 + (0.69\times10^{-6}\times3146.63\,\mathrm{nm})^2 + (1.414\times0.29\,\mathrm{nm})^2\right)\cos^2 2^\circ + \\ \left((8.02\,\mathrm{nm})^2 + (0.69\times10^{-6}\times3242.97\,\mathrm{nm})^2 + (1.414\times11.37\,\mathrm{nm})^2\right)\sin^2 2^\circ \end{array} \right] \\ + (0.048\,\mathrm{nm})^2 + (0.071\,\mathrm{nm})^2 \end{array} \right\}^{1/2} . \\ &= 1.22\,\mathrm{nm} \end{aligned}$$

According to the Welch-Satterthwatte formula [12], the effective degrees of freedom (ν_{eff}) of pitch measurement is derived by:

$$\nu_{eff}(y) = \frac{u_c^{\,4}(y)}{\sum_{i=1}^{n} \frac{u_i^{\,4}(y)}{\nu_i(y)}} \tag{5.15}$$

$$\begin{aligned}\nu_{eff}(P) &= \frac{u_c^{\,4}(P)}{\frac{[c_{x_1}u(x_1)]^4}{\nu(x_1)} + \frac{[c_{x_m}u(x_m)]^4}{\nu(x_m)} + \frac{[c_{y_1}u(y_1)]^4}{\nu(y_1)} + \frac{[c_{y_m}u(y_m)]^4}{\nu(y_m)} + \frac{[c_{\varepsilon_{P_1}}u(\varepsilon_{P_1})]^4}{\nu(\varepsilon_{P_1})} + \frac{[c_{\varepsilon_{P_2}}u(\varepsilon_{P_2})]^4}{\nu(\varepsilon_{P_2})}}, \\ &= \frac{u_c^{\,4}(P)}{\frac{2[c_x u_c(x)]^4}{\nu_c(x)} + \frac{2[c_y u_c(y)]^4}{\nu_c(y)} + \frac{[c_{\varepsilon_{P_1}}u(\varepsilon_{P_1})]^4}{\nu(\varepsilon_{P_1})} + \frac{[c_{\varepsilon_{P_2}}u(\varepsilon_{P_2})]^4}{\nu(\varepsilon_{P_2})}}\end{aligned}$$

where $u_c(y)$ is combined Standard uncertainty of estimated output y, $u_i(y)$ is component of combined Standard uncertainty $u_c(y)$ of input x_i, $\nu_i(y)$ is degrees of freedom of standard uncertainty $u(x_i)$ of estimated input x_i. The sensitivity coefficients, standard uncertainties, and degrees of freedom of displacements in X and Y directions are described as following.

$$c_x = (\cos 2°)/(11-1) = 9.99\times10^{-2}$$

$$c_y = (\sin 2°)/(11-1) = 3.49\times10^{-3}$$

$$c_{\varepsilon_{P_1}} = 1$$

$$c_{\varepsilon_{P_2}} = 1$$

$$u_c(x) = \sqrt{(8.56\,\text{nm})^2 + u^2(L_x) + (0.49\times10^{-6}L_x)^2} = 8.56\,(\text{nm})$$

$$u_c(y) = \sqrt{(5.67\,\text{nm})^2 + u^2(L_x) + (0.49\times10^{-6}L_y)^2} = 12.71\,(\text{nm})$$

$$u(\varepsilon_{P_1}) = 0.071\,(\text{nm})$$

$$u(\varepsilon_{P_2}) = 0.048\,(\text{nm})$$

$$\nu_c(x) = \frac{8.56^4}{\frac{1.15^4}{50} + \frac{(6.99\times10^{-4})^4}{50} + \frac{(1.39\times10^{-3})^4}{50} + \frac{8.36^4}{12.5} + \frac{0.21^4}{12.5} + \frac{1.4^4}{12.5} + \frac{0.29^4}{15}} = 13.73$$

$$\nu_c(y) = \frac{12.71^4}{\frac{1.15^4}{50} + \frac{(7.20\times10^{-4})^4}{50} + \frac{(1.43\times10^{-3})^4}{50} + \frac{5.37^4}{12.5} + \frac{0.21^4}{12.5} + \frac{1.4^4}{12.5} + \frac{11.37^4}{15}} = 22.10$$

$$\nu(\varepsilon_{P_1}) = 15$$

$$\nu(\varepsilon_{P_2}) = 39$$

Then substituting these into equation 5.15, the effective degrees of freedom of pitch measurement can be obtained.

$$\nu_{eff}(P)=\frac{1.22^4}{\frac{2\times(9.99\times10^{-2}\times8.56)^4}{13.73}+\frac{2\times(3.49\times10^{-3}\times12.71)^4}{22.10}+\frac{(1\times0.071)^4}{15}+\frac{(1\times0.048)^4}{39}}\approx29$$

From *t*-distribution, it gives a 2.05 of effective degrees of freedom by a coverage factor *k* of 29 at 95 % confidence level (see table 5.3). So, the expanded uncertainty of any pitch measurement in a measuring area of 100 μm × 100 μm is expressed as:

$$U=k\times u_c(P)=2.05\times\left\{\begin{array}{l}\frac{1}{(m-1)^2}\left[\begin{array}{l}\left((12.11\,\mathrm{nm})^2+(0.69\times10^{-6}L_x)^2+(1.414\,u(L_x)\,\mathrm{nm})^2\right)\cos^2\phi+\\ \left((8.02\,\mathrm{nm})^2+(0.69\times10^{-6}L_y)^2+(1.414\,u(L_x)\,\mathrm{nm})^2\right)\sin^2\phi\end{array}\right]\\ +(0.048\,\mathrm{nm})^2+u^2(\varepsilon_{P1})\end{array}\right\}^{\frac{1}{2}}$$

$$\approx\left[(2.5nm)^2+4.2u^2(\varepsilon_{p1})\right]^{1/2} \tag{5.16}$$

Table 5.3 Coverage factor defined from the degrees of freedom and confidence level

Degrees of freedom (ν)	Fraction in percent					
	68.27	90	95	95.45	99	99.73
1	1.84	6.31	12.71	13.97	63.66	235.80
2	1.32	2.92	4.30	4.53	9.92	19.21
3	1.20	2.35	3.18	3.31	5.84	9.22
4	1.14	2.13	2.78	2.87	4.60	6.62
5	1.11	2.02	2.57	2.65	4.03	5.51
6	1.09	1.94	2.45	2.52	3.71	4.90
7	1.08	1.89	2.36	2.43	3.50	4.53
8	1.07	1.86	2.31	2.37	3.36	4.28
9	1.06	1.83	2.26	2.32	3.25	4.09
10	1.05	1.81	2.23	2.28	3.17	3.96
11	1.05	1.80	2.20	2.25	3.11	3.85
12	1.04	1.78	2.18	2.23	3.05	3.76
13	1.04	1.77	2.16	2.21	3.01	3.69
14	1.04	1.76	2.14	2.20	2.98	3.64
15	1.03	1.75	2.13	2.18	2.95	3.59
16	1.03	1.75	2.12	2.17	2.92	3.54
17	1.03	1.74	2.11	2.16	2.90	3.51
18	1.03	1.73	2.10	2.15	2.88	3.48
19	1.03	1.73	2.09	2.14	2.86	3.45
20	1.03	1.72	2.09	2.13	2.85	3.42
25	1.02	1.71	2.06	2.11	2.79	3.33
30	1.02	1.70	2.04	2.09	2.75	3.27
35	1.01	1.70	2.03	2.07	2.72	3.23
40	1.01	1.68	2.02	2.06	2.70	3.20
45	1.01	1.68	2.01	2.06	2.69	3.18
50	1.01	1.68	2.01	2.05	2.68	3.16
100	1.005	1.660	1.984	2.025	2.626	3.007
∞	1.000	1.645	1.960	2.000	2.576	3.000

5.8 Discussion

A Traceable Atomic Force Microscope has been developed in the Center for Measurement Standards in Taiwan. The TAFM can be used to calibrate the one-dimensional pitch standards and provide the traceability of commercial Scanning Probe Microscope. The TAFM consists of a commercial Atomic Force Microscope, an active-error-compensated flexure stage, two differential plane mirror laser interferometers, a vibration isolator, and a super-Invar metrology frame. The design concepts include the metric, the carriage and driver, the metrology frame, the probe, the isolation, the symmetry, and the alignment [90-91]:

(1). Metric: Differential plane mirror laser interferometer

The displacements of the TAFM should be directly traceable to the SI. The displacements can be measured by different sensors such as optical scale, x-ray interferometer, Fabry-Perot interferometer, linear variable differential transducer (LVDT), capacitance sensor, and laser interferometer. Figure 5.20 shows the limits of realizing a metric. A laser interferometer is one of the instruments to realize the displacement measurement and to trace to the SI. The advantages of laser interferometer are high resolution and large measuring range, direct trace to laser wavelength, fast and ease of use. The limitations are periodic nonlinearity, ghosts and diffraction effects. Figure 2.5 (see page 6) shows the traceability of AFM. In the TAFM, two Differential plane mirror laser interferometers were assembled in X and Y-axes. They were used to measure the displacements of test sample seated on the flexure stage in the X and Y directions.

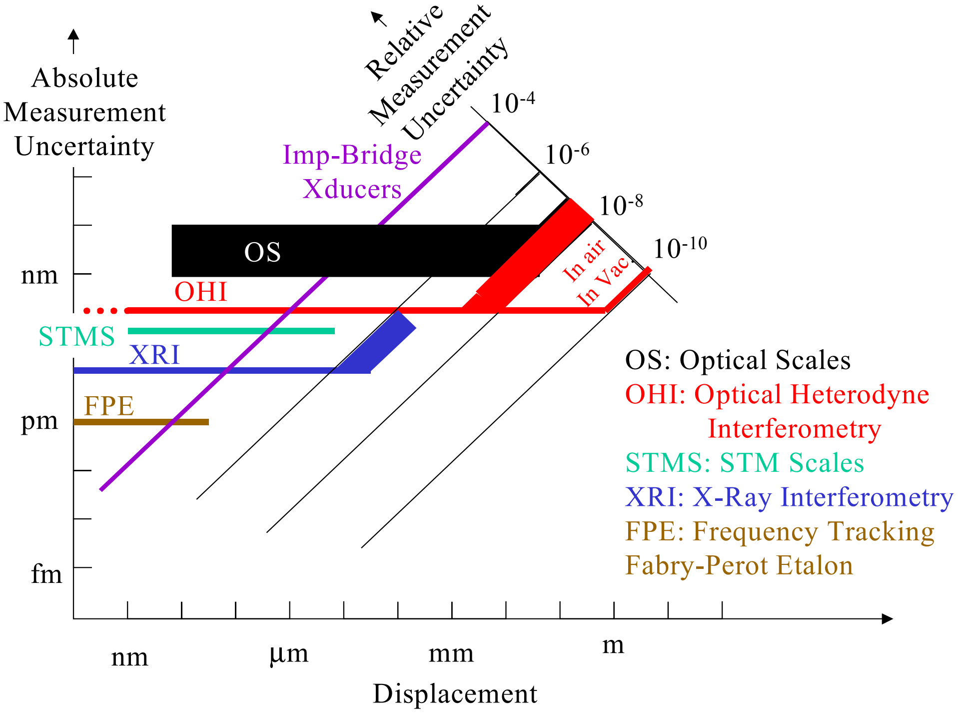

Figure 5.20 Limits of realizing a metric [92]

(2). Carriage and driver: Active error compensation flexure stage

An instrument for displacement measuring should contain a carriage and a driver. The carriage supplies a guide way of linear motion and the driver gives a linear motion. The carriages can be realized by commercial products like sliding bearing guide way, roller bearing guide way, air bearing guide way, magnetic bearing guide way, and flexure stage. The commercial drivers are stepping motor, DC/AC servomotor, friction-driving driver, voice coil, and piezo actuator. For the metrology systems, one should selects a guide way with good straightness error and angular deviation and a driver with high positioning resolution and accuracy. A coarse motion of 120 mm × 100 mm (component of commercial DI AFM) and a fine motion of 100 μm × 100 μm were original designed in the TAFM. The coarse motion system employed the ball bearing guide with stepping motor. The fine motion system was a custom-modified PI flexure stage. But the angular deviations (pitch and yaw) of coarse motion were bigger than 1 arc minute. Therefore, the coarse motion was not used. Then the measuring range was limited to 100μm × 100 μm. To avoid the errors caused by the intrinsic properties of the AFM scanner, a flexure stage gave the sample scanning of the TAFM. A special custom-modified flexure stage made by PI was installed in the TAFM. The stage contains 6 actuators and 6 capacitance sensors for the 3-axis active error compensation. The travel range was 100μm × 100 μm in the XY plane. The out-of-plane motion was 0.5 nm in the Z direction. The angular deviations were less than 0.5 arc sec in pitch and yaw.

(3). Metrology frame: Super-Invar

The relationship between mechanical stiffness and resonance frequency should be considered in mechanical structure design. Two basic design concepts, the structure loop and the metrology loop, are important for the design of measuring instruments. The structure loop is the path (or parallel paths) needed to trace from the probe tip through all parts of its holder and through the overall holding structure back to that part of the structure which holds the workpiece up to the corresponding points on the workpiece surface. To shorten structure loop path from the probe to the sample can achieve an improvement of the stiffness, and reduce the influences from vibration and temperature changes. The metrology loop is the continuous path from the sense point on the probe or contact point on the machine tool to a reference datum and then back to the contacted point on the workpiece [92]. Figure 5.21 shows the structure loop and metrology loop in Y-axis of the TAFM.

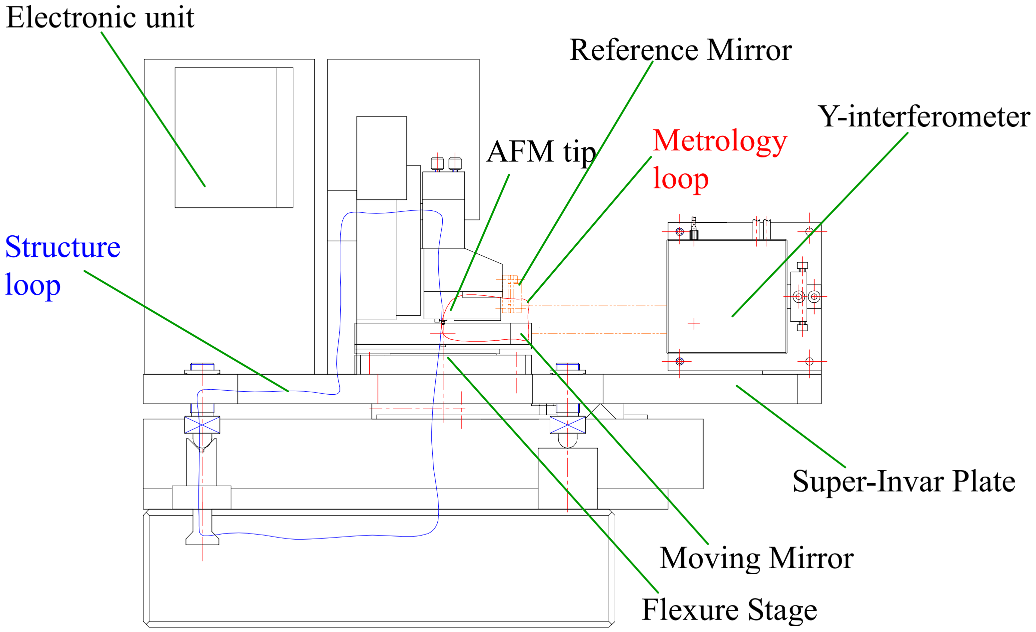

Figure 5.21 Structure loop and metrology loop in Y direction of the TAFM

(4). Probe: Atomic Force Microscope

A probe is any means by which features, edges, and surfaces are located. Figure 5.22 shows the sensitivity of different probes. Figure 5.23 shows the idea probe shape with only one atom on the tip. An AFM, as a probe, was used to measure the surface texture in the TAFM. Figure 5.24 shows the images obtained from different probes. The left image may be captured by a broken tip. So the shape of probe tip should be verified by a standard sample before starting to measure.

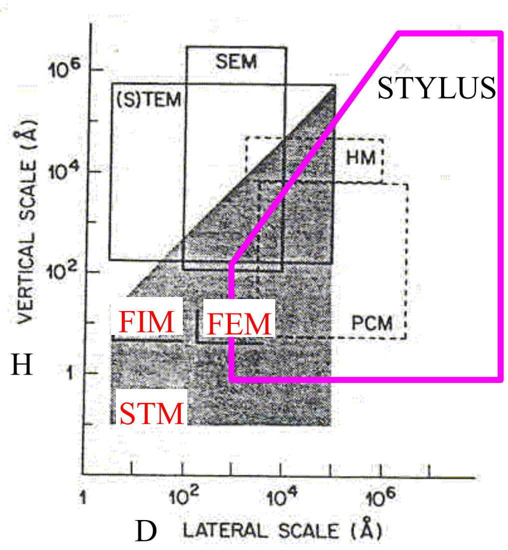

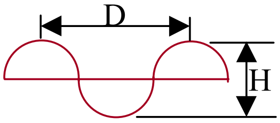

HM: high-resolution optical microscope,
PCM: phase contract microscope
FIM: field ion microscope
FEM: field emission microscope
AfterY. Kuk and P.J. Silverman, Rev. Sci. Instrum. 60, 165-180 1989

Figure 5.22 The sensitivity of different probes [91]

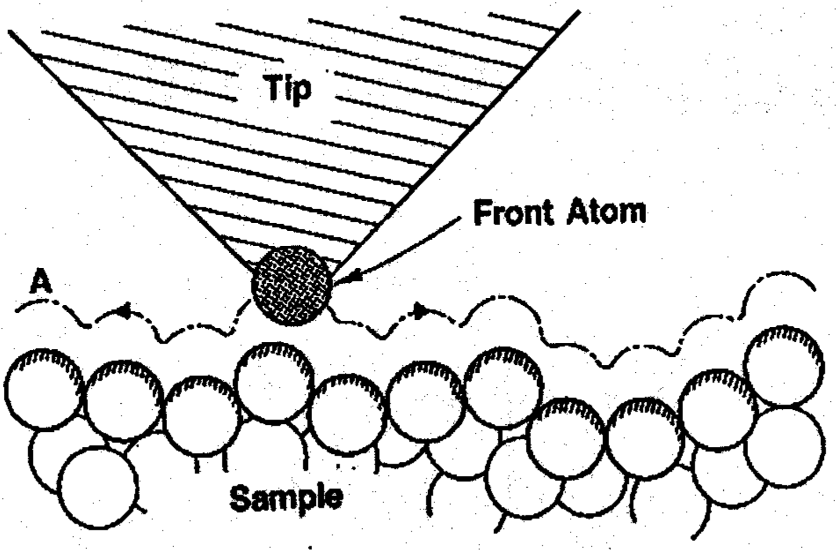

Figure 5.23 The idea AFM probe tip [90]

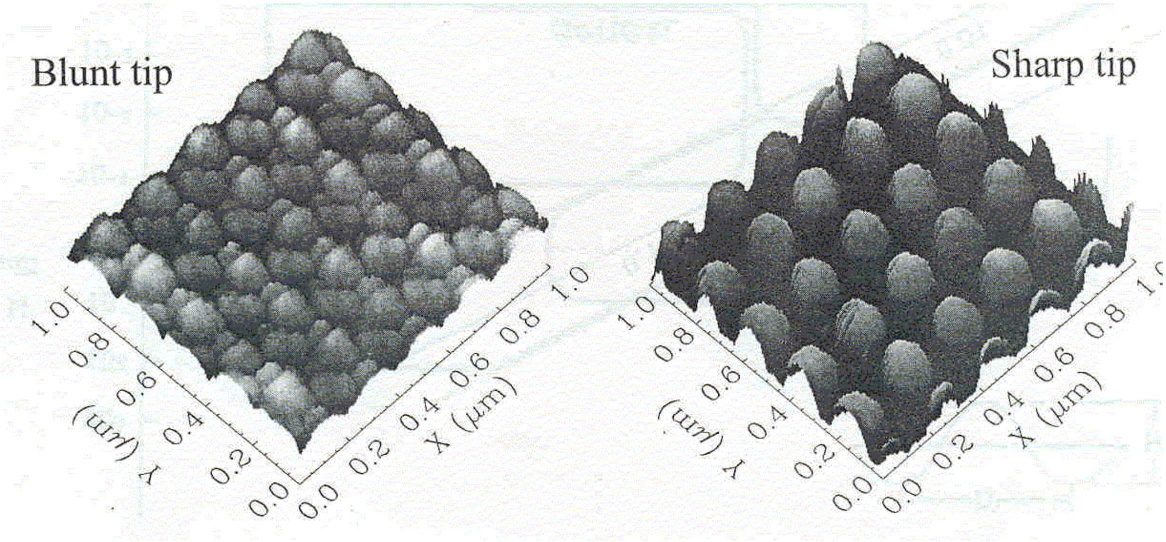

Figure 5.24 Images from different probes [90]

(5). Isolation: vibration isolator and temperature control

"The experiment must be so arranged that the effects of disturbing agents on the phenomena to be investigated are as small as possible" said by James Clerk Maxwell, 1890. Vibration and temperature changes will affect the results of dimensional measurement. Some disturbing agents, for instances, building: 1-10 Hz; traffic: 5-100 Hz; construction: 10-200 Hz; machinery: 10-200 Hz; acoustic: >20 Hz should be isolated. They may cause a noise of 20 nm and a drift of a few micrometers to the laser interferometer. A vibration isolator and a temperature-controlled enclosed box with circulating water can eliminate the noises and drifts from the environment. Figure 5.4

(see page 46) and Figure 5.5 (see page 47) show the laser interferometer test. The measuring noise of laser interferometer affected by conditioning air (in a temperature-controlled laboratory without an enclosed cover) was about 20 nm in 17 second. After adding an enclosed box made of stainless steel sheets and thermal isolation material to cover the whole measuring machine, the noise of laser interferometer was reduced to about 2 nm in 18 seconds.

(6). Symmetry:

The mechanical structure of dimensional measuring instrument with symmetric design will give good repeatability, stability, stiffness, and accuracy. The flexure stage is made with symmetric springs. The metrology frame made of super-Invar was nearly symmetrical in the X direction but asymmetrical in the Y direction (see Figure 5.21on page 70). A nearly symmetric design in the X direction of TAFM is shown in Figure 5.25. The super-Invar frame was supported by a quasi-kinematic mount with a set cone-vee-plane and fixed on the cone, and four screws with spheres on a granite base. The measuring results revealed evidences that the drift reading from the Y laser interferometer was bigger than that from the X laser interferometer. Figure 5.13 (see page 51) shows 1μm drift in X-axis, 3.8 μm drift in Y-axis, and 0.1 μm drift in Z-axis. They were caused by the temperature-change due to heat emission from the electronic unit of AFM. It can be improved by adding a temperature-controlled system with circulating water and changing the mechanical structure to symmetric design.

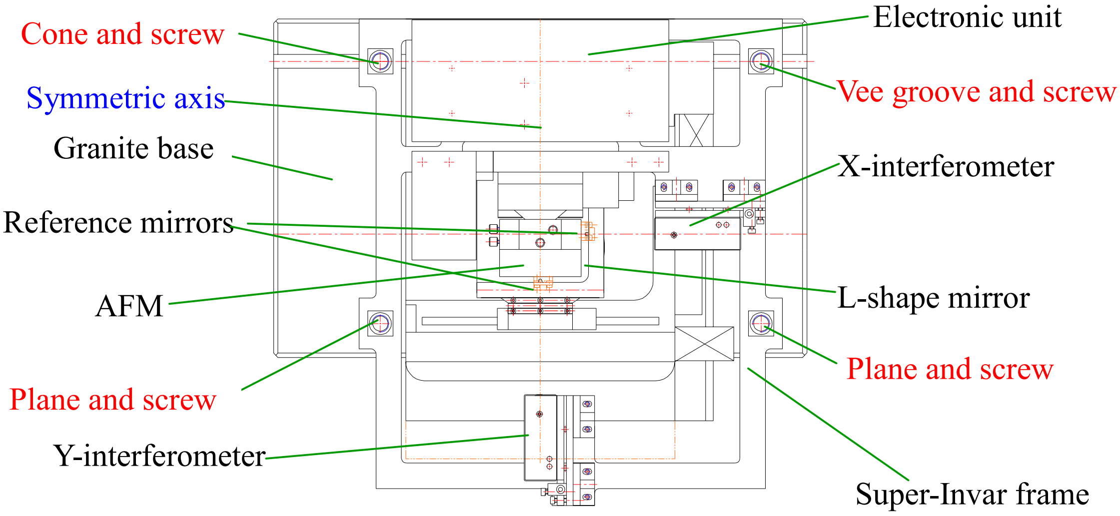

Figure 5.25 Nearly symmetric structure in the X direction of TAFM

(7). Alignment:

The first principle of machine design and dimensional metrology is the Abbe principle [73]. Ernst Abbe said “The measuring instrument is always to be constructed that the

> distance being measured is a straight line extension of the graduations on the scale that serves as the reference …", and "Should the measuring axis and that of the scale belong to two different axes which are separated by a certain distance… that length being read off will be identical to the length being measured in general only when the moving system… undergoes pure parallel motion, with no rotation. If the system undergoes a rotation between the initial and final settings, then the scale reading and the measured length is different".

Figure 5.26 shows the Abbe offsets (Abbe error equals d×sinβ). In the TAFM, a specimen was arranged on the same plane of the X and Y laser interferometers, and the AFM tip was on the intersection point of the lines extended from the laser beams of the X and Y interferometers. The angular deviations of pitch and yaw of flexure stage were less than 0.5 arc sec. Then the error caused by Abbe-offset can be neglected.

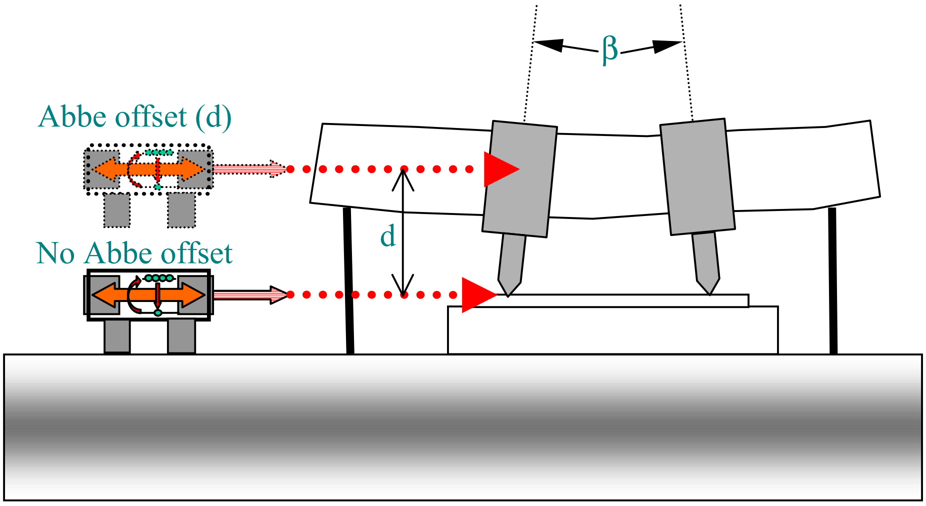

Figure 5.26 Abbe offsets

The TAFM has been established for the one-dimensional pitch calibrations for Taiwan industry. First, to assemble the test specimen on the flexure stage and use the optical microscope to find a suitable testing area. Second, to use the DI AFM to optimize the control parameters only for Z-height sensing (changing scanning range to zero in the XY plane). Then, to use a program developed in LabVIEW to control the two-dimensional scanning of flexure stage and, simultaneously, to capture the displacements from the laser interferometers (X and Y) and capacitance sensor (Z) of AFM. The displacements of X- and Y- axes of flexure stage from laser interferometers via RS232 interfaces and the voltage of Z axis of DI AFM via an AD card are obtained simultaneously while the AFM probe is scanned. Finally, a program written in Matlab is employed to perform the equivalent space interpolation in the X and Y directions, and SPIP software is used to calculate the pitch value and the pattern tilt angle. According to the "Guide to the Expression of Uncertainty in Measurement", the error budget was evaluated. The performances of pitch measurement of the TAFM are as following.

(a). Measuring item: one-dimensional pitch standards
(b). Measuring range: 100μm × 100 μm
(c). Metric (trace to the SI): laser interferometer
(d). Resolution of laser interferometer: 0.078 nm
(e). Expanded uncertainty: $\left[(2.5\,nm)^2 + 4.2\,u^2(\varepsilon_{p1})\right]^{1/2}$ (95 % confidence level)
(f). Effective Degrees of freedom: 29

6. Future Modification

A TAFM has been established at the CMS in Taiwan. It consists of a commercial AFM, two laser interferometers, a flexure stage, a super-Invar metrology frame, a vibration isolator and a temperature-controlled enclosed box with circulating water. The AFM is a DI Dimension Metrology AFM with three capacitance sensors at all axes. The laser interferometers all belong to the type of differential plane mirror laser interferometer made by SIOS Meßtechnik GmbH. The L-shape mirror was 150×18 mm^2 with 30 nm of flatness at each side. The flexure stage was a three-axis active-error-compensated flexure stage made by Physik Instruments in Germany. The out-of-plane motion was 0.5 nm and the angular deviation was 0.5 arc sec. The L-shape mirror was fixed on the flexure stage and the reference mirrors were fixed on the AFM head. A specimen was arranged on the same plane of X and Y laser interferometers, and AFM tip was on the intersection point of the lines extended of laser beams emitted from the X and Y interferometers. The error caused by Abbe-offset can be neglected. The laser interferometers can be used to measure the displacements between the stage and AFM head. The displacements of X- and Y- axes were controlled by capacitance sensors of flexure stage and recorded by laser interferometers. And the Z-height motion was controlled and recorded by a capacitance sensor of the scanner of AFM. The TAFM has been successfully used in pitch measurements. According to the ISO "GUM", [12] the error budget of TAFM was evaluated. The expanded uncertainty was 2.5 nm of a nominal pitch value of 292 nm at 95 % confidence level.

This expanded uncertainty is not satisfactory in the usually use in the nanometrology field. According to the error budget in table 5.2 (see page 64), the mechanical structure of AFM head, vibration noise from water circulatory, asymmetric structure loop and metrology loop, and thermal influence were the main contributors. The metrology frame was nearly symmetric in X direction but asymmetric in Y direction (see Figure 5.21 on page 70 and Figure 5.25 on page 72). And the super-Invar frame was supported by a quasi-kinematic supporting by a set cone-vee-plane and four screws with spherical head on a granite base. For the application in nanometrology, to achieve an expanded uncertainty to be no more than 0.5 nm by improving the flexure stage, AFM, laser interferometers on the same metrology frame, symmetric and shortest designs of structure loop and metrology loop. Additionally, there were only two laser interferometers used in X and Y directions. The displacement in the Z direction is recorded by a capacitance sensor. This sensor should be calibrated by a traceable sensor like a laser interferometer. If a laser interferometer is used to detect the displacement of flexure stage in the Z direction, the TAFM can realize directly traceable to the SI at all three axes. The followings describe some future modifications to reduce the error sources.

6.1 Traceability of Z-axis

Laser interferometer is an instrument to directly realize to trace to the SI unit. In the TAFM, a capacitance sensor of AFM sensed the height variation while the sample was scanning in the XY plane by a flexure stage. Two differential plane mirror laser interferometers recorded the displacements of sample on the flexure stage in X- and Y- axis, and a capacitance sensor recorded the Z-axis displacement. If the TAFM is intentionally used to calibrate the step height or the roughness, a traceable displacement sensor must be assembled in the Z-axis. For this reason, a same differential plane mirror laser interferometer (see Figure 3.5 on page 23) has to be arranged with a prism through the aperture of the flexure stage to detect the displacement and angular deviations in the Z direction. The schematic diagram is depicted in Figure 6.1. The travel range of the flexure stage is 10 μm in the Z direction. The capacitance sensor of the AFM can be directly calibrated by laser interferometer through the flexure stage. With this modification, the three differential plane mirror laser interferometers in the TAFM can be utilized to monitor the displacements in all three axes and angular deviations of pitch, yaw, and roll.

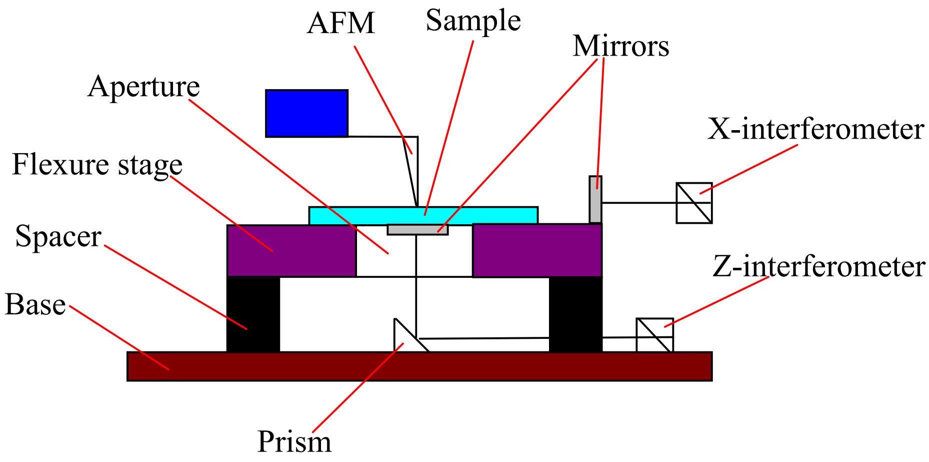

Figure 6.1 The schematic diagram of Z axis traceability

6.2 Vibration noise

A vibration isolator made by Minus-K was used to insulate the vibration from the environment, and an enclosed box with circulating water was used to control the temperature at 20 °C. Unfortunately, a 20 nm noise of laser interferometer was induced by the water circulator. It was caused by the circulating water through the copper pipe of the enclosed box seated on the tabletop of vibration isolator. It is shown in Figure 6.2. The vibration noise came from the water circulator via the copper pipe and the tabletop. If the support of enclosure box is changed from the tabletop to the floor, the noise of laser interferometer can be reduced to about 5 nm.

Additionaly, the AFM head and electronic unit were originally fixed on a granite plate. For the metrology consideration, the AFM head and electronic unit were separated from granite plate and reassembled on a super-Invar plate. The super-Invar frame was seated on a base plate with a cone-vee-plane kinematic mounting. The thickness of super-Invar frame was 25 mm (see Figure 3.12 on page 28). After reassembling, the noise level of AFM became 0.6 nm RMS (The original noise level was 0.04 nm RMS). It caused by an about 9 Hz natural frequency of super-Invar frame as shown in Figure 6.3. It can be improved by increasing the thickness of super-Invar plate and moving the flexure stage from base plate to super-Invar frame to increase the natural frequency of mechanical frame and reduce the noise level of AFM.

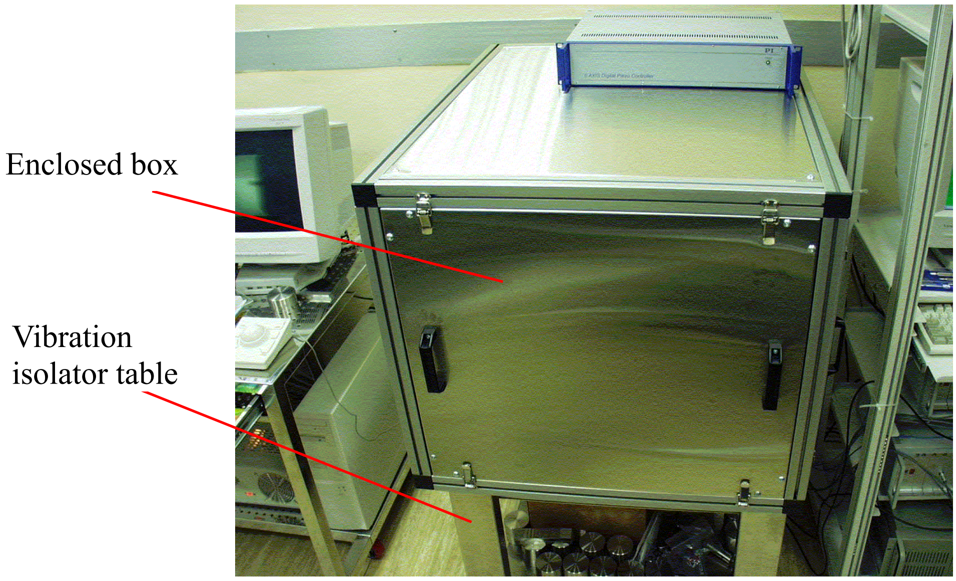

Figure 6.2 Enclosed box seated on the isolator tabletop

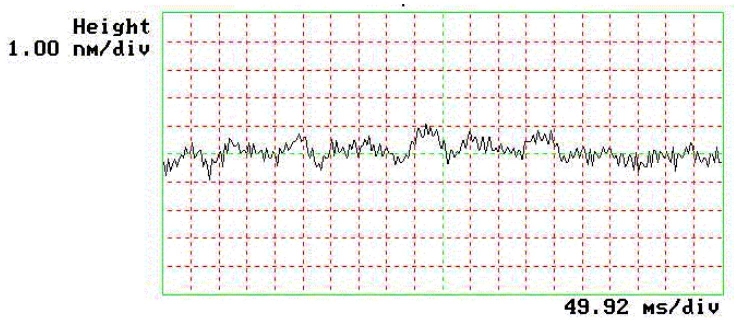

```
Digital Instruments NanoScope
Scan size              1.000 nm
Scan rate             0.5008 Hz
Number of samples        256
Image Data            Height
Data scale          10.00 nm
```

Figure 6.3 Noise of one line scanning of AFM

6.3 Metrology Frame

The structure loop is the path (or parallel paths) needed to trace from the probe tip through all parts of its holder and through the overall holding structure back to that part of the structure which holds the workpiece up to the corresponding points on the workpiece surface. And the metrology loop is the continuous path from the sense point on the probe or contact point on the machine tool to a reference datum and then back to the contacted point on the workpiece [92]. To maximize the resistances of vibration and thermal influences may reach by making the shortest path from the test probe to the test sample. There are some modifications can be used to improve the performance of the TAFM: to change the position of reference mirrors; to design a symmetric mechanism with a single material, and to shorten the structure and metrology loops.

(1). Reference Mirrors

A big error source in measuring uncertainty came from the positions of the reference mirrors. The reference mirrors were fixed on the AFM head. The AFM head was made of an Aluminum alloy box. The coefficient of thermal expansion was $23 \times 10^{-6}\ °C^{-1}$. The distances between the reference mirror and the AFM probe were about 48 mm in X-axis and 30 mm in Y-axis. The thickness of reference mirror mount was 8 mm (super-Invar) and the thickness of reference mirror was 6 mm (Quartz). An estimated material temperature changing was 0.025 °C during one pitch measurement. Therefore, the changings of distances between probe and reference mirrors were $(48\times23+8\times0.6+6\times8)\times10^{-6}\times0.025 = 28.92$ (nm) in X-axis and $(30\times23+8\times0.6+6\times8)\times10^{-6}\times0.025 = 18.57$ (nm) in Y-axis. If the probe is stationary, then it can be improved by moving the reference mirrors to the flexure stage (see Figure 6.4).

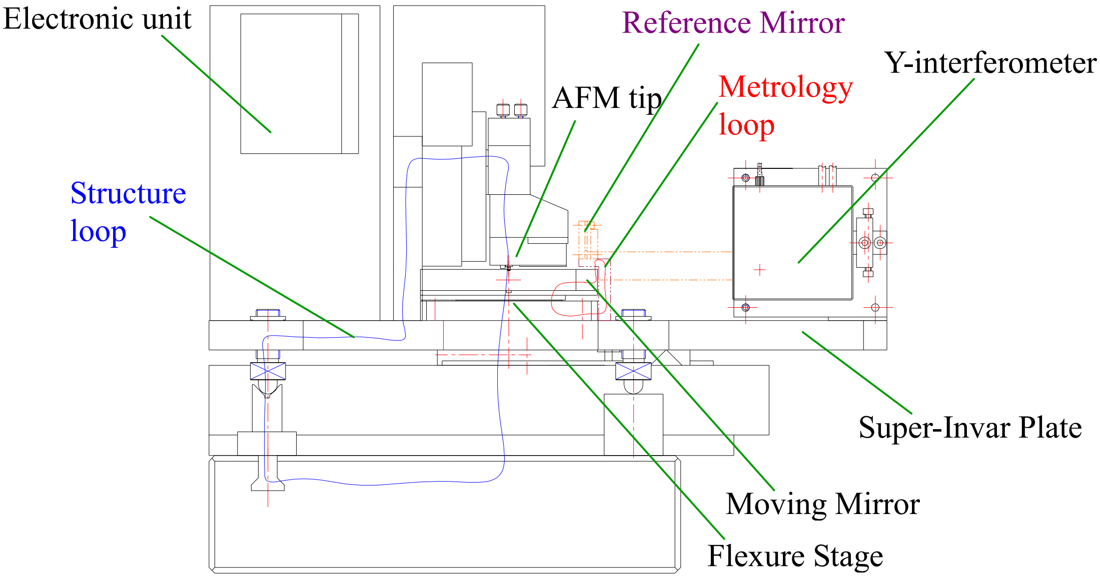

Figure 6.4 New location of reference mirrors

The flexure stage was made of super-Invar with the coefficient of thermal expansion of 0.6×10^{-6} °C $^{-1}$. The changes of distances between probe and reference mirrors were $(48+8+6)\times0.6\times10^{-6}\times0.025 = 0.93$ (nm) in X-axis, and $(30+8+6)\times0.6\times10^{-6}\times0.025 = 0.66$ (nm) in Y-axis. For this reason, the standard uncertainties were 0.27 nm in X direction, and 0.19 nm in Y direction.

(2). Symmetric mechanism and a single material

As mentioned in last paragraph, the probe tip should be stationary in a high stability AFM. The best way is to put the probe on the center of a symmetric mechanism and use a single material. From the mechanical structure of the TAFM, the AFM head was fixed on the middle of a bridge in X-axis. So it was almost symmetrical in the X direction, but asymmetrical in the Y direction (see Figure 5.25 on page 72). The asymmetrical mechanism in the Y direction will cause a big drift between the reference mirror and moving mirror if the temperature is changed.

For the metrology consideration, the AFM probe can be designed on the center of a super-Invar round plate. And the round plate is supported by a kinematic mount with three vee grooves and three spheres. Figure 6.5 shows a commercial AFM in a round plate. But the original design is supported by a set of cone-vee-plane kinematic mounting. It is also an asymmetrical structure. But it can be changed as a symmetrical mechanism by three vee grooves.

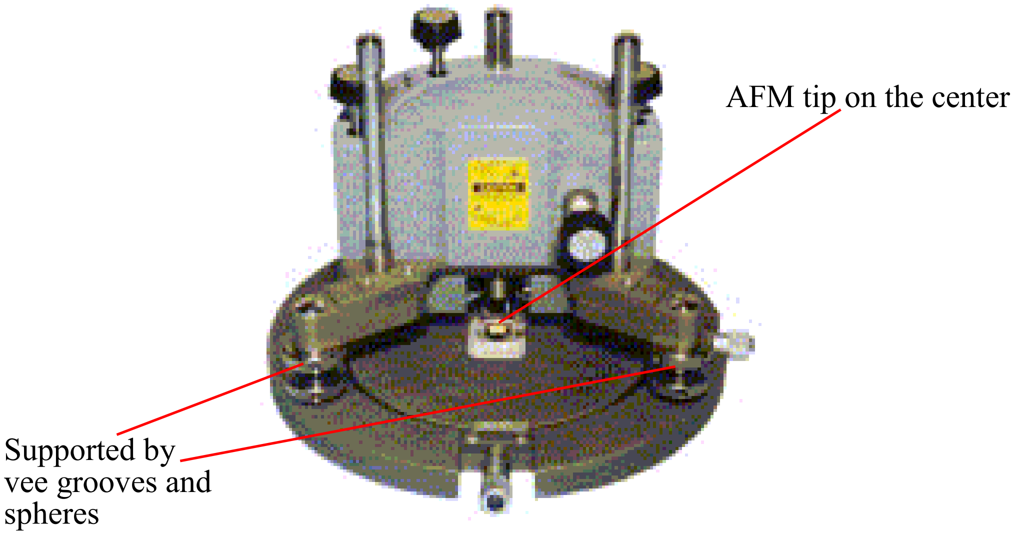

Figure 6.5 Symmetric design of AFM (NT-MDT SMENA)

(3). Metrology loop and structure loop

The metrology and structure loops have been described in section 5.8 (see page 70). There are some guidelines for the metrology loop and structure loop: as short as possible; containing a minimum number of joints; using internally damped materials and damped structures; separating metrology loop, mechanically and thermally, from the structure loop. In the TAFM, the metrology loop and structure loop can be improved as follow: (see Figure 6.6)

(a). Change the flexure stage from the base plate to the super-Invar frame to get a shorter metrology loop and structure loop.

(b). Thicken the super-Invar frame to increase the natural frequency, stiffness, and to reduce the noise level.

(c). To enlarge the travel range 20×20 mm^2 for the coarse motion to move the test sample and find the testing pattern on the nanometer scale standards, add a two-dimensional stage onto the same metrology frame. The original coarse motion stage (120×100 mm^2) of AFM had a big angular deviation (bigger than 60 arc sec.). It has been disconnected in the TAFM. A custom-made roller bearing stage provides better angular deviations: 2 arc sec in yaw and 6 arc sec in pitch.

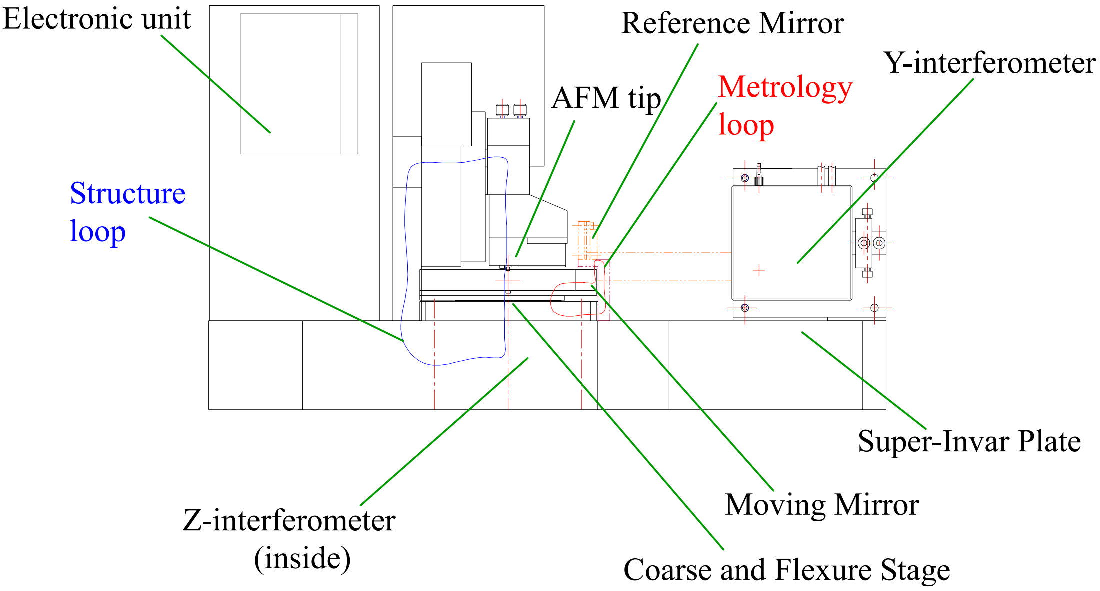

Figure 6.6 New Metrology loop and structure loop

6.4 Thermal drift

Indirect temperature-controlled circulating water through copper pipe was applied to control the temperature within (20±0.3) °C in the enclosed box. The thermometer was put in the water tank. The temperature of water must be adjusted manually to compensate the conditioning changes of enclosed box. It may be improved by changing the temperature-controlled system by an external thermometer putting on the testing area in the enclosed box. The temperature in measurement volume can be achieved to (20±0.1) °C.

The measurement results were affected, due to the long-term thermal drift, by the measuring time interval. The TAFM took 42 minutes long for each pitch measurement by use of the RS232 interface. The RS232 interface has been replaced by USB interface. The measuring time interval was reduced to 20 minutes for each pitch measurement.

6.5 Nanometer scale standards in nanotechnology

(1) Nanometer scale standards

The TAFM has been applied to calibrate the pitch standards for the semiconductor industry in Taiwan. In the semiconductor manufacturing industry, the pitch and linewidth are the important factors of the manufacturing roadmap. Some of the manufacturers in Taiwan, for example the Taiwan Semiconductor Manufacturing Company (TSMC) and the United Microelectronics Corporation (UMC), announced that their manufacturing techniques would be forward to nanotechnology in this year. They are forcing the NML to supply the calibration of nanometer scale standards, like pitch and thickness.

A prototype pitch standard on photo-resister was designd by the CMS and manufactured by National Nano-Device Laboratory in Hsinchu. This prototype included pitches of 200 nm, 320 nm, 400 nm, and 600 nm in 2×2 mm^2. Figure 6.7 shows the images of 200 nm and 320 nm pitch patterns. A nanometer scale of pitch standard on silicon will be developed in next step.

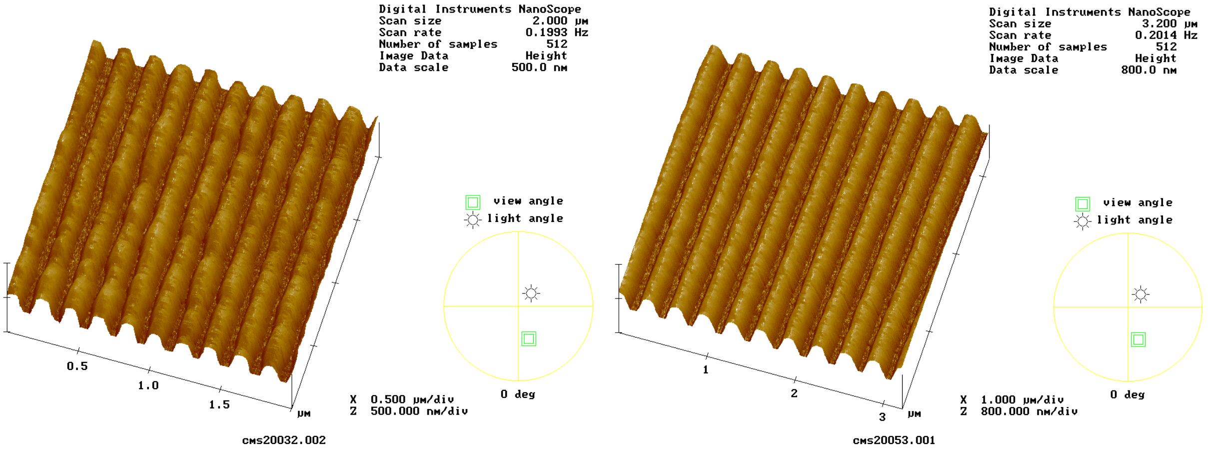

Figure 6.7 Pitch standards on photo-resister

(2) Comparison with laser diffractometer

After establishing the TAFM [93], a laser diffractometer was also setup to measure the grating pitch. Both measurement systems are based on different measurement principles. Light Diffraction is a well-know phenomenon in the modern optical physics. Laser diffractometer consists of a red or green He-Ne laser, a precision angular positioning stage, a four-quadrant detector, a beam splitter, and few mirrors (see Figure 6.8). The measurement principle is based on the Littrow configuration, i.e. the diffraction beam is coincident with the incident beam. The pitch value is determined by the diffraction angle γ and laser wavelength λ. The pitch P measured by the Littrow configuration is expressed as $m_d\lambda = 2P\sin\gamma$, where m_d is diffraction order [94].

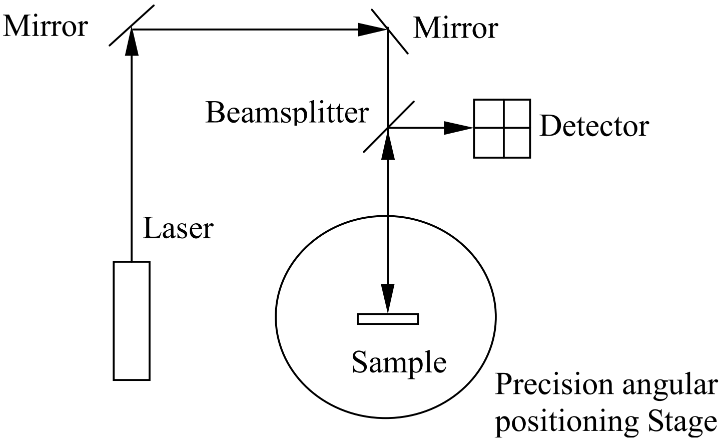

Figure 6.8 Laser diffractometer [95]

Figure 6.9 depicts the principle of grating diffraction. The incident laser beam has an angle γ to the normal of grating sample. The diffraction beams include zero order diffraction with an angle η_0 to the normal, first order diffraction with an angle η_1, negative first order diffraction with an angle η_{-1}, and other high-order diffraction beams.

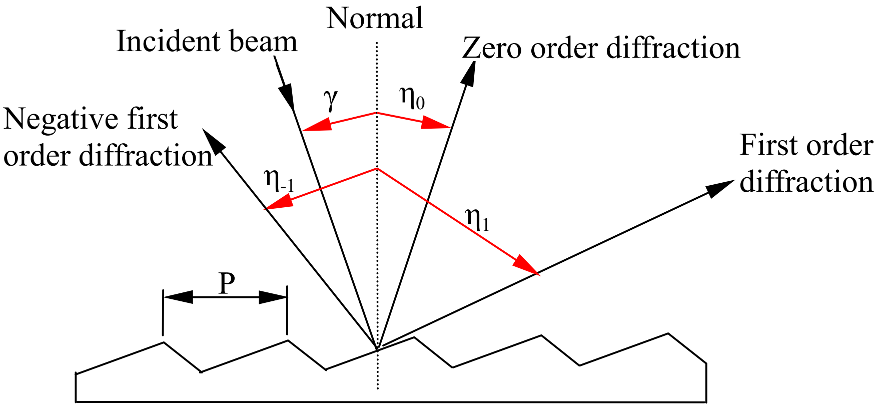

Figure 6.9 Principle of grating diffraction [95]

By applying, e.g., a frequency stabilized 633 nm laser on a grating sample with an incident angle of γ, the diffraction can be expressed as equation 6.1, where P is pitch of grating, λ is the laser wavelength, m_d is the diffraction order.

$$m_d \lambda = P(\sin\gamma + \sin\eta) \tag{6.1}$$

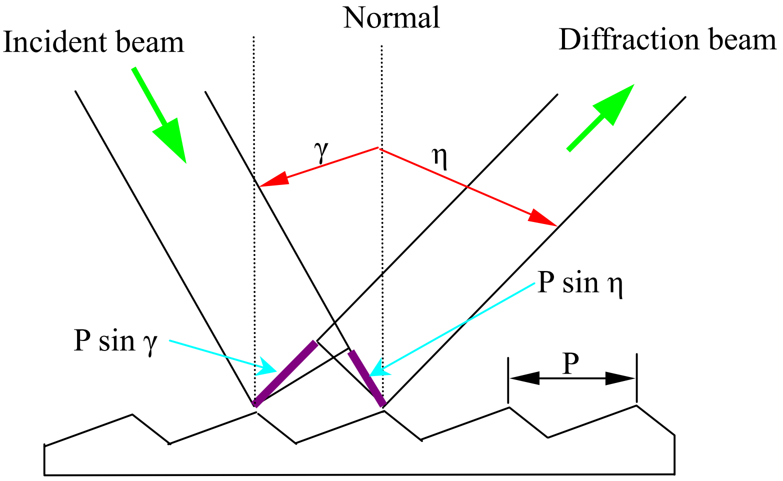

Figure 6.10 Grating diffraction

The incident light coincident to the reflection light is the so-called “Littrow configuration” shown in Figure 6.11. Then the diffraction equation is modified as: (equation 6.2)

$$m\lambda = 2P\sin\gamma \tag{6.2}$$

The laser diffractometer is constructed as the “Littrow configuration”. The grating pitch can be calculated by the laser wavelength and the Littrow diffraction angle (equation 6.3).

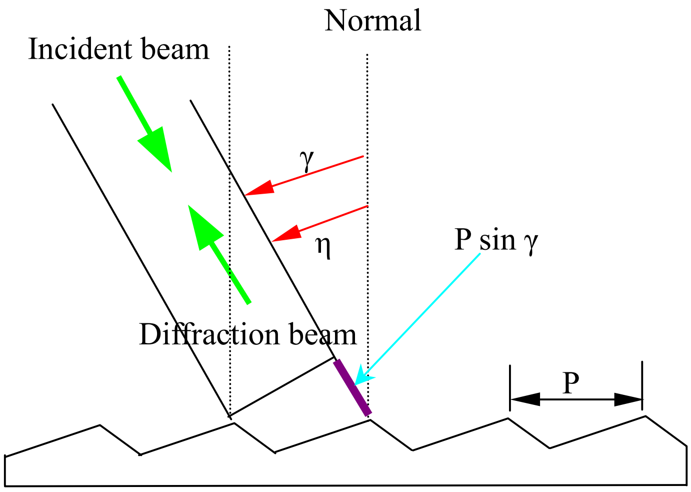

Figure 6.11 Littrow diffraction configuration

$$P = \frac{m\lambda}{2\sin\gamma} \tag{6.3}$$

The measuring results will be compared and verified by The TAFM and laser diffractometer. They will also provide the pitch traceability paths for different measuring method (see appendix 9.4). The major difference of AFM and laser diffractometer is that AFM takes every pitch data in a localized area, and the laser diffractometer takes the dominating pitch in the area of laser spot. Although the laser diffractometer has the high resolution measuring ability, the measuring range of pitch is limited by laser wavelength. The laser source should change to ultraviolet laser if the pitch grating measurement under 200 nm is needed (see appendix 9.5).

7. Summary

Surface textures were observed to atomic resolution using a Scanning Tunneling Microscope (STM) in 1982 and an Atomic Force Microscope (AFM) in 1986. Nowadays, the Scanning Probe Microscopes (SPMs), such as STMs, AFMs, are widely applied to measure engineering surfaces in a variety of fields, for example material sciences, semiconductor industry and biotechnology. It is also tool with potential use in nanotechnology, including nanolithography, atom manipulation, and nanometrology.A commercial AFM consists of a scanner, a laser, a photo-detector, a controller, and a cantilever tip. The scanner is normally designed with a tube piezoelectric actuator for three-dimensional scanning. However, some intrinsic properties of the piezo-actuator, such as non-linearity, hysteresis, aging, thermal drift, creep and coupling error, can cause measurement errors, which may reach 20 % of the reading. To reduce major measurement errors mentioned above, an AFM should be periodically calibrated using a traceable standard.

A state-of-the-art AFM should be directly traceable to the International System of Units (SI). It can be met by adding a laser interferometer, obeying the Abbe principle, and employing a high precision flexure stage. Establishing the traceability of the SPM to trace to the SI unit is a responsibility of the National Measurement Institute. Some national standard laboratories have developed metrological AFMs with a traceable displacement sensor, such as the calibrated AFM (C-AFM) developed at the National Institute of Standards and Technology (NIST) in the U.S.A., the metrological AFM (MAFM) at the Physikalisch-Technische-Bundesanstalt (PTB) in Germany, and the long-range profiler at the Metrology and Accreditation in Switzerland (METAS).

The goal of my study was conducted to develop a Traceable Atomic Force Microscope (TAFM) to be as a primary realization of nanometer scale standards for Taiwan industry. The TAFM includes a commercial AFM, a flexure stage, two laser interferometers, a vibration isolator and a super-Invar metrology frame, as depicted in Figure 7.1. The design concepts relate to the metric, the carriage and driver, the metrology frame, the probe, the isolation, the symmetry, and the alignment.

(1) Metric: A laser interferometer is one of the devices direct traceability to the definition of meter for taking displacement measurements. The advantages of laser interferometry are widely used in industry, including high resolution, a large measuring range, direct tracing to laser wavelength, and ease of use. Two differential plane mirror laser interferometers, made by SIOS, were assembled on X and Y-axes of the TAFM, and the reference mirrors were fixed on the AFM head to eliminate the error caused by the dead path. They were used to measure the X and Y displacements of the test sample on the flexure stage.

(2) Carriage and driver: An instrument for measuring displacement should have a carriage and a driver. A special custom-modified flexure stage, made by PI, was installed in the TAFM. It contains six piezo-actuators and six capacitance sensors to compensate actively for the three-axis errors. The range of displacement was 100μm × 100 μm in the XY plane. The out-of-plane displacement was 0.5 nm in the Z direction. The angular deviations were less than 0.5 arc sec in pitch and yaw.

(3) Metrology frame: Two basic design concepts, the structure loop and the metrology loop, are important in designing measuring instruments. The resistance of the instrument to vibration and thermal influence must be maximized by determining the shortest path from the test probe to the test sample. A super-Invar metrology frame was used to install the AFM and laser interferometers.

(4) Probe: A probe is any device using which features, edges, and surfaces are located. Examples include the scanning probe microscope, the scanning electron microscope, the stylus and the optical microscope. An AFM as a probe was used to measure the surface texture in the TAFM.

(5) Isolation: Vibration and temperature changes may influence measurements of displacement. A vibration isolator and a temperature-controlled enclosed box with circulating water can eliminate noise and drift caused by the environment. The enclosed box, made of stainless steel sheets and thermally isolating material, reduced the noise level of laser interferometer from 20 nm in 17 second to 2 nm in 18 seconds affected by conditioned air. The measuring volume of the TAFM was maintained at (20±0.3) °C.

(6) Symmetry: The mechanical structure of the symmetrically designed instruments for measuring displacement gives good repeatability, stability, stiffness and accuracy. The flexure stage was made with symmetric springs. The metrology frame, made of super-Invar, was almost symmetrical in the X direction but asymmetrical in the Y direction. The super-Invar frame was supported by a quasi-kinematic supporting with a set of cone-vee-plane and four screws with spherical heads on a granite base.

(7) Alignment: Ernst Abbe said, "The measuring instrument is always to be constructed such that the distance that is measured is a straight line extension of the graduations on the scale that serves as the reference…" [73]. In the TAFM, a specimen was arranged on the same plane as the X and Y laser interferometers on the flexure stage, and the AFM tip was on the intersection of the lines extended from the laser beams of the X and Y interferometers. The angular deviations of the pitch and the yaw of the flexure stage were less than 0.5 arc sec. Then, the error caused by the Abbe-offset could be neglected.

The uncertainty in the measurement was evaluated following the "Guide to the expression of the uncertainty in measurement" (GUM), published by the International Organization of Standards (ISO). The expanded uncertainty of a nominal pitch of 292 nm was 2.5 nm at a confidence level of 95 % and 29 effective degrees of freedom.

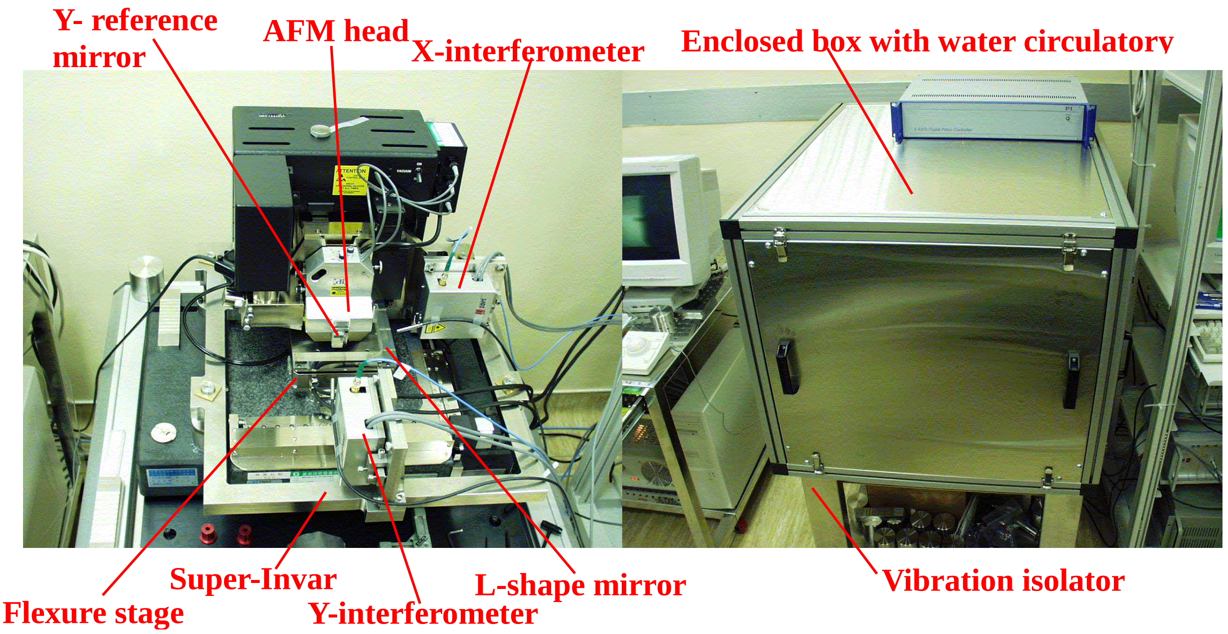

Figure 7.1 Traceable Atomic Force Microscope

The first step in measuring pitch is to position the test specimen on the flexure stage and then use an optical microscope to find a suitable area for testing. Secondly, the DI AFM is utilized to optimize the control parameters for Z-height sensing. Then, a program written in LabVIEW is used to control the motion of the flexure stage, and simultaneously capture the displacements by the laser interferometers (X and Y) and the capacitance sensor (Z) in the AFM. The displacements along the X and Y axes of the flexure stage measured by laser interferometers, via RS232 interfaces, and the voltage on the Z axis of the DI AFM measured using an AD card, are obtained while the AFM probe is scanning. Finally, a program written in Matlab is employed to perform the equivalent space interpolation in the X and Y directions and SPIP software is used to calculate the pitch value and the pattern tilt angle. The following are the performances of pitch measurement by the TAFM.

- Measuring item: one-dimensional pitch standards
- Measuring range: 100µm × 100 µm
- Metric (trace to the SI): laser interferometer
- Resolution of laser interferometer: 0.078 nm
- Expanded uncertainty: $\left[(2.5\,nm)^2 + 4.2u^2(\varepsilon_{p1})\right]^{1/2}$ (95 % confidence level)
- Effective Degrees of freedom: 29

The TAFM has successfully provided services for calibrating the one-dimensional pitch standards for the semiconductor industry. However, the expanded uncertainty of one-dimensional pitch is not satisfactory and there is no traceability in the Z direction. The main contributors to measurement uncertainty are the supports of the flexure stage and the AFM, the mechanical structure of the AFM head, vibration from circulating water, the near symmetry of the metrology frame in the X direction but the asymmetry in the Y direction, and the thermal influence. The aim of the TAFM is to reach an expanded uncertainty of no more than 0.5 nm at 95 % confidence level at all three axes. It can be achieved by the following future modifications.

(1) Add another differential plane mirror laser interferometer on the flexure stage. It can calibrate the z-height of the capacitance sensor of the AFM and monitor the displacement of the flexure stage.

(2) The vibration noise was caused by the circulating water of copper pipe via tabletop of the vibration isolator. Move the enclosed box from the tabletop to the floor. The noise level of the laser interferometer caused by circulating water can be reduced to no more than 5 nm.

(3) Improve the metrology frame to yield high repeatability, stability, stiffness and accuracy. Improvements may include moving the reference mirrors from the AFM head to the flexure stage, thickening the super-Invar frame, shortening the structure loop and the metrology loop, using a single material and a symmetrical mechanism in the Y direction.

(4) Change the passive temperature control to active temperature control in the measuring volume of the TAFM to achieve a temperature of (20±0.1) °C.

(5) Develop the nanometer scale pitch and step height standards, and compare the pitch measurement to that measured by the laser diffractometer.

The above modifications will soon be made at the Center for Measurement Standards to provide the best nanometer scale traceability in Taiwan.

References

[1] *Binnig, G., Rohrer, H., Gerber, Ch., and Weibel, E.:* Tunneling through a controllable vacuum gap, Applied Physical Letters 40 (1982), p. 178-179.

[2] *Binnig, G., Quate, C. F., and Gerber, Ch.:* Atomic Force Microscope, Physical Review Letters 56 (1986), p. 930-933.

[3] *Meli, F. and Thalmann, R.:* Long-range AFM profile used for accurate pitch measurements, Measurement Science Technology 9 (1998), p. 1087-1092.

[4] *Hasche, K., Herrmann, K., Büchner H.-J., Pohlenz, F., Seemann, R.:* Lösungsbeispiele für quantitative Rastersondenmikroskopie in der Mikro- und Nanotechnik, 44. Internationales Wissenschaftlisches Kolloquium, Technische Universität Ilmenau, September 1999, p. 68-73.

[5] *Büchner, H., Jäger, G., and Manske, E.:* Laser-interferometrically assisted 3D-nanometrology on the atomic force microscope type VERITEKT, Proceedings of 1st international conference and general meeting of the european soceity for precision engineering and nanotechnology vol. 2, p. 161-164.

[6] *Jäger, G., Manske, E., Hausotte T., and Büchner, H.:* Nanomessmaschine zur abbefehlerfreien Koordinatenmessung, Technisches Messen 67 (2000), p. 319-323.

[7] *Tsai, Vincent Wen-Chieh.:* Calibration of Atomic Force Microscopes with Silicon Atomic Step Artifact, Dissertation (1998).

[8] *Image Metrology:* Scanning Probe Image Processor, SPIP™ User's and Reference Guide (1999).

[9] *NT-MDT:* What is Scanning Probe Microscope (2002).

[10] *Park:* A Practical Guide to Scanning Probe Microscope, www.park.com.

[11] *Digital Instruments:* Dimension 3100 Series Scanning Probe Microscope Instruction Manual, Version 4.31ce (1997).

[12] *ISO:* Guide to the Expression of Uncertainty in Measurement. Corrected and reprinted (1995).

[13] *Paul Kam-Wa Lui, Sheau-shi Pan, Chao-Jung Chen, and Gwo-Sheng Peng:* Uncertainty Estimation of 1D Pitch Measurement by AFM, Proceedings of the 3rd Conference of Chinese Metrology Society and Chinese Measurement Society, p. 187-191 (2000).

[14] *J. Kramar, J. Jun, F. Scire, C. Teague, J. Villarrubia, E. Amatucci, D. Gilsinn:* The Molecular Measuring Machine, Proceedings of the 1998 ICMT, p. 477-487 (1998).

[15] *E. Clayton Teague:* Generating and Measuring Displacements Up To 0.1 m To An Accuracy of 0.1 nm: Is It Possible?, SPIE Handbook "The Technology of Proximal Probe Lithography" (1993).

[16] *E.C. Teague, L.W. Linholm, M.W. Cresswell, W.B. Penzes, J.A. Kramar, F.E. Scire, J.S. Villarrubia, J.S. Jun:* Metrology Standards for Advanced Semiconductor Lithography Referenced to Atomic Spacings and Geometry, Proc. IEEE Int. p. 213-217 (1993).

[17]*E. Clayton Teague:* The National Institute of Standards and Technology molecular measuring machine project: Metrology and precision engineering design, J. Vac. Sci. Technol. B7 (6), p. 1898-1902 (1989).

[18]*M.W. Cresswell, R.A. Allen, L.W.Linholm, C.H. Ellenwood, W.B. Penzes, and E.C. Teague:* Test structure for the In-Plane Locations of Projected Features with Nanometer-Level Accuracy Traceable to a Coordinate Measurement System, Proc. IEEE Int. Vol. 6, p. 255-261 (1993).

[19]*L.W. Linholm, R.A. Allen, M.W. Cresswell, R.N. Ghoshtagore, S. Mayo, H.A. Schafft, J.A. Kramar, and E.C. Teague:* Measurement of Patterned Film Linewidth for Interconnect Characterization, Proc. IEEE Int. Vol. 8, p. 23-26 (1995).

[20]*N.M. Oldham, J.A. Kramar, P.S. Hetrick, and E.C. Teague:* Electronic limitations in phase meters for heterodyne interferometry, Precision Engineering 15 (3), p. 173-179 (1993).

[21]*T.V. Vorburger, J.A. Dagata, G. Wilkening, and K. Iizuka:* Industrial Uses of STM and AFM, CIRP (1999).

[22]*J.S. Villarrubia, R. Dixon, S. Jones, J.R. Lowney, M.T. Postek, R.A. Allen, and M.W. Cresswell:* Intercomparison of SEM,AFM,and Electrical Linewidths, SPIE Vol. 3677 (1999).

[23]*J.E. Griffith, H.M. Marchman, and L.C. Hopkins:* Edge position measurement with a scanning probe microscope, J. Vac. Sci. Technol. B 12(6), p. 3567-3570 (1994).

[24]*J. Fu, R.D. Young, and T.V. Vorburger:* Long-range scanning for scanning tunneling microscope, Review of Scientific Instruments, Vol. 63, No. 4, p. 2200-2205 (1992).

[25]*J. Schneir, T.H. Mcwaid, J. Alexander and B.P. Wilfley:* Design of an atomic force microscope with inteferometric position control, J. Vac. Sci. Technol. B 12(6). p. 3561-3566 (1994).

[26]*R. Köning, R. Dixson, J. Fu, V.W. Tsai, T.V. Vorburger, E.D. Williams, X.S. Wang:* Pitch and Step Height Measurement using the Calibrated Atomic Force Microscope, Proceedings of 1st euspen conference, p. 172-176 (1998).

[27]*J. Schneir, T. McWaid, R. Dixon, V.W. Tsai, J.S. Villarrubia, E.D. Williams, and E. Fu:* Progress on Accurate Metrology of Pitch, Height, Roughness, and Width Artifacts Using an Atomic Force Microscope, SPIE Vol. 2439, p. 401-415 (1995).

[28]*R. Dixon, J. Schneir, T. McWaid, N. Sullivan, V.W. Tsai, S.H. Zaidi, S.R.J. Brueck:* Toward Accurate Linewidth Metrology using Atomic Force Microscopy and Tip Characterization, SPIE Vol. 2725 (1996).

[29]*Herschel Marchman:* Nanometer-scale dimensional metrology with noncontact atomic force microscopy, SPIE Vol. 2725, p. 527-539 (1996).

[30]*Vincent Tsai, X.-S. Wang, and Ellen D. Williams:* Conformal oxides on Si surfaces, Appl. Phys. Lett. 71(11), p. 1495-1497 (1997).

[31]*R. Dixon, R. Köning, V.W. Tasi, J. Fu, T.V. Vorburger:* Dimensional Metrology with the NIST Calibrated Atomic Force Microscope, SPIE Vol. 3677 (1999).

[32]*Joseph E. Griffith, David A. Grigg:* Dimensional metrology with scanning probe

microscope, J. Appl. Phys. 74(9), p. R83-R109 (1993).

[33] *O. Jusko, X. Zhao, H. Wolff, and Wilkening:* Design and three dimensional calibration of a measuring scanning tunneling microscope for metrological applications, Rev. Sci. Instrum. 65(8), p. 2514-2517 (1994).

[34] *K. Hasche, O. Jusko, L. Koenders, K. Thiele, G. Wilkening, X. Zhao:* Scanning Probe Microscope for dimensional length measurements, Proceedings of ASPE conference, Vol. 14, p. 369-374 (1996).

[35] *M. Bienias, K. Hasche, R. Seemann, K. Thiele, Zhao Kegong, Gao Sitian, Xu Yi:* A Metrology Atomic Force Microscope(Chinese), ACTA METRLOGICA SINICA 19(1), p. 1-8 (1998).

[36] *Gerd Jäger:* Precision distance measurement by means of miniaturized interferometers, Proceedings of the XIII. IMEKO World Congress, Vol. 3, S. 1712-1716 (1994).

[37] *Gerd Jäger:* Laser-Nano-Multicoordinate Mmeasurement, Proceedings of the XIV. IMEKO World Congress (1997).

[38] *Gerd Jäger, Eberhard Manske und Holger Wurzbacher:* Optische Kopplung zwischen Laserinterferometern, Technisches Messen 65 (3), p. 109-115 (1998).

[39] *H. Büchner, G. Jäger, E. Manske:* Laser-interferometrically assisted 3D-nanometrology on the atomic force microscope type VERITEKT, Proceedings of the 1st Euspen international conference, Vol. 2, p. 161-164 (1999).

[40] *Gerd Jäger, Eberhard Manske, Tino Hausotte und Hans-Joachim Büchner:* Nano Measuring Machine for zero Abbe Offset Coordinate-Measuring, Technisches Messen 67 (7-8), p. 319-323 (2000).

[41] *G. Jäger, E. Manske, T. Hausotte und H.-J. Büchner:* Nanomeasuring Machine, MICRO.tec 2000 Hanover, S. 551-556 (2000).

[42] *G. Jäger, E. Manske, T. Hausotte:* Nanopositioning and measuring Machine, Proceedings of the 2nd Euspen international conference, Vol. 2, S. 290-293 (2001).

[43] *F. Meli:* International comparison in the field of nanometrology: Pitch of 1D gratings (Nano4), Proceedings of 2nd euspen International Conference, p. 358-361 (2001).

[44] *F. Meli, R. Thalmann:* Long-range AFM profiler used for accurate pitch measurements, Meas. Sci. Technol. 9, p. 1087-1092 (1998).

[45] *M.J. Downs, and W.R.C. Rowley:* A proposed design for a polarization-insensitive optical interferometer system with subnanometric capability, Precision Engineering 15 (4), p. 281-286 (1993).

[46] *M.J. Downs and J.W. Nunn:* Verification of the sub-nanometric capability of an NPL differential plane mirror interferometer with a capacitance probe, Meas. Sci. Technol. 9, S. 1437-1440 (1998).

[47] *Chao-Jung Chen, Sheau-shi Pan, and Gwo-Sheng Peng:* Development of Traceable Atomic Force Microscope, Proceedings of the 8th Conference of the Chinese Metrology Society, p. 31-37 (2001).

[48] *Chao-Jung Chen, Paul Kam-Wa Lui, and Gwo-Sheng Peng:* Introduction of Traceable

Atomic Force Microscope, Measurement Information 80, p. 21-26 (2001).

[49] *Chao-Jung Chen, Sheau-shi Pan, Paul Kam-Wa Lui, and Gwo-Sheng Peng:* The Nano-scale Measuring Application and calibration of Atomic Force Microscope, Mechanical tech. Magazine 197, p. 202-209 (2001).

[50] *Paul Kam-Wa Lui, Gwo-Sheng Peng, Chao-Jung Chen, and Sheau-shi Pan:* Traceability of 1D Gratings Standards Accomplished via International Comparison, Proceedings of the 8th Conference of the Chinese Metrology Society, p. 51-55 (2001).

[51] *Digital Instruments:* Training Book, Rev. 3.0 (1998).

[52] *Digital Instruments:* Nanoscope Command Reference Manual, Version 4.42 (1999).

[53] *Digital Instruments:* Metrology Scanning Microscope –Description & Use, Version 243.B (1998).

[54] *C.R. Steinmetz:* Sub-micron position measurement and control on precision machine tools with laser interferometry, Precision Engineering 12 (1), p. 12-24 (1990).

[55] *C.R. Steinmetz:* Sub-Micron Displacement Masurement Repeatability on Precision Machine Tools with Laser Interferometry, SPIE 959, p. 178-192 (1988).

[56] *H.-J. Büchner and G. Jäger:* Contactless interferometric incremental measurement technique, Measurement 6 (4), S. 146-150 (1998).

[57] *SIOS Meßtechnik GmbH:* Model SP500DD Differential Plane Mirror Optical interferometers (2000).

[58] *R.V. Jones, C.B., C.B.E., D. Phil., F. Inst. P.:* Parallel and rectilinear spring movements, J. Sci. Instrum. 28, p. 38-41 (1951 Feb.).

[59] *J.M. Paros and L. Weisbord:* How to design flexure hinges, Machine design, p. 151-156 (1965 Nov.).

[60] *Fredric E. Scire and E. Clayton Teague:* Piezodriven 50-μm range stage with subnanometer resolution, Rev. Sci. Instrum. 49 (12), p. 1735-1740 (1978).

[61] *S.T. Smith, D.G. Chetwynd and D.K. Bowen:* Design and assessment of monolithic high precision translation mechanisms, J. Phys. E: Sci. Instrum. 20, p. 977-983 (1987).

[62] *Chr. Hoffrogge and H.-J. Rademacher:* Eine Doppelparallelfeder als Präzisionsführung, PTB-Mitteilungen 2, p. 79-82 (1973).

[63] *Gao Hong, Li Qingxiang, Yan Puqiang:* Design and Accuracy Analysis of Submicron Positioning Flexure Fine Stage System, J. Tsinghua Uni. 28 (5), p. 19-28 (1983).

[64] *Kazuyoshi Sugihara, Ichiro Mori, Toru Tojo, Chikara Ito, Mitsuo Tabata, and Toshiaki Shinozaki:* Piezoelectrically driven Xyθ table for submicron lithography systems, Rev. Sci. Instrum. 60 (9), p. 3024-3029 (1989).

[65] *S.H. Chang, N.N. Rogacheva, and C.C. Chou:* Analysis of Methods for Determining Electromechanical Coupling Coefficients of Piezoelectric Elements, IEEE transactions on Ultrasonics, Ferroelectrics, and Frequency Control 42 (4), p. 630-640 (1995).

[66] *Renyi Yang, Musa Jouaneh, and Rudolph Schweizer:* Design and characterization of a low-profile micropositioning stage, Precision Engineering 18 (1), p. 20-29 (1996).

[67] *Jae W. Ryu and Dae-Gab Gweon:* Error analysis of a flexure hinge mechanism induced by machining imperfection, Precision Engineering 21 (2-3), p. 83-89 (1997).

[68] *Chang-Woo Lee and Seung-Woo Kim:* An ultraprecision stage for alignment of wafers in advanced microlithography, Precision Engineering 21 (2-3), p. 113-122 (1997).

[69] *S.H. Chang and B.C. Du:* A precision piezodriven micropositioner mechanism with large travel range, Rev. Sci. Instrum. 69 (4), p. 1785-1791 (1998).

[70] *Shuo Hung Chang:* An Ultra-Precision XYθz Piezo-Micropositioner Part I: Design and Analysis, IEEE transactions on Ultrasonics, Ferroelectrics, and Frequency Control 46 (4), p. 897-9050 (1995).

[71] *Hsien-Chi Yeh:* Study in Subnanometer Laser Metrology and Subnanometer Real-time Motion Control, Dissertation of National Chin-Hwa University (1998).

[72] *PI:* www.physikinstrumente.com.

[73] *E. Abbe:* Messaparate für Physiker, Zeitschrift für Instrumentenkunde, p446-448 (1890).

[74] *Minus-K Technology:* www.minusk.com.

[75] *Chao-Jung Chen, Sheau-Shi Pan, Paul Kam-Wa Lui, Norbert Hofmann:* Traceable Atomic Force Microscope, CMS/ITRI Technical report 073890115 (2000).

[76] *F. Meli:* WGDM-7: Preliminary comparison on nanometrology, According to the rules of CCL key comparisons, Nano4: 1D gratings Final report Draft B, Swiss Federal Office of Metrology (2000).

[77] *National Institute of Standards and Technology:* Reference Material 8090, SEM Magnification Reference Material, www.nist.gov.

[78] *National Physical Laboratory:* SEM and SPM standards, www.npl.co.uk.

[79] *Molecular Devices and Tools for NanoTechnology (NT-MDT):* Diffraction grating TDG01, www.ntmdt.ru.

[80] *Moxtek:* www.moxtek.com.

[81] *VLSI Standards Incorperated:* NanoLattice™ Pitch Standard (2001).

[82] *Chao-Jung Chen, Paul Kaw-Wa Lui, Yeng-Liang Chen, Liang-cha Chang:* Instrument Calibration Technique for Pitch Standards, CMS/ITRI Technical Report (2001).

[83] *Sheau-Shi Pan, Yeh, Chao-Jung Chao:* The test results of DI Atomic Force Microscope, CMS/ITRI Technical Report (1999).

[84] *VLSI Standards Incorporated:* Certificate of Calibration, Model Number: STS3-1800P, Serial Number: 4478-012-002 (1998).

[85] *PI:* PZT Performance Test Document, Job Nr: 126012 (2000).

[86] *B. Edlén:* The Refractive Index of Air, Metrologia 2, p. 71-80 (1966).

[87] *K.P. Birch, F. Reinboth, R.E. Ward and G. Wilkening:* The Effect of Variations in the Refractive Index of Industrial Air upon the Uncertainty of Precision Length Measurement, Metrologia 30, p. 7-14 (1993).

[88] *K.P. Birch and M.J. Downs:* An Updated Edlén Equation for the Refractive Index of Air,

Metrologia 30, p. 155-162 (1993).

[89] *G. Bönsch and E. Potulski:* Measurement of the refractive index of air and comparison with modified Edlén's formulae, Metrologia 35, p. 133-139 (1998).

[90] *Chien-ming Wu:* System Practice for Precision Instruments, (2001).

[91] *G. Wilkening:* Metrological Aspects of SPM Developments, (1997).

[92] *E. Clayton Teague:* Basic Concepts for Precision Instrument Design: Designing Instruments and Machines to Have a High Degree of Repeatability, (1999).

[93] *Chao-Jung Chen, Paul Lui and Gwo-Sheng Peng:* Introduction to metrology AFM, Measurement Information (in Chinese), Vol. 80, No.7, pp21-26, 2001.

[94] *Christopher Palmer:* Diffraction Grating Handbook, 4th edition, Richardson Grating Laboratory, 2000.

[95] *San-Peng Pan, Chao-Jung Chen and Liang-Chin Chang:* 1-D Pitch Measurements by Laser Diffractometer and Atomic Force Microscope, Proceedings of International Symposium Precision Mechanical Measurements, p. 5-059~5-063 (2002).

8. Appendix

9.1 LabVIEW program for TAFM

(1). 2d_scan_frontend_h.vi (Pitch measurement)

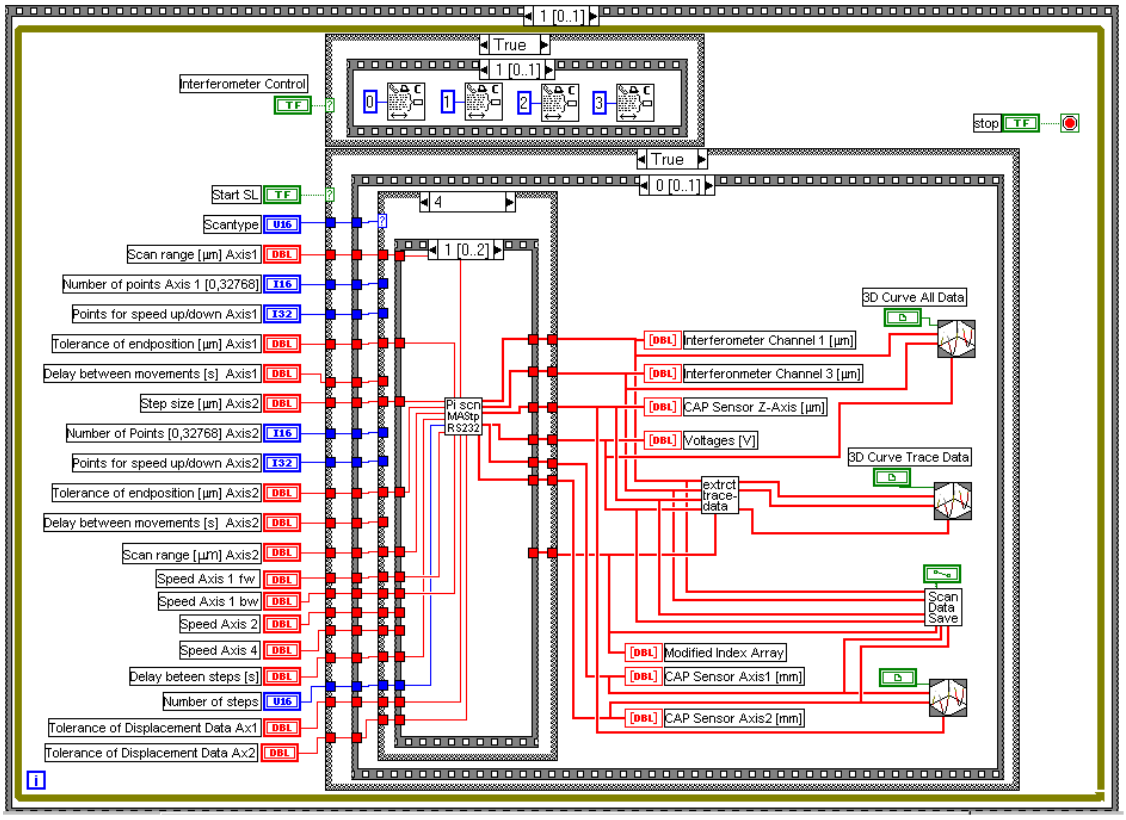

(2). drift.vi (Drift test of laser interferometer)

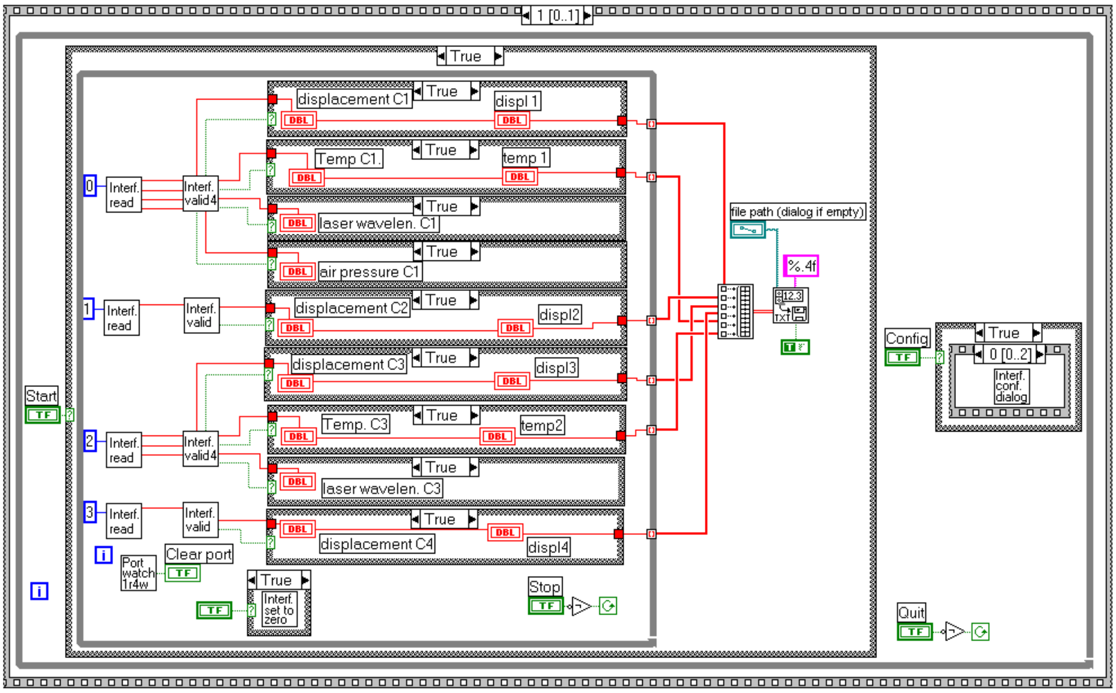

(3). pi.vi (Moving test of PI flexure stage)

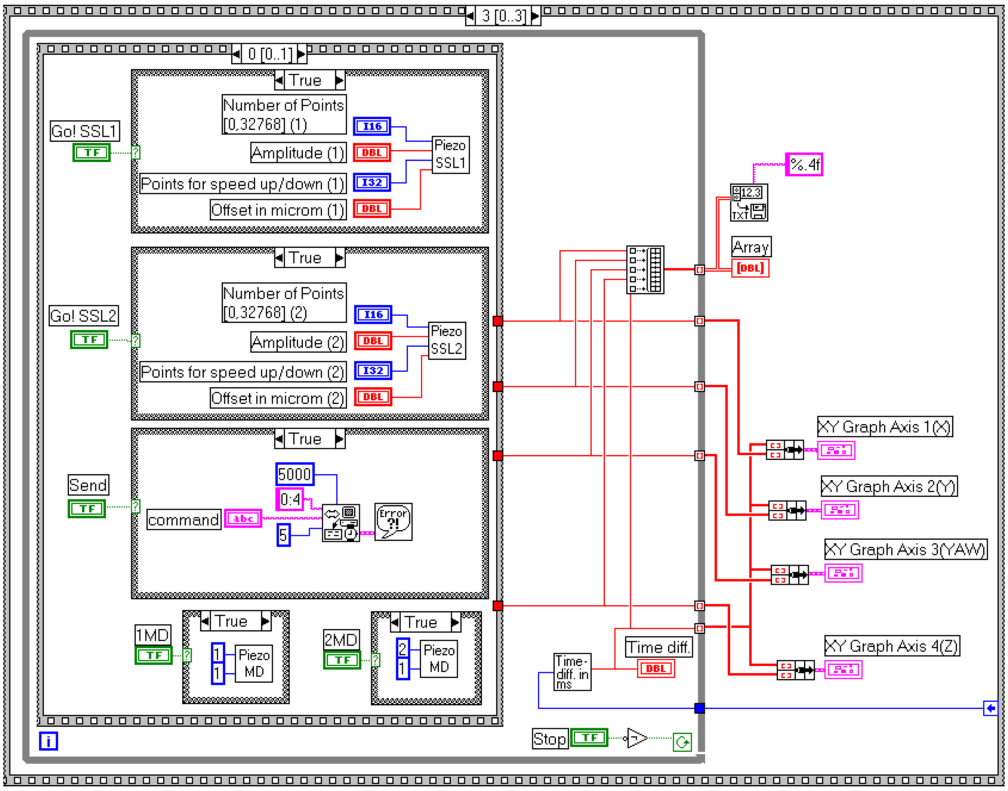

9.2 Interpolation program (Matlab)

```
clear
clc
name=input('File name:','s');
na=sprintf('d: %s.dat',name);
na1=sprintf('d: %s.txt',name);
afm=load(na);
n=length(afm);
x1=afm(:,1);
y1=-afm(:,2);
z2=afm(:,6).*0.5;
z1=detrend(z2);

txx=prctile(x1(:),95)-prctile(x1(:),5)
tyy=prctile(y1(:),95)-prctile(y1(:),5)
tx=linspace(prctile(x1(:),5),prctile(x1(:),95),512);
ty=linspace(prctile(y1(:),5),prctile(y1(:),95),(n/512));
[x,y]=meshgrid(tx,ty);
z=griddata(x1,y1,z1,x,y);
%w=detrend(z);

save(na1,'z','-ascii');
%fid=fopen(na1,'wt');
%fprintf(fid,'%12.8f',z);
%fclose(fid);

mesh (x,y,z);
axis ([0,3.5,0,3.5,-0.1,0.1]);
xlabel('x (micrometer)');
ylabel('y (micrometer)');
zlabel('z (micrometer)');
title('1D-Pitch Measurement');
view(-25,80);
```

9.3 Software verification (Matlab)

```
clear
clc
a=1:1:512;
bb=512/(2*11);
y=floor(bb);
b=[ones(1,23) zeros(1,23)];
ab=[b b b b b];
b=[ab ab ab ab ab];
ab=[b b b b b];
b=ab(1,1:1000);
b=(b-0.5).*65;
(3250)*(2*y)/512
[X,Y]=meshgrid(0:(3250/511):3250,0:(3250/63):3250);
c=ones(1000,1);
d=c*b;
R=(rand(1000,1000)-0.5).*44;
R2=R./2;
for i=1:1:43;
    R(:,4+(23*(i-1)):20+(23*(i-1)))=0;
end
d=d+R+R2;
dd=d(1:64,1:512);
dd=imresize(dd,[64 512],'bicubic');
figure(1)
mesh (X,Y,dd);
axis ('equal');

e=imrotate(d,+0.5);
[l1,l2]=size(e);
f1=round((l1/2)-256);
f2=round((l2/2)-256);
e=e(f1+1:512+f1,f2+1:512+f2);
e=imresize(e,[64 512],'bicubic');
save c:\scan\05.txt dd -ASCII

e=imrotate(d,+1);
```

```
[l1,l2]=size(e);
f1=round((l1/2)-256);
f2=round((l2/2)-256);
e=e(f1+1:512+f1,f2+1:512+f2);
e=imresize(e,[64 512],'bicubic');
save c:\scan\10.txt e -ASCII

clear e l1 l2 f1 f2
e=imrotate(d,+1.5);
[l1,l2]=size(e);
f1=round((l1/2)-256);
f2=round((l2/2)-256);
e=e(f1+1:512+f1,f2+1:512+f2);
e=imresize(e,[64 512],'bicubic');
save c:\scan\15.txt e -ASCII

clear e l1 l2 f1 f2
e=imrotate(d,+2);
[l1,l2]=size(e);
f1=round((l1/2)-256);
f2=round((l2/2)-256);
e=e(f1+1:512+f1,f2+1:512+f2);
e=imresize(e,[64 512],'bicubic');
save c:\scan\20.txt e -ASCII

clear e l1 l2 f1 f2
e=imrotate(d,+2.5);
[l1,l2]=size(e);
f1=round((l1/2)-256);
f2=round((l2/2)-256);
e=e(f1+1:512+f1,f2+1:512+f2);
e=imresize(e,[64 512],'bicubic');
save c:\scan\25.txt e -ASCII

clear e l1 l2 f1 f2
e=imrotate(d,+3);
[l1,l2]=size(e);
f1=round((l1/2)-256);
f2=round((l2/2)-256);
```

```
e=e(f1+1:512+f1,f2+1:512+f2);
e=imresize(e,[64 512],'bicubic');
save c:\scan\30.txt e -ASCII

clear e l1 l2 f1 f2
e=imrotate(d,+3.5);
[l1,l2]=size(e);
f1=round((l1/2)-256);
f2=round((l2/2)-256);
e=e(f1+1:512+f1,f2+1:512+f2);
e=imresize(e,[64 512],'bicubic');
save c:\scan\35.txt e -ASCII

clear e l1 l2 f1 f2
e=imrotate(d,+4);
[l1,l2]=size(e);
f1=round((l1/2)-256);
f2=round((l2/2)-256);
e=e(f1+1:512+f1,f2+1:512+f2);
e=imresize(e,[64 512],'bicubic');
save c:\scan\40.txt e -ASCII

clear e l1 l2 f1 f2
e=imrotate(d,+4.5);
[l1,l2]=size(e);
f1=round((l1/2)-256);
f2=round((l2/2)-256);
e=e(f1+1:512+f1,f2+1:512+f2);
e=imresize(e,[64 512],'bicubic');
save c:\scan\45.txt e -ASCII

clear e l1 l2 f1 f2
e=imrotate(d,+5);
[l1,l2]=size(e);
f1=round((l1/2)-256);
f2=round((l2/2)-256);
e=e(f1+1:512+f1,f2+1:512+f2);
e=imresize(e,[64 512],'bicubic');
save c:\scan\50.txt e –ASCII
```

9.4 Uncertainty Evaluation of Laser Diffractometer

(1). Measuring equation

$$P_{20} = [1+\alpha(20-t_s)]P = [1+\alpha(20-t_s)]\frac{\lambda}{2\sin\gamma} = [1+\alpha_s(20-t_s)]\frac{\lambda_0}{2n_{tpf}\sin\gamma},$$
$$= F(\lambda_0, n_{tpf}, \alpha, t_s, \gamma)$$

where

P_{20} : Pitch value calibrated at 20 °C,
P : Pitch measuring value at temperature t_s,
λ_0 : Laser wavelength in vacuum,
n_{tpf} : Refraction index of air,
γ : First order diffraction angle,
t_s : Smple temperature,
α : The coefficient of thermal expansion.

(2) Sensitivity coefficient

$$\frac{\partial F}{\partial \lambda_0} = \frac{1}{2n_{tpf}\sin\gamma} = \frac{P}{\lambda_0}$$
$$\frac{\partial F}{\partial n_{tpf}} = \frac{\lambda_0}{-2{n_{tpf}}^2\sin\gamma} = -\frac{P}{n_{tpf}}$$
$$\frac{\partial F}{\partial \gamma} = \frac{\lambda_0}{-2n_{tpf}\sin^2\gamma}\cos\gamma = -\frac{P}{\tan\gamma}$$
$$\frac{\partial F}{\partial t_s} = -\alpha P$$
$$\frac{\partial F}{\partial \alpha} = (20-t_s)P$$

(3) Standard uncertainty (Error budget)

Error(x_i)	Estimated value	Type	Distribution	Standard uncertainty	$\dfrac{\partial F}{\partial x_i}$	$\left\lvert\dfrac{\partial F}{\partial x_i}u(x_i)\right\rvert$	υ_i
Wavelength (λ_0)	3.55×10^{-6}	B	$1/\sqrt{3}$	2.05×10^{-6}	$1.84\,P$	$3.77\times10^{-6}\,P$	50
Refraction index of air					$-1\,P$	$5.99\times10^{-7}\,P$	50
Edlén formula	3×10^{-8}	B	$1/\sqrt{3}$	1.732×10^{-8}	$-0.9997\,P$	$1.73\times10^{-8}\,P$	(50)
Temperature(t)	1 °C	B	$1/\sqrt{3}$	0.577 °C	$9.53\times10^{-7}\,P$°C^{-1}	$5.50\times10^{-7}\,P$	(50)
Pressure(p)	150 Pa	B	$1/\sqrt{3}$	86.6 Pa	$-2.68\times10^{-9}P$Pa^{-1}	$2.32\times10^{-7}\,P$	(50)
Vapor pressure(f)	10 %	B	$1/\sqrt{3}$	5.77 %	$8.5\times10^{-9}\,P$%$^{-1}$	$4.95\times10^{-8}\,P$	(50)
Sample temperature(t_s)	1 °C	B	$1/\sqrt{3}$	0.577 °C	$-2.55\times10^{-6}P$ °C^{-1}	$1.47\times10^{-6}P$	50
Coefficient of thermal expansion (α)	1×10^{-6} °C^{-1}	B	$1/\sqrt{3}$	0.577×10^{-6} °C^{-1}	$-3\,P$ °C	$1.73\times10^{-6}P$	50
Diffraction angle (γ)				1.43×10^{-5}	$-P\cot\alpha$	$0.56\times10^{-5}\,P$	16.5
Angular resolution	0.36”	B	$1/\sqrt{3}$	0.21 ”			(50)
Angular accuracy	1”	B	$1/\sqrt{3}$	0.58 ”			(50)
Repeatability	$u(r)$	A	1	2.87 ”			(15)

9.5 Limitations of Laser Diffractometer

P (nm)	λ (nm)	Sin γ	γ (°)	δγ (”, $\Delta p/p=1\times10^{-5}$)
200	325	0.8125	54.34	2.88
	488	(1.22)	×	×
	543	(1.3575)	×	×
	633	(1.5825)	×	×
300	325	0.5417	32.80	1.33
	488	0.8133	54.42	2.87
	543	0.905	64.82	4.38
	633	(1.055)	×	×
500	325	0.325	18.96	0.71
	488	0.488	29.21	1.15
	543	0.543	32.89	1.33
	633	0.633	39.27	1.68
700	325	0.232	13.42	0.49
	488	0.3486	20.40	0.76
	543	0.3878	22.82	0.86
	633	0.4521	26.88	1.04
1000	325	0.1625	9.35	0.34
	488	0.244	14.12	0.51
	543	0.2715	15.75	0.58
	633	0.3165	18.45	0.68

$$\frac{\delta P}{P}=\frac{\delta\lambda}{\lambda}-\frac{\delta\gamma}{\tan\gamma}$$

10. Resume

Personal Information:

Name: Chao-Jung Chen
Date of Birth: 19. January 1960
Place of Birth: Taoyuan, Taiwan
Marital status: Married
Phone: 886-3-5743769
E-mail: Chao-Jung.Chen@itri.org.tw
Address: Bldg. 16, 321 Kuang-Fu Road, Section 2, Hsinchu, 300 Taiwan
Title of Position: Researcher

Education:

Oct. 1988 ~ Jun. 1990: M.S., Mechanical Engineering, National Taiwan University of Science and Technology in Taipei, Taiwan

Oct. 1978 ~ Jun. 1982: B.S., Mechanical Engineering, National Taiwan University of Science and Technology in Taipei, Taiwan

Sep. 1975 ~ Jun. 1978: Taipei Senior Technical High School in Taipei, Taiwan

Aug. 1972 ~ Jun. 1975: Wen-Chang Junior High School in Taoyuan, Taiwan

Aug. 1966 ~ Jun. 1972: Chung-Pu Elementary School in Taoyuan, Taiwan

Experiences:

Jan. 1994 ~ Present: Researcher, Center for Measurement Standards/Industrial Technology Research Institute in Hsinchu, Taiwan
Jun. 1990 ~ Dec. 1993: Associate Researcher, Center for Measurement Standards/Industrial Technology Research Institute in Hsinchu, Taiwan

Nov. 1984 ~ Oct. 1988: Assistant Engineer, Chung-Shan Institute of Science and Technology in Taoyuan, Taiwan
Jul. 1982 ~ May 1984: Lieutenant, Army in Kin-Men, Taiwan

Awards:

Nov. 1997: Best Young Engineer Award of Chinese Society of Mechanical Engineering in 1997.
Jun. 2002: The first place of the Metrology Essay Award of the Chinese Metrology Society in 2002.

Development of a Traceable Atomic Force Microscope with Interferometer and Compensation Flexure Stage

Abstract

Scanning Probe Microscopes (SPMs), generally including such instruments as Scanning Tunneling Microscopes (STMs) and Atomic Force Microscopes (AFMs), have been widely applied to measure engineering surfaces in a variety of fields, such as material sciences, semiconductor industry, and biotechnology. SPMs will also be a potential tool in nanotechnology, for example nanolithography, atom manipulation, and nanometrology. Normally, a commercial AFM consists of a laser, a photo-detector, a controller, a piezo-scanner, and a cantilever tip. The piezo-scanner is critical to the performance of AFMs. The intrinsic properties of piezo-scanners, for instance non-linearity, hysteresis, aging, thermal drift, creep, and coupling effect will result in measurement errors that may reach up to 20 % of the reading. To reduce major measurement errors mentioned above, an AFM should be periodically calibrated with a traceable standard.

The goal of my research study was to design a state-of-the-art Traceable Atomic Force Microscope (TAFM) to be used as a primary realization of nanometer scale standards for Taiwan industry. The TAFM was composed of a commercial AFM, two laser interferometers, a 3-axis active compensation flexure stage, a super-Invar metrology frame, a vibration isolator, and a temperature-controlled enclosed box with circulating water. To eliminate the Abbe-offset, the surface-plane of specimens was arranged on the same plane-level to the laser beams emitted by interferometers. The compensation flexure stage was aimed to provide a perfect reference motion mechanism. To achieve the direct traceability to the definition of meter, two interferometers were added to the flexure stage. The TAFM was evaluated to have an expanded uncertainty of 2.5 nm at a confidence level of 95 % and 29 degrees of freedom for a nominal pitch value of 292 nm.

Since the expanded uncertainty of pitch measurement is not satisfactory and there is no traceability in the Z direction. The TAFM needs to be improved to meet the requirement of an expanded uncertainty of no more than 0.5 nm at 95 % confidence level at all three axes. The requirement can be achieved by the following improvements: A laser interferometer is added to the flexure stage for Z-height calibration. To reduce the noise of laser interferometer to about 5 nm, the support of the enclosed box is moved from tabletop to the floor. The metrology frame is improved by changing the reference mirrors from AFM to flexure stage, thickening the super-Invar frame, shortening the structure loop and metrology loop, using one material, and realizing a symmetrical mechanism design. The passive temperature control is changed to active temperature control, which will approach an anticipative temperature stability of (20±0.1) °C in the measuring volume.

Entwicklung eines rückführbaren Rasterkraftmikroskops auf der Basis von Interferometern und einer geregelten Einkörperführung

Abstrakt

Rastersondenmikroskope, zu denen unter anderem Rastertunnelmikroskope (STM) und Rasterkraftmikroskope (AFM) gezählt werden, werden an vielen Stellen in der Material- und Oberflächenforschung, der Halbleitertechnologie sowie der Biotechnologie angewendet. Sie sind zudem denkbare Werkzeuge der Nanotechnologien, so beispielsweise der Nanolithographie. Zudem können sie der Manipulation von Atomen und zur Nanometrologie dienen. Kommerzielle AFM bestehen unter anderem aus einem Laser, Photoempfänger, Regler, Piezoantriebssystem sowie einem Tastsystem. Dabei kommt den Piezoelementen des Antriebssystems besondere Bedeutung zu. Die von Piezoelementen bekannten Nachteile, wie Nichtlinearität, Hysterese, Alterung, thermische Drift, Kriechen und Übersprechen, können durchaus 20% der Messabweichungen bei Vorwärtssteuerung verursachen. Daher sollten AFM, Metrologiestandards entsprechend, zur Reduzierung der Meßunsicherheit regelmäßig rückführbar kalibriert werden.

Das Ziel der vorliegenden Arbeit bestand in der Entwicklung eines rückführbaren Rasterkraftmikroskops (Traceable Atomic Force Microscope, TAFM) zum Einsatz als staatliches Normal zur rückführbaren Vermessung von Normalen im Nanometer-Bereich für die taiwanesische Industrie. Das TAFM wurde als Kombination eines kommerziellen AFM, zwei Laserinterferometern, einer aktiv geregelten dreiachsigen Präzisionsführung, einem Metrologierahmen aus Super-Invar, einer Schwingungsdämpfung sowie einer temperaturgeregelten Umhausung konzipiert und aufgebaut. Zur Reduzierung des Abbe-Offsets wurden die Interferometer derart angeordnet, dass sich ihre virtuell verlängerten Messstrahlen im Antastpunkt des Cantilevers und damit direkt auf der Probenoberfläche im Messpunkt schneiden. Eine einwandfreie Referenzbewegung des Systems wurde durch die eingesetzten Präzisionsführungen sichergestellt, während die direkte Rückführbarkeit auf die Definition der Längeneinheit „Meter“ durch den Einsatz von zwei Laser-Interferometern erreicht wurde. Die ermittelte erweiterte Messunsicherheit des TAFM für die laterale Messung einer Länge von 292 nm betrugt bei einer statistischen Sicherheit von 95% unter Berücksichtigung von 29 Freiheitsgraden 2,5 nm.

Da die ermittelte erweiterte Messunsicherheit für laterale Längenmessungen noch nicht zufriedenstellend und die Rückführbarkeit in Richtung der Z-Achse nicht gewährleistet ist, soll das TAFM verbessert werden, um perspektivisch eine Messunsicherheit von 0,5 nm in allen drei Messachsen zu erreichen. Dieses Ziel kann zunächst durch den Einbau eines weiteren Laserinterferometers zur Kalibrierung des Meßsystems der Z-Achse erreicht werden. Zusätzlich sollte die Umhausung statt auf einem Tisch auf dem schwingungsärmeren Boden platziert werden, was das Rauschen der Interferometer auf weniger als 5 nm reduzieren sollte. Ein verstärkter Metrologierahmen, die Verlagerung der Referenzspiegel vom AFM auf die Präzisionsführung und verkürzte Messkreise, die Konstruktion aller Teile aus dem gleichen Material, ein symmetrischer mechanischer Aufbau und der Einsatz einer aktiven Temperaturregelung mit einer Temperaturstabilität von 20±0.1 °C sind weitere wichtige Schritte.